

Department of Physics and Astronomy

University of Heidelberg

Master thesis

in Physics

submitted by

Beatrice Marie Latz

born in Saarbrücken

2019

Multipartite Entanglement
from Quench Dynamics in Spinor Bose Gases
using Bogoliubov Theory

This Master thesis has been carried out by Beatrice Marie Latz

at the

Kirchhoff Institute of Physics

under the supervision of

Dr. Philipp Hauke

Abstract

Studying the entanglement among many particles is a central topic of current research in quantum many-body systems and has great importance to the field of quantum metrology. In this context, the quantum Fisher information (QFI) provides a powerful framework for assessing, classifying and understanding the multipartite entanglement, and its metrological applications. Spinor Bose-Einstein condensates (BECs) constitute a particularly versatile platform for experimental investigations in this matter, however, a general and efficient experimental scheme for measuring the QFI in spinor BECs is still missing. The aim of this Master's thesis is therefore to bring these two important concepts together by developing a protocol for the extraction of multipartite entanglement in spin-1 BECs. To this end, we derive an overarching framework relying on the computation of the QFI from quench dynamics and mean-field Bogoliubov theory. In a first study, we examine the strong influence of spontaneous symmetry breaking on the many-particle entanglement in single-mode BECs and compare our analysis to exact numerical calculations. We expand this study to an one-dimensional system by extending the Bogoliubov formalism to spin-1 quasi-condensates and deriving bounds for the entanglement of generic many-spin states. In this way, we compute the finite temperature amount of entanglement in a spin-1 BEC from dynamic susceptibilities after a weak quench. Our studies reveal the presence of multipartite entanglement in spin-1 BECs and the growth of correlations in regions close to quantum phase transitions. This work therefore paves the way towards the detection of multipartite entanglement in spinor BECs.

Zusammenfassung

Quanten-Vielteilchen-Systeme sind ein wichtiger Gegenstand heutiger Forschung, insbesondere durch ihren potentiellen Nutzen für Präzisionsmessungen. Die Quanten Fisher Information (QFI) ist hierbei eine Größe mit welcher die Verschränkung vieler Quanten berechnet, klassifiziert und besser verstanden werden kann. Experimentell bilden Spinor Bose-Einstein Kondensate (BECs) ideale Möglichkeiten um Quantenphänome zu untersuchen, derzeit gibt es jedoch noch kein Messprotokoll, welches die QFI in Spinor BECs bestimmt. Diese Masterarbeit hat daher zum Ziel ein solches Messprotokoll auf der Grundlage von Bogoliubov Theorie und Quenchedynamik zu entwickeln. Zunächst untersuchen wir die QFI für ein spin-1 BEC unter Vernachlässigung räumlicher Abhängigkeiten. Hierbei liegt ein besonderes Augenmerk auf dem Einfluss spontaner Symmetriebrechung des Grundzustandes. Anschließend wenden wir eine Erweiterung der Bogoliubov Theorie für eindimensionelle Quasikondensate an. Diese ermöglicht uns, die QFI sowohl im Grundzustand als auch bei endlichen Temperaturen mit Hilfe der dynamischen Suszeptibilität nach einem Quench in einem ausgedehnten spin-1 BEC zu berechnen. Nicht zuletzt zeigen wir, wie aus der QFI einer beliebigen Spin-Konfiguration untere Schranken für ihre Mehrfachverschränkung hergeleitet werden können. Zusammenfassend legen unsere Ergebnisse nahe, dass Vielteilchenverschränkung insbesondere nahe Quantenphasenübergängen in spin-1 BECs vorhanden ist und auf Grundlage dieser Arbeit möglicherweise gemessen werden könnte.

Acknowledgments

This thesis closes my studies of physics. I am grateful to all the friends, colleagues, teachers and family members encouraging me to start and persevere with this adventure. Thanks for being part of this journey!

First and foremost, I would like to thank my advisor Philipp Hauke for the continuous support of my Master's thesis, for his motivation, patience, and immense knowledge. You have introduced me to the tools of quantum many-body theory and I am very grateful for always finding you ready to listen to my questions. Your expertise was invaluable in all the time of research and your guidance helped me in the writing of this thesis!

I give also deep thanks to the professors and lecturers awakening my curiosity about the quantum world. In particular, I thank Markus Oberthaler for encouraging me to work on this project and for all the opportunities I was given to conduct my thesis in his supporting working environment. Thank you, Markus, for also becoming the second reader of this thesis! Moreover, I sincerely acknowledge the valuable and productive discussions with Martin Gärttner and Thomas Gasenzer.

A big thanks goes out to all QOT members, the SynQS collaborators as well as the members of the Berges group for their insightful comments and the fantastic opportunity to work with you. With a special mention to Ricardo Costa de Almeida: The results outlined in this thesis were accomplished with the help of your passionate input and our fruitful discussions! Moreover, I wish to thank Kevin Geier for providing his code for benchmark studies.

I would like to also convey my heartfelt thanks to our team assistants, Dagmar Hufnagel and Christiane Jäger, for their various acts of support and the invaluable help with the paper works.

A thank you to the Cave54 Jazz family, the Beatschuppen band and all the people running: I owe my personal balance to your cracking distraction!

To Vaso and Bruno, for always sharing your truthful and inspiring views on a number of issues, may it be related to Physics or not.

Finally, I am profoundly grateful to my mother, my brother and my grandparents for providing me with never ending support. With all my heart, I thank my dad, whose dreams aroused my enthusiasm for research and technology.

And, most importantly, I am deeply grateful to Tim: There is nothing more marvelous than sharing life with you!

Contents

Abstract	5
Acknowledgments	7
List of Abbreviations	11
Motivation	12
Thesis Outline	14
I. Concepts	17
1. Many-Body Physics of Spinor Bose Gases	18
1.1. Spin-1 Bose-Einstein Condensates	18
1.2. The Lie Algebra $su(3)$	24
1.3. Coherent Spin States and Wigner Function	26
1.4. Spontaneous Symmetry Breaking	26
2. Bogoliubov Theory	30
2.1. Diagonalization of Quadratic Bosonic Hamiltonians	30
2.2. Examples	32
2.2.1. Bosonic, Interacting Hamiltonian	32
2.2.2. Single-Mode Approximation Hamiltonian of Spin-1 BEC in Polar Phase	34
2.3. Wick's Theorem for Gaussian Fields	35
3. Quantum Fisher Information	37
3.1. Multipartite Entanglement	37
3.2. Classical and Quantum Phase Estimation	37
II. Studying Multipartite Entanglement in Spin-1 BECs	41
4. Extracting Quantum Fisher Information from Quench Dynamics	42
4.1. Linear Response Theory	42
4.2. Quantum Fisher Information through Dynamic Susceptibilities	44
4.3. Correlation Functions from Bogoliubov Theory	45
4.3.1. Thermal Equilibrium	46
4.3.2. Time-Evolution Following a Weak Quench	47
5. Quantum Fisher Information of a Spin-1 BEC in Single-Mode Approximation	50
5.1. Single-Mode Approximation	50
5.2. Lipkin-Meshkov-Glick Representation	52
5.3. Self-Consistent Mean-Field Bogoliubov Theory	53
5.3.1. Mean-Field Description	54

5.3.2.	Quadratic Form of the Single-Mode Approximation Hamiltonian	56
5.3.3.	Numerical Implementation	57
5.4.	Quantum Fisher Information at Zero Temperature	58
5.4.1.	Spontaneous Symmetry Breaking of the Ground State	60
6.	Multipartite Entanglement in Spin-1 Quasi-Condensate (1D)	64
6.1.	Extension of Bogoliubov Theory to Spin-1 Quasi-Condensates	64
6.1.1.	Effective Interaction in One Dimension	64
6.1.2.	Discretization of Space	66
6.1.3.	Dimensionless Formulation	67
6.1.4.	Mean-Field Description	68
6.1.5.	Characteristic Properties	70
6.1.6.	Bogoliubov Hamiltonian	71
6.1.7.	Density and Phase Fluctuations	72
6.2.	Entanglement Bounds for Spin Systems	76
6.2.1.	Generic Configuration of Quantum-Mechanical Spins	76
6.2.2.	Spinor BEC on a Spatial Grid	80
6.3.	Signatures of Multipartite Entanglement in spin-1 BECs	82
6.3.1.	Experimental Considerations	85
	Conclusion and Outlook	88
	Appendices	90
A.1.	Wick's Theorem	90
A.2.	Thermal Phase Diagram in Single-Mode Approximation	91
A.3.	Analytical Approach towards SMA Bogoliubov Transformations	93
A.4.	Energy Spectrum of spin-1 BEC in SMA from Exact Diagonalization	97
A.5.	Equations of Motion in Extended Spin-1 BEC	98
A.6.	Cumulant Expansion	99
	Bibliography	101

List of Abbreviations

AFM	Anti-Ferromagnetic
AOD	Acousto-Optic Deflector
BA	Broken-Axisymmetry
BEC	Bose-Einstein Condensate
CSS	Coherent Spin State
EA	Easy-Axis
EP	Easy-Plane
HL	Heisenberg Limit
P	Polar
RF	Radiofrequency
SBB	Spontaneous Symmetry Breaking
SCC	Spin Changing Collisions
SMA	Single Mode Approximation
SQL	Standard Quantum Limit
QFI	Quantum Fisher Information
QPT	Quantum Phase Transition

Motivation

Quanta are the very building blocks of our world. Many of their special and fascinating properties, however, remain insufficiently explained. At the same time, quantum physics has become a cornerstone of today's research and modern industry.

The phenomenon of entanglement among many particles is a topic at the leading edge of science and the verge of breaking through into major applications such as quantum computing. In addition to being intrinsically fascinating, a better understanding of the mingling and tangling between quantum particles could unravel fundamental questions concerning, for example, the underlying mechanisms of quantum magnetism and high temperature superconductivity.

In this regard, ultracold quantum gases provide an exceptionally well-developed experimental platform to investigate quantum many-body systems with a broad range of techniques for trapping, counting, and manipulating particles [1, 2]. Groundbreaking experiments, such as with spinor Bose-Einstein condensates (BECs), have demonstrated the generation of entangled states in many-particle systems [3, 4, 5, 2, 6].

In comparison to single-component BECs, spinor condensates exhibit a particularly rich quantum structure, raising new questions about spin dynamics, such as the formation of spin domains [7]. In these systems, spin exchange interactions among Zeeman sub-levels lead to dynamical redistribution of the population of modes, thereby driving the growth of quantum correlations and the creation of entanglement.

Spinor BECs are therefore widely considered to be a good way of investigating many-particle entanglement. A particularly promising application is quantum-enhanced metrology, constituting a gradually broadening field of experimental and theoretical efforts with the aim to overcome classical bounds in precision measurements by exploiting quantum resources such as squeezing and entanglement. A typical precision experiment estimates the measure of a physical quantity by means of a phase shift observed in an interferometer [8, 9]. Here, quantum correlations are the very key component that makes it possible to achieve phase sensitivities beyond the standard quantum limit. The strong connection between phase estimation and many-particle entanglement is formalized within the highly useful framework of quantum Fisher information.

The quantum Fisher information classifies metrologically advantageous states by their multipartite entanglement content and gives a limit to the ultimate precision achievable in a phase

estimation protocol [10, 11]. Recent theoretical developments have revealed a close relation to dynamical susceptibilities of quantum many-body system [12]. This relation not only permits a natural view on the differences between non-entangled and entangled states, where the latter are more sensitive towards a transformation of the state. It also provides the possibility of extracting the quantum Fisher information from well-established linear response protocols. Additionally, it is capable of classifying multipartite entanglement at finite temperatures and allows one to identify strongly entangled phase transitions through its universal scaling behavior close to the critical point.

The overall goal of this thesis is to combine the two exceptionally fascinating and versatile concepts of spinor Bose gases and quantum Fisher information. We particularly focus on the development of an overarching framework to extract the quantum Fisher information from quench dynamics using mean-field Bogoliubov theory. To this end, we also implement an extended Bogoliubov theory for spin-1 quasi-condensates [13] and relate entanglement bounds to general density distributions of bosons on a spatial grid. By making extensive use of these concepts, we calculate correlation functions in the Broken-Axisymmetry (i. e. Easy-plane) phase of a spin-1 BEC both, in single-mode approximation and in an extended one-dimensional geometry. The quantum Fisher information is extracted at zero and finite temperature after a weak quench, thereby witnessing multipartite entanglement and the growth of correlations especially in regions close to quantum phase transitions.

This thesis therefore constitutes a contribution towards a spin-1 measurement protocol relying on the extraction of the quantum Fisher information from quench dynamics and mean-field Bogoliubov theory. It opens a door to revealing the beauty of entanglement among many particles which remains to be further explored and is possibly still hidden in its applications.

Thesis Outline

This thesis comprises some of the major steps towards a protocol for measuring multipartite entanglement in spin-1 Bose-Einstein condensates. While Part I summarizes the underlying concepts of this work, the main studies performed are discussed in Part II.

- Part I starts out with an introduction to the many-body physics of spinor Bose gases (chapter 1), including convenient approximations and mathematical descriptions [14, 15, 16]. We discuss the $su(3)$ Lie algebra as an apt representation for a three-level system such as the spin-1 BEC and introduce coherent spin states [17] and Wigner quasi-probability distributions [18] as very helpful tools to describe ensembles of quantum-mechanical spins. Moreover, we elaborate the notion of spontaneous symmetry breaking, becoming particularly relevant to the amount of entanglement in spin-1 BECs.
- Since a full quantum mechanical treatment of spinor Bose gases can become exponentially difficult, further assumptions are required. We therefore introduce mean-field Bogoliubov theory [19], relying on the description of the characteristic low-energy excitations of a quadratic theory in chapter 2. In the so-called Bogoliubov quasi-particle picture the physical sense is readily visible and explainable, thereby significantly simplifying calculations.
- The main building block allowing for the investigation of entanglement among many particles is the quantum Fisher information [8, 11], outlined in chapter 3. As a central quantity in quantum metrology, it is capable of classifying multipartite entanglement and identifying strongly entangled phase transitions [1, 12]. In particular, the QFI is related to dynamical quantities from linear response measurements, which is straightforward to measure, even for large systems, at finite temperatures and in real time.
- Bridging these three central concepts, spinor Bose-Einstein condensates, Bogoliubov theory and quantum Fisher information, is our main objective. Therefore Part II starts with the outline towards reaching this goal and presents the methodology used in this thesis for the extraction of the quantum Fisher information from dynamical susceptibilities after a weak quench using mean-field Bogoliubov theory in chapter 4.
- Subject to our first study (chapter 5) is the spin-1 BEC in single-mode approximation (SMA) and Broken-Axisymmetry (BA) phase at zero temperature, where the QFI can be computed from the variance of a pure state. By comparing results for the mean-field ground state of a spin-1 BEC with 12000 particles and the exact ground state [20, 21] for 500 particles, we discuss the strong influence of spontaneous symmetry breaking on the amount of entanglement in this system.
- In chapter 6 we introduce spatial degrees of freedom and study the considerably more involved spin-1 BEC in an one-dimensional setting. An extension of Bogoliubov theory [13] for quasi-

condensates allows us to again describe the system withing the quasi-particle picture. Another important ingredient for this study is obtained by the analysis of generic entanglement bounds for collective spin states. This enables us to compute the QFI at finite temperatures from dynamic susceptibilities following a weak quench. Using the derived entanglement bounds, we observe signatures of multipartite entanglement in the system. As a natural consequence of this finding, we close this work by discussing a possible implementation of our studies for experimentally extracting the multipartite entanglement content of spin-1 BECs.

Part I.
Concepts

1 Many-Body Physics of Spinor Bose Gases

This chapter gives an overview of the basic concepts used within this thesis in order to describe the many-body physics of spinor Bose gases. First, we review the main characteristics and mathematical descriptions of spin-1 Bose-Einstein condensates (BECs). Second, we discuss the underlying $su(3)$ -algebra of spin-1 systems and its implications on the representation of operators. Moreover, coherent spin states (CSS) and Wigner quasi-probability distributions are introduced as very helpful tools to describe ensembles of quantum-mechanical spins. The chapter closes with a review of spontaneous symmetry breaking (SSB), as this notion can significantly influence the characteristics and, especially, the entanglement content of large quantum systems.

1.1 Spin-1 Bose-Einstein Condensates

Spinor Bose-Einstein Condensates are ideal model systems to study quantum many-body physics. They feature additional degrees of freedom compared to single component BECs due to the Zeeman splitting of magnetic sublevels. Engineering their internal states with optical and magnetic fields offers a wide range of possibilities to study quantum phenomena [15, 22]. First, they exhibit various phases with different spinor order parameters due to the competition between interatomic interactions and the coupling to an external field [23, 7]. Second, their dynamics feature a variety of physical effects, including formation of spin domains, Josephson-like tunneling [24] and spontaneous symmetry-breaking. Besides, spin-mixing dynamics, generating entanglement via spin-changing collisions, can be used to create metrologically favourable states. Quantum metrology with spin-1 BECs has therefore received substantial interest and the field is maturing, with a wealth of well-understood experimental and theoretical methods [1]. Gaussian spin-squeezed states as well as the enhanced sensitivity of atom interferometers using spinor BECs have been demonstrated [2, 4] and there is growing interest in investigating the quantum Fisher information as an entanglement witness for spinor Bose gases [25, 21].

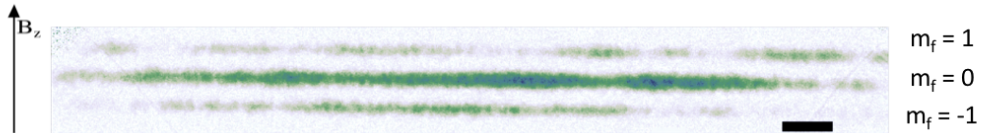


Figure 1.1.: An absorption image after a short time of flight allows one to experimentally map out the distribution of the hyperfine components of the spinor BEC when applying a magnetic field B_z . Figure courtesy of Philipp Kunkel and Maximilian Prüfer, SynQS Heidelberg.

The basis for a general mathematical description of spinor Bose gases is the second quantized

form of the so-called Gross-Pitaevski equation [26, 27] for multi-component Bose-Einstein condensates in a magnetic field ($\hbar = 1$) [28]

$$\mathcal{H} = \sum_{m, m' = -f}^f \int d^3r \Psi_m^\dagger(\mathbf{r}) \left(-\frac{\nabla^2}{2M} + V_T(\mathbf{r}) - \mu - p(f_z)_{mm'} + q(f_z^2)_{mm'} \right) \Psi_{m'}(\mathbf{r}) + V_{\text{int}}. \quad (1.1)$$

It comprises the kinetic term ($\propto \nabla^2$) for particles with mass M , the potential energy of the confining trap V_T , the chemical potential μ , and terms proportional to the linear ($\propto p$) and quadratic ($\propto q$) Zeeman shift of the hyperfine spin states. The trapping potential $V_T(\mathbf{r})$ and the chemical potential μ are assumed to be the same for all components of the Bose gas. The Zeeman energy shifts are specified by $p = -\mu_B B_z g_f$ and $q = \mu_B^2 B_z^2 / (\hbar^2 E_{\text{HFS}})$, where E_{HFS} is the ground state hyperfine splitting, B_z is the magnetic field in z -direction, g_f is the Landé g -factor, and μ_B is the Bohr magneton. The spin matrix elements are given by $(f_z)_{mm'} = m \delta_{mm'}$ and hence, $(f_z^2)_{mm'} = m^2 \delta_{mm'}$. The interaction energy V_{int} is added to the Hamiltonian and can be obtained from the two-body interaction model

$$V_{\text{int}} = \frac{1}{2} \int d^3r \sum_{m_1, m_2, m'_1, m'_2} \Omega_{m'_1, m'_2}^{m_1, m_2} \hat{\psi}_{m_1}^\dagger(\mathbf{r}) \hat{\psi}_{m_2}^\dagger(\mathbf{r}) \hat{\psi}_{m'_1}(\mathbf{r}) \hat{\psi}_{m'_2}(\mathbf{r}). \quad (1.2)$$

Assuming a dilute system in the low temperature limit at which the range of the interaction is negligible compared to the inter-particle spacing, the interaction is described by a pseudo-interaction $\sum_{i < j} g_F \delta(r_i - r_j)$. Accordingly, the parameters $\Omega_{m'_1, m'_2}^{m_1, m_2}$ can be computed using the projection operator \mathcal{P}_F for a two-body state with total spin angular momentum¹ F and Glebsch-Gordan coefficients $\langle f_1, m_{f_1}; f_2, m_{f_2} | F, m_F \rangle$

$$\sum_{i < j} g_F \delta(r_i - r_j) = \delta(r_i - r_j) \underbrace{\sum_{F=0}^{2f} \sum_{M_F=-F}^F |F, M_F\rangle \langle F, M_F|}_{\mathcal{P}_F} \quad (1.3)$$

$$\text{and } \Omega_{m'_1, m'_2}^{m_1, m_2} = \sum_{F=0}^{2f} g_F \langle f, m_1; f, m_2 | \mathcal{P}_F | f, m'_1; f, m'_2 \rangle. \quad (1.4)$$

A detailed review on Bose-Einstein condensates can be found in A. Leggett's book [14]. For a more involved description of multi-component Spinor Bose-Einstein condensates see also reviews by Y. Kawaguchi and D. Stamper-Kurn [15, 16].

For the remaining part of this thesis, we focus on a spin-1 system featuring three magnetic sublevels. A Stern-Gerlach type experiment reveals the splitting of these sublevels as showcased in Figure 1.1. According to their hyperfine state, the atom cloud splits up into several clouds which

¹The total spin state $|F, M_F\rangle$ is expanded in terms of basis vectors $|f, m_f\rangle \otimes |f, m'_f\rangle$.

can be detected by a time-of-flight measurement (Figure 1.1).

In order to investigate the dynamics of a spin-1 BEC, it is convenient to rewrite the Hamiltonian (1.1) as a sum of a symmetric, spin-independent part \mathcal{H}_S , an anti-symmetric, spin-dependent part \mathcal{H}_A and the Zeeman energies \mathcal{H}_B [15]

$$\mathcal{H}_S = \sum_{i=0,\pm 1} \int d^3r \hat{\psi}_i^\dagger \left(-\frac{\nabla^2}{2M} + V_T - \mu \right) \hat{\psi}_i + \frac{\lambda_s}{2} \sum_{i,j=0,\pm 1} \int d^3r \hat{\psi}_i^\dagger \hat{\psi}_j^\dagger \hat{\psi}_i \hat{\psi}_j \quad (1.5)$$

$$\begin{aligned} \mathcal{H}_A = \frac{\lambda_a}{2} \int d^3r & \hat{\psi}_1^\dagger \hat{\psi}_1^\dagger \hat{\psi}_1 \hat{\psi}_1 + \hat{\psi}_{-1}^\dagger \hat{\psi}_{-1}^\dagger \hat{\psi}_{-1} \hat{\psi}_{-1} + 2\hat{\psi}_1^\dagger \hat{\psi}_0^\dagger \hat{\psi}_1 \hat{\psi}_0 + 2\hat{\psi}_{-1}^\dagger \hat{\psi}_0^\dagger \hat{\psi}_{-1} \hat{\psi}_0 \\ & - 2\hat{\psi}_1^\dagger \hat{\psi}_{-1}^\dagger \hat{\psi}_1 \hat{\psi}_{-1} + \underbrace{2\hat{\psi}_0^\dagger \hat{\psi}_0^\dagger \hat{\psi}_1 \hat{\psi}_{-1} + 2\hat{\psi}_1^\dagger \hat{\psi}_{-1}^\dagger \hat{\psi}_0 \hat{\psi}_0}_{\text{SCC}} \end{aligned} \quad (1.6)$$

$$\mathcal{H}_B = \int d^3r p \left(\hat{\psi}_1^\dagger \hat{\psi}_1 - \hat{\psi}_{-1}^\dagger \hat{\psi}_{-1} \right) + q \left(\hat{\psi}_1^\dagger \hat{\psi}_1 + \hat{\psi}_{-1}^\dagger \hat{\psi}_{-1} \right). \quad (1.7)$$

The symmetric, spin-independent part (1.5) determines the overall spatial and motional wavefunction, whereas the anti-symmetric, spin-dependent portion (1.6) drives so-called spin-mixing dynamics. The coupling strengths λ_s and λ_a will be further specified later. The dynamics is sensitive to the distribution of atomic populations among the individual components of the condensate shown in Figure 1.1 [7, 28]. The interchange of hyperfine states among the m_F - components through spin-changing collisions (SCC) transfers population from one spin state to another, thereby preserving the overall spin. SCC are incorporated into the Hamiltonian (1.6) by terms of the form $\hat{\psi}_1^\dagger \hat{\psi}_{-1}^\dagger \hat{\psi}_0 \hat{\psi}_0$ describing, for instance, the process of annihilating to particles in the central mode ($m_F = 0$) and creating one particle in each side mode ($m_F = \pm 1$). These s-wave type collisions are a key component for the emergence of dynamical phenomena involving the creation of entanglement. They can be, for example, exploited to create metrologically useful states [1, 29, 30, 4]. Spin changing collisions are therefore of special interest for the investigation and comprehensive description of multipartite entanglement in spin-1 BECs.

Furthermore, the phase diagram of a spin-1 BEC is determined by symmetries associated with the magnetic order of the system [15] (Figure 1.2). The mean-field parametrization is given by the ground state magnetism for specific linear and quadratic Zeeman shifts (p and q , respectively) and spin-spin interaction parameters (we use $c_1 \propto \lambda_s$ in the following). The ferromagnetic phases I and II are fully polarized with respect to the applied magnetic field \mathbf{B} . The anti-ferromagnetic phase III has a longitudinal magnetization that depends on the linear Zeeman shift p . Because the rotational symmetry about \mathbf{B} is spontaneously broken, phase IV refers to the Broken-Axisymmetry (BA) phase, marked by the shaded regions in Figure 1.2. The polar phase V does not possess any polarization. In Figure 1.2, the yellow boundaries indicate second-order phase boundaries across which the derivative of the ground state energy with respect to the Zeeman shifts p and q changes continuously. The red lines correspondingly describe first-order

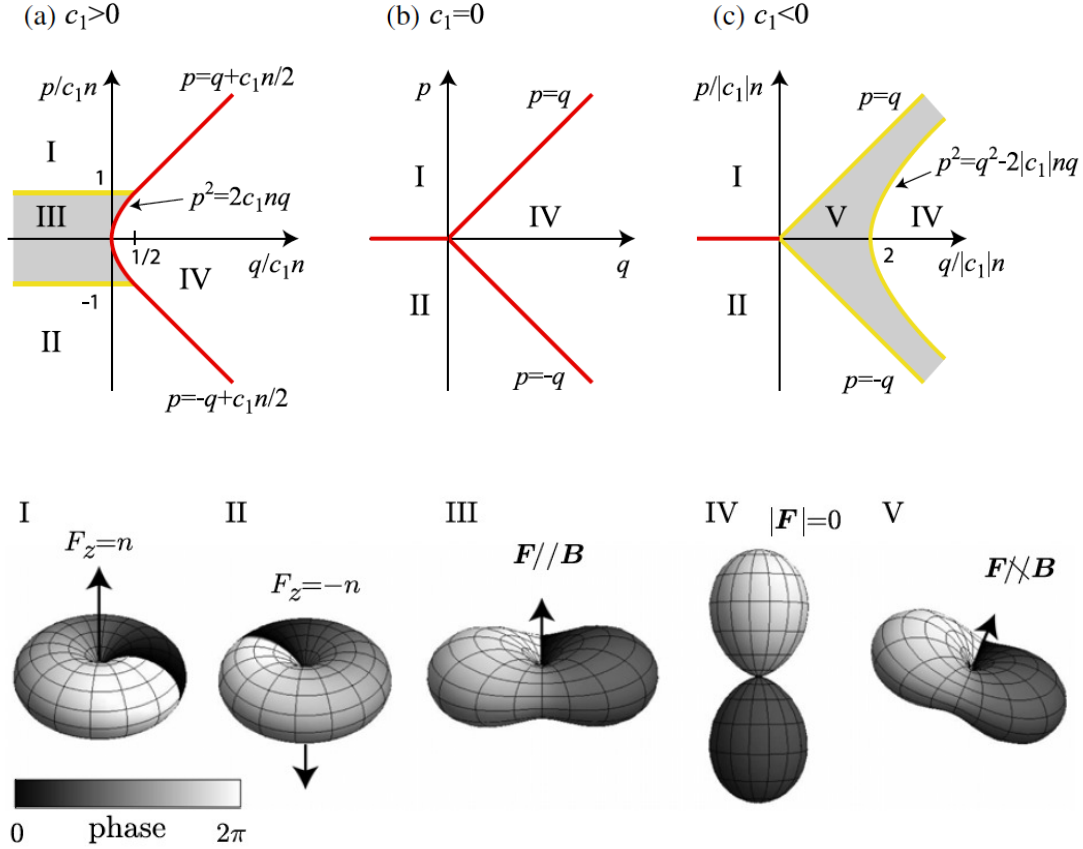
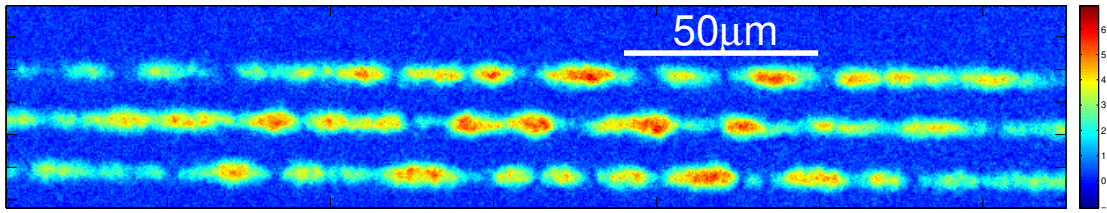


Figure 1.2.: The upper panel shows the mean-field phase diagrams [15] of a spin-1 Bose–Einstein condensates with repulsive ($c_1 > 0$) and attractive ($c_1 < 0$) spin-spin interactions. The linear and quadratic Zeeman shift is parametrized by p and q , respectively. The phase diagram exhibits various transitions between different magnetically ordered states, further specified and visualized in the lower panel. Here, there magnetization is given in terms of F_z which denotes the spin expectation value in z direction of a uniform system with a fixed number density n . \mathbf{B} gives the direction of the external magnetic field. The complex wave function of the mean-field ground state is depicted in terms of the spherical harmonics $Y_F^m(\mathbf{s})$, according to $\Psi(\mathbf{s}) = \sum_m \sqrt{n} \zeta_m Y_F^m(\mathbf{s})$, where \mathbf{s} is a unit vector in spin spaces and ζ_m the mean-field value of the $m_F = m$ hyperfine spin state. The order parameters are shown as the surface plot of $|\Psi(\mathbf{s})|$ with a gray scale representing $\arg(\Psi(\mathbf{s}))$. Further details, as for example on the parametrization ζ_m of the mean-field ground state, can be found in Table 3 of [15].

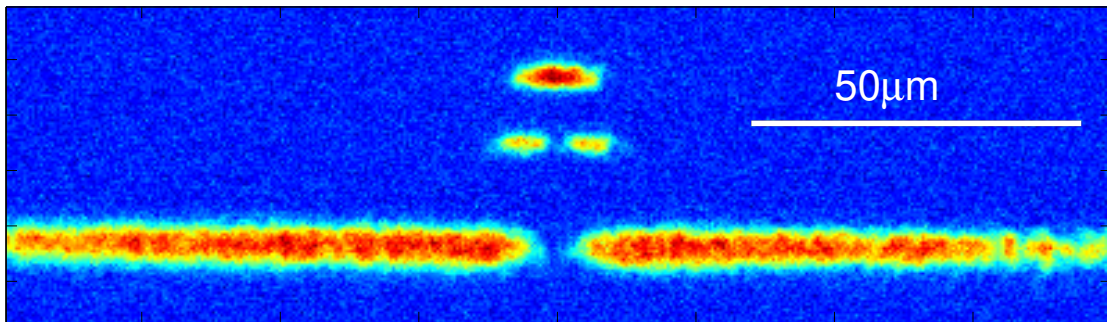
quantum phase transition (QPT) with an abrupt change in the order parameter. The other lines indicate first-order QPTs. In either way, the regions in vicinity of the QPTs offer a fascinating interplay of effects driven by quantum and thermal fluctuation [31]. In addition to that, these effects are strongly involved in the creation of entanglement and can lead to a scaling growth of the quantum Fisher information [12].

In the course of this thesis, we will examine the dynamics of a spin-1 BEC after a weak quench, which means a sudden change of a characteristic parameter of the system. In experiments, magnetic and electric fields allow one to carefully address a broad range of parameters, as demonstrated in Figure 1.3. For example, spin-changing collisions can be enhanced by tuning the magnetic field parameter q which leads to spin excitations (Figure 1.3a). Moreover, acousto-optic deflectors (AODs) allow for local manipulations of the BEC with the use of radiofrequency (RF) pulses, thereby creating local spin rotations (Figure 1.3b). Most interestingly, the development of experimental tools went already so far to make geometries beyond the typical harmonic trapping potential possible. Especially box potentials allow for a reduction of trap effects and a more straightforward comparison to theoretical studies (Figure 1.3c). Thus, there is a variety of experimental tools already available to examine quantum dynamics in spinor Bose gases.

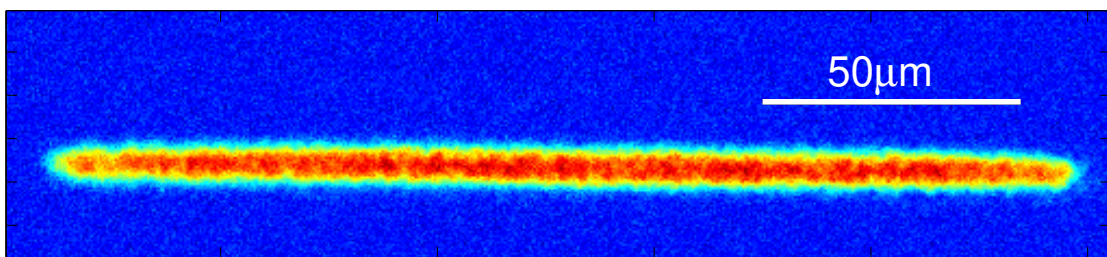
From the short review above, we summarize that many features of the spin-1 BEC can be attributed to its quantum-mechanical spin. In first place, the phase diagram is determined by magnetic order parameters. Moreover, spin-changing collisions are involved in the growth of entanglement. Most interestingly, the spin dynamics as well as spin-spin interactions and spin rotations can be experimentally manipulated in a well-controlled manner. To this end, it is natural to describe spinor Bose gases with the language of spin systems. In the following, we introduce the $su(3)$ group as a particularly apt representation for spin-1 BECs.



(a) In a Stern-Gerlach type configuration, the atom cloud splits up according to the m_F hyperfine spin states, where $m_F = 1$ refers to the upper, $m_F = 0$ to the central, and $m_F = -1$ to the lower cloud. Spin excitations can be observed via time-of-flight absorption imaging as shown here after 4 seconds of time evolution under spin-changing collisions.



(b) The time-of-flight image shows a change of the orientation of the spin from $F_z = -1$ (lower clouds) to $F_z = +1$ (upper cloud). Local spin rotations of this type can be performed by specifically addressing RF-pulses to the BEC with the help of AODs, thereby locally changing the Rabi-coupling between different m_F components.



(c) Using AODs also allows one to cut-off the wings of an elongated atom cloud, such that the system resembles a box.

Figure 1.3.: Well-developed experimental techniques allow for the specific and local manipulation of a spin-1 BEC in an elongated trap. The colorbar is proportional to the number of atoms observed via time-of-flight absorption imaging. Red refers to the maximal atom count and blue to the shot noise limit. Images were captured and kindly provided by Stefan Lannig, SynQS Heidelberg.

1.2 The Lie Algebra $su(3)$

The simplest case of a spin system and one of the most widely used models in quantum physics is the two-level system, often just referred to as qubit. In general, the state of such a system can be represented by a complex two-component vector on the Bloch sphere [32, 33]. Transformations to these states are formalized in the $su(2)$ Lie Algebra which comprises a set of 2×2 complex unitary matrices. For a spin- $\frac{1}{2}$ particle, this matrix decomposition is generated by the Pauli matrices $\hat{\sigma}$, which is the fundamental representation of the $su(2)$ group [34]

$$\hat{\mathbf{L}} = \frac{\hbar}{2} \hat{\boldsymbol{\sigma}}. \quad (1.8)$$

The spin operator $\hat{\mathbf{L}}$ preserves the spin length and satisfies the commutation relation

$$[\hat{L}_i, \hat{L}_j] = i\hbar \sum_k \epsilon_{ijk} \hat{L}_k. \quad (1.9)$$

There are further extensions to this formalism: A system consisting of N qubits is, for example, described within the $su(2^N)$ algebra.

Three-level quantum systems are the simplest multi-valued systems and the spin-1 BEC is a common example of a three-level system. In contrast to the two-level system, their set of possible physical transformations is larger. Hence, more operators are needed to fully describe the spin-1 states. In general, any interaction Hamiltonian coupling a spin-1 system can be constructed by 3×3 complex unitary matrices. An orthogonal basis of the $su(3)$ algebra is built by the identity matrix $\mathbb{1}$ and the following, so-called Gell-Mann operators:

$$\begin{aligned} G_1 &= \frac{1}{2} \begin{pmatrix} 0 & 1 & 0 \\ 1 & 0 & 0 \\ 0 & 0 & 0 \end{pmatrix}, & G_2 &= \frac{1}{2} \begin{pmatrix} 0 & -i & 0 \\ i & 0 & 0 \\ 0 & 0 & 0 \end{pmatrix}, & G_3 &= \frac{1}{2} \begin{pmatrix} 1 & 0 & 0 \\ 0 & -1 & 0 \\ 0 & 0 & 0 \end{pmatrix} \\ G_4 &= \frac{1}{2} \begin{pmatrix} 0 & 0 & 1 \\ 0 & 0 & 0 \\ 1 & 0 & 0 \end{pmatrix}, & G_5 &= \frac{1}{2} \begin{pmatrix} 0 & 0 & -i \\ 0 & 0 & 0 \\ i & 0 & 0 \end{pmatrix}, & G_6 &= \frac{1}{2} \begin{pmatrix} 0 & 0 & 0 \\ 0 & 0 & 1 \\ 0 & 1 & 0 \end{pmatrix} \\ G_7 &= \frac{1}{2} \begin{pmatrix} 0 & 0 & 0 \\ 0 & 0 & -i \\ 0 & i & 0 \end{pmatrix}, & G_8 &= \frac{1}{2\sqrt{3}} \begin{pmatrix} 1 & 0 & 0 \\ 0 & 1 & 0 \\ 0 & 0 & -2 \end{pmatrix}. \end{aligned} \quad (1.10)$$

This representation can be seen as arising from the Pauli matrices. The matrices $G_1 - G_7$ contain one Pauli matrix each and a third column/row filled up with zeros. $\{G_1, G_2, G_3\}$, $\{G_4, G_5, G_6\}$ and $\{G_6, G_7, G_8\}$ form $su(2)$ -subspaces of the $su(3)$ Lie Algebra. Here, G_8 is chosen in such a way that the matrix completes the corresponding subspace. These operators generally describe a

single spin-1 state. Here, it is important to mention that we seek to study ensembles of interacting spins as described by the Hamiltonian (1.5) - (1.7). Therefore, we first relate the Gell-Mann matrices to the modes of a spin-1 BEC and, second, introduce the notion of coherent spin states (CSS) which significantly simplifies the description of collective spins.

The formalism of second quantization can be used in order to rewrite the total spin angular momentum in terms of the creation \hat{a}^\dagger and annihilation operators \hat{a} . It is convenient to introduce the symmetric (\hat{g}) and anti-symmetric (\hat{h}) creation and annihilation operators $\hat{g}^\dagger = \frac{1}{\sqrt{2}}(\hat{a}_1^\dagger + \hat{a}_{-1}^\dagger)$ and $\hat{h}^\dagger = \frac{1}{\sqrt{2}}(\hat{a}_1^\dagger - \hat{a}_{-1}^\dagger)$ and the corresponding Schwinger-representation using the three non-commuting sets of collective pseudo-spin-1/2 operators $\hat{\mathbf{S}}$, $\hat{\mathbf{A}}$ and $\hat{\mathbf{J}}$, which can be straightforwardly related to the Gell-Mann operators [4, 21]

$$\begin{aligned}\hat{S}_x &= \frac{\hat{a}_0^\dagger \hat{g} + \hat{g}^\dagger \hat{a}_0}{2} = \frac{\hat{G}_1 + \hat{G}_6}{\sqrt{2}}, & \hat{J}_x &= \frac{\hat{a}_1^\dagger \hat{a}_{-1} + \hat{a}_{-1}^\dagger \hat{a}_1}{2} = \hat{G}_4, \\ \hat{S}_y &= \frac{\hat{a}_0^\dagger \hat{g} - \hat{g}^\dagger \hat{a}_0}{2i} = \frac{-\hat{G}_2 + \hat{G}_7}{\sqrt{2}}, & \hat{J}_y &= \frac{\hat{a}_1^\dagger \hat{a}_{-1} - \hat{a}_{-1}^\dagger \hat{a}_1}{2i} = -\hat{G}_5, \\ \hat{S}_z &= \frac{\hat{a}_0^\dagger \hat{a}_0 - \hat{g}^\dagger \hat{g}}{2} = \frac{-3\hat{G}_3 - 2\hat{G}_4 + \sqrt{3}\hat{G}_8}{4}, & \hat{J}_z &= \frac{\hat{a}_1^\dagger \hat{a}_1 - \hat{a}_{-1}^\dagger \hat{a}_{-1}}{2} = \frac{\hat{G}_3 + \sqrt{3}\hat{G}_8}{2}.\end{aligned}\tag{1.11}$$

The operator $\hat{\mathbf{S}}$ describes the two-level system composed by (\hat{a}_0, \hat{g}) . $\hat{\mathbf{A}}$ corresponds to (\hat{a}_0, \hat{h}) and is constructed in an analogous way. Both, $\hat{\mathbf{S}}$ and $\hat{\mathbf{A}}$ describe the annihilation of a particle in the central-mode ($m_F = 0$) and the creation of a particle in the side mode ($m_F = \pm 1$) and vice versa. They are therefore closely related to the process of spin-changing collisions. In contrary, $\hat{\mathbf{J}}$ generates rotations in the $(\hat{a}_1, \hat{a}_{-1})$ subspace. Most notably, \hat{J}_z accounts for the imbalance between the side modes and, thus, the magnetization of the system.

We explicitly note the relation between the operator \hat{S}_x , most relevant throughout discussions in this thesis, and the operator \hat{F}_x , typically found in literature

$$\hat{S}_x = \frac{1}{2\sqrt{2}} \left(\hat{a}_0^\dagger \hat{a}_1 + \hat{a}_0^\dagger \hat{a}_{-1} + \hat{a}_1^\dagger \hat{a}_0 + \hat{a}_{-1}^\dagger \hat{a}_0 \right) = \frac{1}{2} \hat{F}_x.\tag{1.12}$$

The choice of \hat{S}_x instead of \hat{F}_x is rationalized by aiming to compute the quantum Fisher information from an interferometric type of measurement without having to account for additional correction factors when using the corresponding $su(3)$ representation from the outset (see also section 3.2, equation (3.7)).

1.3 Coherent Spin States and Wigner Function

In general, many body spin states of N particles, as considered in this thesis, can become exceedingly complicated. Here, the notion of coherent spin states (CSS) [17] is very useful in order to describe collective spin state and their properties. The simplest useful state for metrology is the non-entangled coherent spin state [35] satisfying

$$\hat{S} |\theta, \varphi\rangle = \hat{S}_x \sin(\theta) \cos(\varphi) + \hat{S}_y \sin(\theta) \sin(\varphi) + \hat{S}_z \cos(\theta) \quad (1.13)$$

We use the Wigner function $W(\theta, \varphi)$ [18] to visualize these quantum states as a function of the angles θ and φ on the Bloch sphere [32, 33]. For a j -spin system it is given by

$$W(\theta, \varphi) = \sum_{k=0}^{2j} \sum_{q=-k}^k \rho_{kq} Y_{kq}(\theta, \varphi), \quad (1.14)$$

where the entries of the density operator ρ_{kq} determine the contribution of the spherical harmonics Y_{kq} . A detailed mathematical description of ρ_{kq} in terms of spherical transformations and Clebsch-Gordan coefficients is given by R. Schmied [36]. The Wigner function constitutes a generalization of classical probability distributions with the central objective to represent quantum states and their properties. In contrast to its classical analogues, it is called a quasi-probability distribution because of its possible negativity.

To make this more clear and gain an intuitive understanding of the consequences of this quasi-probability distribution, we briefly discuss the example of a classical and superimposed state as shown in Figure 1.4. Figure 1.4a illustrates the intrinsic quantum spin noise of a coherent spin state equally distributed between quadratures

$$\langle \Delta \hat{S}_y^2 \rangle = \langle \Delta \hat{S}_z^2 \rangle = \frac{1}{2} |\langle \hat{S}_x \rangle| = \frac{S}{2}. \quad (1.15)$$

We observe that the Wigner function of this spin state shows no negativity [37]. In contrast, the representation of a superimposed state (Figure 1.4b) demonstrates that the negativity of the Wigner distribution can be associated with interference of quantum states. Fringes along the equator exhibit negative regions in the Wigner representation. The emerging interference pattern already hints that rotations along the \hat{S}_x -axis become more distinguishable when compared to the non-superimposed coherent state (Figure 1.4a). This so-called phase sensitivity is an interesting aspect of metrological enhancement using spin-states, becoming quite important in the course of this work.

1.4 Spontaneous Symmetry Breaking

Another highly useful concept in the context of many-body spin systems is spontaneous symmetry breaking (SBB), describing the emergence of a non-unique equilibrium state of a quantum

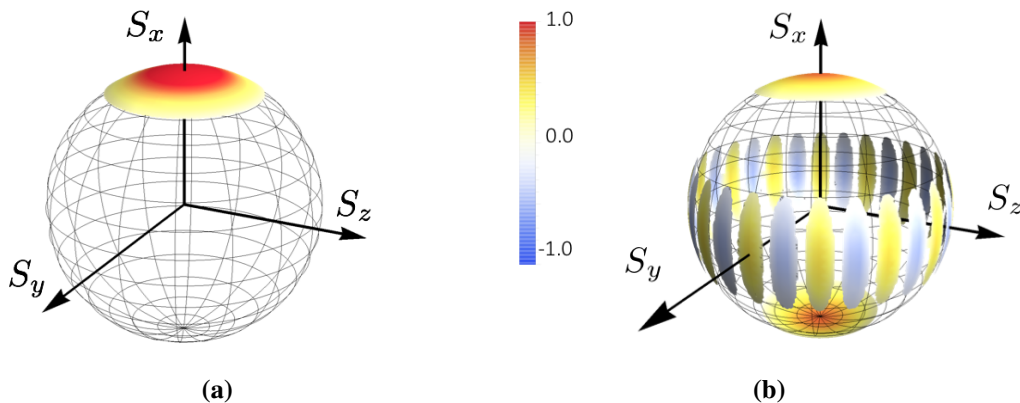


Figure 1.4.: Wigner function of a coherent spin state (left) and a superimposed on the Bloch sphere ($N = 14$). The negativity of the quasi-probability distributions accounts for the quantum mechanical character, especially interference. We observe, that the coherent spin state along the \hat{S}_x axis shows no negativity, whereas the Wigner function of the superimposed states attains positive as well as negative values. To be precise, the superimposed state considered here is a NOON state along the \hat{S}_x axis, discussed in greater detail in section 5.2.

system in the thermodynamic limit [38]. The general idea states that as the size of a quantum system grows, superpositions of the system as a whole become unstable against small perturbations. In the limit of large particle numbers and low temperatures, even infinitesimal small perturbations such as thermal or quantum fluctuation suffice to force the system into a state which does not conform to the symmetry of the Hamiltonian anymore. As outlined in greater detail below, SBB can then be explained from two non-commuting limits: In a macroscopic system without perturbations the underlying symmetry of the Hamiltonian should not be broken. However, if the system grows in the presence of an infinitesimal perturbation, it will be able to evolve into a symmetry broken state [39].

One way to formalize a mathematical description [40] of this process is by using the effective action² $\Gamma[\phi]$, which generalizes the concept of classical action to quantum states

$$e^{-\Gamma[\phi]} = \int \mathcal{D}\varphi e^{-S[\varphi] + \int_X j[\phi] \cdot (\varphi - \phi)}. \quad (1.16)$$

It comprises the microscopic action $S[\varphi]$ and the source term $j[\phi]$ by means of all possible field configurations φ with expectation value ϕ , i.e. $\phi = \langle \varphi \rangle$. A non-vanishing source ($j[\phi] \neq 0$) typically leads to explicit symmetry breaking by terms in the effective action which are non-invariant under symmetry transformations. Setting the external source to zero ($j[\phi] = 0$), we see that any symmetry of the microscopic action will be shared by the effective action. Nevertheless, the ground state of the theory may have a non-zero expectation value according to

²Technically speaking, the effective action is the generating functional of one-particle irreducible (1PI) correlation functions [40, 41].

$\phi_0 := \langle \varphi \rangle_{j \rightarrow 0} \neq 0$. Spontaneous symmetry breaking refers to the case, where this expectation value transforms non-trivially under rotations.

We elucidate this on the most prominent example of this phenomenon, namely ferromagnetism [42]. At high temperatures the electron spins inside a ferromagnet are uncorrelated. By lowering the temperature, the spins get aligned which gives rise to a phase transition characterized by a finite magnetization in a particular direction. This effect appears, for instance, within the framework of the transverse field Ising model with ferromagnetic interactions ($J_{ij} > 0$)

$$\hat{\mathcal{H}} = - \sum_{\langle i,j \rangle} J_{ij} \hat{s}_i \hat{s}_j + \sum_i h_i \hat{s}_i, \quad (1.17)$$

where \hat{s}_i is a binary Ising variable on site i of a lattice. The first term represents short ranged interactions making it energetically favorable for spins to align parallel with one another. The magnetic field h_i in the second term can be regarded as a source of magnetization at site i . The amount of magnetic order is given by the magnetization $M(h, N, T) = \langle \sum_i^N \hat{s}_i \rangle$, which is also the order parameter of the phase transition from an ordered to a disordered state.

The classical Ising model has two ground states for ferromagnetic interactions: One with all spins pointing *up*, the other with all spins pointing *down*. The quantum Ising model, however, has a single ground state $|\hat{\Psi}\rangle = \frac{1}{\sqrt{2}}(|\uparrow\rangle - |\downarrow\rangle)$, which is a *superposition of up and down*. Setting the external field parameter h_i to zero, the Hamiltonian becomes invariant under a spin flip: $\hat{s}_i \rightarrow -\hat{s}_i$. Each configuration with a certain number of spins has a corresponding configuration with all spins reversed and they should cancel when summing over all configurations. So, we expect $\langle \sum_i^N \hat{s}_i \rangle = 0$. This reasoning, however, can only be applied to finite systems. If we first enlarge the system to infinite volume and then remove the field, we have

$$\lim_{h \rightarrow 0} \lim_{N \rightarrow \infty} M(h, N, T) \begin{cases} \neq 0 & \text{symmetry broken state} \\ 0 & \text{symmetry un-broken state.} \end{cases} \quad (1.18)$$

Interchanging these limits always yields vanishing magnetization.

Another argument can be found in the structure of the eigenstates. The first excited state of the quantum Ising model corresponds to the triplet $|\hat{\Psi}\rangle = \frac{1}{\sqrt{2}}(|\uparrow\rangle + |\downarrow\rangle)$. As $N \rightarrow \infty$, it can be shown that the energy gap between the ground state and first excited states decays like $\exp(-N)$. Any quantum or thermal fluctuation will therefore lead to a collapse of the state into a configuration where all spins are either pointing *up* or *down*. That is why the quantum Ising model shows phases of non-vanishing spontaneous magnetization in the infinite volume limit, most prominently in the exact solution of the two-dimensional Ising model by L. Onsager ([43]). T. Koma and H. Tasaki (1994) [44] prove analogous results for a broader class of lattice models which

display degenerate ground states in the thermodynamic limit.

In the course of this thesis, SBB becomes particularly relevant to the discussion of highly entangled many-particle states. The latter often correspond to inherently fragile superposition states which might experience SBB. For this reason, a clear distinction between symmetry broken and symmetry unbroken states is necessary in order to properly estimate the amount of entanglement in spin-1 BECs as we will see in chapter 5.

2 Bogoliubov Theory

A full quantum mechanical treatment of spinor Bose gases in extended systems is exponentially difficult. Here, Bogoliubov theory is a versatile tool that enables one to describe the characteristic low-energy excitations of quantum many-body systems. It is usually employed to diagonalize the quadratic form of a Hamiltonian by means of so-called Bogoliubov transformations of the state. The obtained quasi-particle modes can be employed to calculate operator eigenvalues, which are directly connected to observables of the initial basis states. Furthermore, assessing the energy spectrum allows for the description of finite-temperature effects as presented in this chapter. In order to evaluate correlation functions using Bogoliubov theory, we additionally discuss the use of Wick's theorem for Gaussian states.

2.1 Diagonalization of Quadratic Bosonic Hamiltonians

First, we focus on the most general case of a Bogoliubov transformation for quadratic, bosonic Hamiltonians as, for instance, outlined by J. van Hemmen [45]. Consider a system described by a quadratic Hamiltonian of the form

$$\mathcal{H} = \begin{pmatrix} \hat{\alpha}^\dagger & \hat{\alpha} \end{pmatrix} \begin{pmatrix} \mathcal{A} & \mathcal{B} \\ \mathcal{C} & \mathcal{D} \end{pmatrix} \begin{pmatrix} \hat{\alpha} \\ \hat{\alpha}^\dagger \end{pmatrix} = \hat{\mathbf{a}}^\dagger \mathcal{M} \hat{\mathbf{a}}. \quad (2.1)$$

Here, \mathcal{M} is a quadratic $2N \times 2N$ matrix and, correspondingly, $\mathcal{A}, \mathcal{B}, \mathcal{C}, \mathcal{D}$ are $N \times N$ matrices¹. The entries of the operator $\hat{\mathbf{a}}^\dagger = (\hat{\alpha}^\dagger, \hat{\alpha})$ refer to bosonic annihilation and creation operators

$$\hat{\mathbf{a}} = \begin{pmatrix} \hat{\alpha} \\ \hat{\alpha}^\dagger \end{pmatrix} = \begin{pmatrix} \hat{\alpha}_1 \\ \vdots \\ \hat{\alpha}_N \\ \hat{\alpha}_1^\dagger \\ \vdots \\ \hat{\alpha}_N^\dagger \end{pmatrix}, \quad \hat{\mathbf{a}}^\dagger = (\hat{\alpha}^\dagger \quad \hat{\alpha}) = (\hat{\alpha}_1^\dagger \quad \dots \quad \hat{\alpha}_N^\dagger \quad \hat{\alpha}_1 \quad \dots \quad \hat{\alpha}_N), \quad (2.2)$$

satisfying bosonic commutation relations

$$[\hat{\alpha}_i, \hat{\alpha}_j^\dagger] = \hat{\alpha}_i \hat{\alpha}_j^\dagger - \hat{\alpha}_j^\dagger \hat{\alpha}_i = \delta_{ij}, \quad [\hat{\alpha}_i, \hat{\alpha}_j] = [\hat{\alpha}_i^\dagger, \hat{\alpha}_j^\dagger] = 0. \quad (2.3)$$

¹We use the following notation in this thesis: \mathcal{A}^\dagger denotes the hermitian conjugate, $\bar{\mathcal{A}}$ the complex conjugate and \mathcal{A}^T the transpose of the matrix \mathcal{A}

This leads to the commutation relation for the compound operator $\hat{\mathbf{a}}$

$$[\hat{\mathbf{a}}_\mu, \hat{\mathbf{a}}_\nu^\dagger] = \mathcal{I}_{\mu\nu} \quad \text{with} \quad \mathcal{I} = \begin{pmatrix} \mathbb{1} & 0 \\ 0 & -\mathbb{1} \end{pmatrix}. \quad (2.4)$$

\mathcal{H} being hermitian implies together with the commutation relations (2.4) that the matrix \mathcal{M} takes the form

$$\mathcal{M} = \begin{pmatrix} \mathcal{A} & \mathcal{B} \\ \overline{\mathcal{B}} & \overline{\mathcal{A}} \end{pmatrix}. \quad (2.5)$$

The problem of diagonalizing the Hamiltonian \mathcal{H} amounts to finding a new basis $\mathbf{b}, \mathbf{b}^\dagger$ with a linear transformation \mathcal{T} such that the Hamiltonian can be expressed by a diagonal $2N \times 2N$ matrix \mathcal{D} as follows

$$\mathcal{H} = \mathbf{b}^\dagger \underbrace{\mathcal{T}^\dagger \mathcal{M} \mathcal{T}}_{\mathcal{D}} \mathbf{b} = \mathbf{b}^\dagger \mathcal{D} \mathbf{b}. \quad (2.6)$$

The transformed basis states $\hat{\mathbf{b}}$ and $\hat{\mathbf{b}}^\dagger$, in which the problem (2.6) becomes diagonal, describe the energetically low-lying excitations of the system. They are called quasi-particle modes and resemble the structure of the initial modes $\hat{\mathbf{a}}$ and $\hat{\mathbf{a}}^\dagger$

$$\hat{\mathbf{b}} = \begin{pmatrix} \hat{\beta} \\ \hat{\beta}^\dagger \end{pmatrix} = \begin{pmatrix} \hat{\beta}_1 \\ \vdots \\ \hat{\beta}_N \\ \hat{\beta}_1^\dagger \\ \vdots \\ \hat{\beta}_N^\dagger \end{pmatrix}. \quad (2.7)$$

The canonical transformation \mathcal{T} comprises the $N \times N$ matrices \mathcal{U} and \mathcal{V}

$$\mathcal{T} = \begin{pmatrix} \mathcal{U} & \overline{\mathcal{V}} \\ \mathcal{V} & \overline{\mathcal{U}} \end{pmatrix} \quad (2.8)$$

and relates the quasi-particle modes to the initial modes via $\hat{\mathbf{a}} = \mathcal{T} \hat{\mathbf{b}}$. Because of the underlying commutation relations, the diagonalization of bosonic Hamiltonians further requires that \mathcal{T} is a pseudo-unitary transformation in the sense that $\mathcal{I} = \mathcal{T} \mathcal{I} \mathcal{T}^\dagger = \mathcal{T}^\dagger \mathcal{I} \mathcal{T}$ with \mathcal{I} from (2.4). By inverting this expression one finds that there exists an inverse transformation

$$\mathcal{T}^{-1} = \begin{pmatrix} \mathcal{U}^\dagger & -\mathcal{V}^\dagger \\ -\overline{\mathcal{V}}^\dagger & \overline{\mathcal{U}}^\dagger \end{pmatrix}, \quad (2.9)$$

such that the components of the quasi-particle state $\hat{\mathbf{b}}$ become a linear combination of the initial ones by $\hat{\mathbf{b}} = \mathcal{T}^{-1} \hat{\mathbf{a}}$. Because of their structure

$$\hat{\beta} = \mathcal{U}^\dagger \hat{\alpha} - \mathcal{V}^\dagger \hat{\alpha}^\dagger, \quad \hat{\beta}^\dagger = \bar{\mathcal{U}}^\dagger \hat{\alpha}^\dagger - \bar{\mathcal{V}}^\dagger \hat{\alpha}, \quad (2.10)$$

the quasi-particle excitations are often referred to as a particle- and hole-like excitation. Moreover, they fulfill bosonic commutation relations

$$[\hat{\beta}_i, \hat{\beta}_j^\dagger] = \delta_{ij} \quad \text{and} \quad [\hat{\beta}_i, \hat{\beta}_j] = [\hat{\beta}_i^\dagger, \hat{\beta}_j^\dagger] = 0. \quad (2.11)$$

Finding the correct transformation \mathcal{T} of the state, such that the Hamiltonian becomes diagonal in the quasi-particle modes, amounts for solving the eigenvalue equations [45]

$$\mathcal{I} \mathcal{M} \mathbf{x} = \omega \mathbf{x}. \quad (2.12)$$

The Bogoliubov transformation \mathcal{T} can then be constructed from the eigenvectors \mathbf{x} according to $\mathcal{T} = \{\mathbf{x}_1, \dots, \mathbf{x}_n, \mathcal{J} \mathbf{x}_1, \dots, \mathcal{J} \mathbf{x}_n\}$, where the operator \mathcal{J} is defined as $\mathcal{J} \begin{pmatrix} \mathbf{a} \\ \mathbf{b} \end{pmatrix} = \begin{pmatrix} \bar{\mathbf{b}} \\ \mathbf{a} \end{pmatrix}$. As a consequence, the spectrum of the Bogoliubov Hamiltonian is given by $\mathcal{D} = \text{diag}(\omega_1, \dots, \omega_n, \omega_1, \dots, \omega_n)$ such that the final, diagonalized form of the Hamiltonian becomes

$$\mathcal{H} = \hat{\mathbf{b}}^\dagger \mathcal{D} \hat{\mathbf{b}} = \sum_{i=1}^N \hbar \omega_i \left\{ \hat{\beta}_i^\dagger \hat{\beta}_i + \hat{\beta}_i \hat{\beta}_i^\dagger \right\} \cong \sum_{i=1}^N 2 \hbar \omega_i \hat{\beta}_i^\dagger \hat{\beta}_i \quad (2.13)$$

up to an additive constant.

To conclude, a diagonal Bogoliubov Hamiltonian can be obtained by a corresponding transformation of the state. Physically this implies that the problem becomes diagonal in the basis of quasi-particle modes, describing the characteristic and energetically low-lying excitations of the system. Therefore, computing observables of the transformed state becomes significantly easier [46].

2.2 Examples

Before discussing the calculation of observables from Bogoliubov theory in greater detail, we consolidate our understanding by two simple examples.

2.2.1 Bosonic, Interacting Hamiltonian

As a first, pedagogical example, we discuss the simplest case of a single bosonic mode Hamiltonian with interactions²

$$(E_{kin} - \mu) \hat{a}^\dagger \hat{a} + E_{int} \hat{a}^\dagger \hat{a}^\dagger \hat{a} \hat{a}, \quad (2.14)$$

²The Hamiltonian (2.14) can be also seen as the equivalent to an anharmonic oscillator.

where \hat{a} and \hat{a}^\dagger are bosonic annihilation and creation operators. All relevant parameters are assumed to be real-valued for simplicity. The model is parameterized by the kinetic energy E_{kin} associated with the total number of atoms and the interaction energy E_{int} associated with pairing and collision processes. The chemical potential μ fixes the particle number. In the following mean-field approximation (see also subsection 5.3.1), we treat the operators as uncorrelated in the sense that $\langle \hat{a}^\diamond \hat{a}^\circ \rangle = \langle \hat{a}^\diamond \rangle \langle \hat{a}^\circ \rangle$, where \diamond and \circ denote whether the hermitian conjugate is applied to the operator \hat{a} . The semi-classical expansion

$$\hat{a} \cong \langle \hat{a} \rangle + \hat{\alpha} = \zeta + \hat{\alpha} \quad (2.15)$$

decomposes the fields into its real-valued expectation value³ $\langle \hat{a} \rangle = \zeta$ and fluctuations $\hat{\alpha}$. It follows from direct computation that the fluctuations fulfill bosonic commutation relations as well. The mean-field decomposition brings the Hamiltonian (2.14) into quadratic form when considering only terms up to second order in fluctuations

$$\begin{aligned} H \cong & (E_{kin} - \mu) \zeta^2 + E_{int} \zeta^4 \\ & + [(E_{kin} - \mu) \zeta + E_{int} \zeta^3] (\hat{\alpha}^\dagger + \hat{\alpha}) \\ & + (E_{kin} - \mu) \hat{\alpha}^\dagger \hat{\alpha} + E_{int} \zeta^2 (\hat{\alpha}^\dagger \hat{\alpha}^\dagger + \hat{\alpha} \hat{\alpha}^\dagger + \hat{\alpha}^\dagger \hat{\alpha} + \hat{\alpha} \hat{\alpha}) + \mathcal{O}(\hat{\alpha}^3). \end{aligned} \quad (2.16)$$

The constant term $E_0 = E_{kin} - \mu \zeta^2 + E_{int} \zeta^4$ gives the ground state energy. Minimizing E_0 with respect to the parameter ζ implies $\zeta^2 = \frac{(\mu - E_{kin})}{2E_{int}} = N_0$. This equation gives the relation between the chemical potential μ and the total number of particles N_0 . Inherent to the expansion around the mean-field solution ζ , minimizing the ground state energy, the linear term in (2.16) vanishes. Hence, the Hamiltonian (2.16) attains a quadratic form

$$\mathcal{H} = E_0 + \underbrace{\begin{pmatrix} \hat{\alpha}^\dagger & \hat{\alpha} \end{pmatrix} \begin{pmatrix} \frac{E_{kin} - \mu}{2} + E_{int} \zeta^2 & E_{int} \zeta^2 \\ E_{int} \zeta^2 & \frac{E_{kin} - \mu}{2} + E_{int} \zeta^2 \end{pmatrix} \begin{pmatrix} \hat{\alpha} \\ \hat{\alpha}^\dagger \end{pmatrix}}_{\mathcal{M}} \quad (2.17)$$

It is characterized by the matrix $\mathcal{M} = \begin{pmatrix} A & B \\ B & A \end{pmatrix}$ with entries $A = \frac{E_{kin} - \mu}{2} + E_{int} \zeta^2$ and $B = E_{int} \zeta^2$. In order to apply Bogoliubov theory for bosonic systems as described above, we compute the eigenvalue equation

$$\mathcal{I} \mathcal{M} \mathbf{x} = \omega \mathbf{x} \quad \text{with} \quad \mathcal{I} \mathcal{M} = \begin{pmatrix} A & B \\ -B & -A \end{pmatrix}. \quad (2.18)$$

This gives the eigenenergies $\omega = \pm \sqrt{A^2 - B^2}$. The positive-definiteness of the Hamiltonian is required in order to assure stable dynamics [46] in bosonic systems, i.e. $\omega > 0$. The diagonalization problem $\mathcal{D} = \mathcal{T} \mathcal{M} \mathcal{T}$ and the bosonic commutation relations $\mathcal{I} = \mathcal{T} \mathcal{I} \mathcal{T}^\dagger$ imply the

³In general, if $\zeta \in \mathbb{C}$, the phase may play an important role, see also subsection 5.3.1.

following constraint

$$\begin{pmatrix} \omega & 0 \\ 0 & \omega \end{pmatrix} = \begin{pmatrix} U & V \\ V & U \end{pmatrix} \begin{pmatrix} A & B \\ B & A \end{pmatrix} \begin{pmatrix} U & V \\ V & U \end{pmatrix}. \quad (2.19)$$

Solving this set of equations yields the entries of the transformation matrix $\mathcal{T} = \begin{pmatrix} U & V \\ V & U \end{pmatrix}$

$$V = -\sqrt{\frac{1}{2} \left(\pm \frac{B}{\omega} - 1 \right)} \quad \text{and} \quad U = \sqrt{\frac{1}{2} \left(\pm \frac{B}{\omega} + 1 \right)}. \quad (2.20)$$

Accordingly, the quasi-particle modes $\hat{\beta}$ and $\hat{\beta}^\dagger$ read:

$$\begin{aligned} \hat{\beta} &= \sqrt{\frac{1}{2} \left(\pm \frac{B}{\omega} + 1 \right)} \hat{\alpha} + \sqrt{\frac{1}{2} \left(\pm \frac{B}{\omega} - 1 \right)} \hat{\alpha}^\dagger, \\ \hat{\beta}^\dagger &= \sqrt{\frac{1}{2} \left(\pm \frac{B}{\omega} + 1 \right)} \hat{\alpha}^\dagger + \sqrt{\frac{1}{2} \left(\pm \frac{B}{\omega} - 1 \right)} \hat{\alpha}. \end{aligned} \quad (2.21)$$

As one can see, equation (2.21) shows that the quasi-particle modes can be expressed as a linear combination of the initial modes. In the limit of $\frac{B}{\omega} \rightarrow 1$ the particle- and hole-like excitations resemble the annihilation and creation operators, $\hat{\alpha}$ and $\hat{\alpha}^\dagger$, respectively.

2.2.2 SMA Hamiltonian of Spin-1 BEC in Polar Phase

As a second example, we discuss the single-mode approximation (SMA) Hamiltonian (see also chapter 5) of the spin-1 Bose-Einstein condensate in the Polar phase

$$H \simeq [\lambda (N - \frac{1}{2}) + q] (\hat{a}_1^\dagger \hat{a}_1 + \hat{a}_{-1}^\dagger \hat{a}_{-1}) + \lambda N (\hat{a}_1^\dagger \hat{a}_{-1}^\dagger + \hat{a}_1 \hat{a}_{-1}). \quad (2.22)$$

In order to arrive at this Hamiltonian, we apply similar approximations as those guiding us from (2.14) to (2.17). Here, q denotes the magnetic field parameter, N the particle number and λ the interaction constant. Up to an additive constant and defining $c(q, N) = \lambda (N - \frac{1}{2}) + q$, $A_\pm = \frac{c(q, N) \pm E_{\lambda q}}{2}$ and $B = \frac{\lambda N}{2}$, the Hamiltonian can be rewritten in matrix form

$$H \simeq \begin{pmatrix} \hat{a}_1^\dagger & \hat{a}_{-1} & \hat{a}_{-1}^\dagger & \hat{a}_1 \end{pmatrix} \begin{pmatrix} A_+ & B & 0 & 0 \\ B & A_- & 0 & 0 \\ 0 & 0 & A_+ & B \\ 0 & 0 & B & A_- \end{pmatrix} \begin{pmatrix} \hat{a}_1 \\ \hat{a}_{-1}^\dagger \\ \hat{a}_{-1} \\ \hat{a}_1^\dagger \end{pmatrix}. \quad (2.23)$$

The upper left and lower right sub-matrix $\begin{pmatrix} A_+ & B \\ B & A_- \end{pmatrix}$ can be diagonalized in analogy to the above example. We find the following expressions

$$U = \sqrt{\frac{c(q, N) + E_{\lambda q}}{2E_{\lambda q}}}, \quad V = -\sqrt{\frac{c(q, N) - E_{\lambda q}}{2E_{\lambda q}}}, \quad (2.24)$$

where $E_{\lambda q} = \sqrt{(\frac{\lambda}{2} - q)(\frac{\lambda}{2} - q - 2\lambda N)}$ is the ground state energy. The new quasi-particle operators read

$$\hat{\beta}_1 = U\hat{a}_1 + V\hat{a}_{-1}^\dagger, \quad \hat{\beta}_{-1} = U\hat{a}_{-1} + V\hat{a}_1^\dagger \quad (2.25)$$

and the Hamiltonian becomes

$$H = \begin{pmatrix} \hat{\beta}_1^\dagger & \hat{\beta}_{-1} & \hat{\beta}_{-1}^\dagger & \hat{\beta}_1 \end{pmatrix} \begin{pmatrix} E_{\lambda q} & 0 & 0 & 0 \\ 0 & 0 & 0 & 0 \\ 0 & 0 & E_{\lambda q} & 0 \\ 0 & 0 & 0 & 0 \end{pmatrix} \begin{pmatrix} \hat{\beta}_1 \\ \hat{\beta}_{-1}^\dagger \\ \hat{\beta}_{-1} \\ \hat{\beta}_1^\dagger \end{pmatrix} = E_{\lambda q} (\hat{\beta}_1^\dagger \hat{\beta}_1 + \hat{\beta}_{-1}^\dagger \hat{\beta}_{-1}). \quad (2.26)$$

Equation (2.26) demonstrates once again that the Hamiltonian becomes diagonal after the correct transformation of the state. Thus, the main conclusion that can be drawn from the introduction on Bogoliubov theory and the two examples is that Bogoliubov transformations considerably simplify calculations within a quadratic theory. Often -and also in the course of this thesis-, further approximations are needed in order to arrive at a quadratic Hamiltonian in the first place. On this level, the Bogoliubov descriptions is equivalent to the initial basis, though the physical sense is readily visible and explainable in the quasi-particle picture. We will exploit this in order to calculate the quantum Fisher information of a spin-1 BEC, first, in single mode approximation (chapter 5) and second, in the extended system (chapter 6).

2.3 Wick's Theorem for Gaussian Fields

In order to fully reap the potential of Bogoliubov theory, we examine the consequence of Wick's theorem [47] to the computation of observables. The most general formulation of this theorem can be found in Appendix A.1. Within a quadratic theory, Wick's theorem is a particularly helpful tool to deal with real-valued operators having a joint Gaussian distribution with zero means, such as the (vacuum) expectation value of particle annihilation and creation operators. We denote the Gaussian bosonic operators by \hat{a} and find that Wick's theorem gives an identity for the N -point correlation function with N being an even number

$$\langle \hat{a}_1 \hat{a}_2 \dots \hat{a}_N \rangle = \langle \hat{a}_{i_1} \hat{a}_{i_2} \rangle \dots \langle \hat{a}_{i_{N-1}} \hat{a}_{i_N} \rangle, \quad (2.27)$$

Hence, the expectation value of the product of an even number N of creation and annihilation operators can be expressed as a sum of contracted normally ordered⁴ terms. The N - point correlation function can thus be calculated from first order correlation function⁵. In particular, the second order correlation function for bosonic operators becomes

$$\langle \hat{a}_1 \hat{a}_2 \hat{a}_3 \hat{a}_4 \rangle = \langle \hat{a}_1 \hat{a}_2 \rangle \langle \hat{a}_3 \hat{a}_4 \rangle + \langle \hat{a}_1 \hat{a}_3 \rangle \langle \hat{a}_2 \hat{a}_4 \rangle + \langle \hat{a}_1 \hat{a}_4 \rangle \langle \hat{a}_2 \hat{a}_3 \rangle. \quad (2.28)$$

This is a practical rule for calculating the variance $(\Delta \hat{O})^2 = \langle \hat{O}^2 \rangle - \langle \hat{O} \rangle^2$ of a bosonic operator of the form $\hat{O} = \sum_{i,j} \hat{a}_i \hat{a}_j$ which will be used later to calculate the quantum Fisher information for spin-1 BECs.

⁴For the definition of normal ordering see Appendix A.1.

⁵In this thesis, the term *first order correlation function* refers to the two-point correlator $g^1(x_1, x_2) = \langle \hat{O}(x_1) \hat{O}(x_2) \rangle$ and, correspondingly, *second order correlation function* refers to the four-point correlator $g^2(x_1, x_2, x_3, x_4) = \langle \hat{O}(x_1) \hat{O}(x_2) \hat{O}(x_3) \hat{O}(x_4) \rangle$.

3 Quantum Fisher Information

The classical Fisher information is a fundamental quantity in estimation theory [48, 9]. Correspondingly, its quantum analogue, the quantum Fisher information (QFI), is a central quantity in quantum metrology [8, 11, 1]. The QFI is closely related to well-established experimental protocols such as quantum interferometry [10] and dynamical susceptibilities measures [12] of quantum many-body systems. The QFI is also capable of classifying multipartite entanglement, both at zero and finite temperature. Furthermore, it allows to identify strongly entangled phase transitions through its universal scaling behavior [12, 49] when approaching the critical point. Before outlining mathematical formulations of the quantum Fisher information, we introduce the notion of multipartite entanglement.

3.1 Multipartite Entanglement

The classification of multipartite entanglement is closely related to the definition of k -producible states [50, 11]: A pure state $|\Psi\rangle$ of a quantum system with N particles is called k -producible if we can write

$$|\Psi\rangle = |\Psi_1\rangle \otimes |\Psi_2\rangle \otimes \cdots \otimes |\Psi_k\rangle, \quad (3.1)$$

where the $|\Psi_i\rangle$ are states of maximally k particles. The state contains genuine k -particle entanglement if it is k -producible but not $(k-1)$ -producible. Therefore, a k -partite entangled state can be written as a product state

$$|\Psi_{k-ent}\rangle = \otimes_{l=1}^M |\Psi_l\rangle \quad (3.2)$$

with the normalization condition $\sum_{l=1}^M N_l = N$. Here, at least one state $|\Psi_l\rangle$ of $N_l = k$ particles does not factorize and is therefore k -partite entangled. k -producibility can be readily extended to mixed states $\rho = \sum_i p_i |\Psi_i\rangle \langle \Psi_i|$. Such a state is called k -producible if it can be written as a mixture of $(k_l \leq k)$ -producible pure states [11], that is,

$$\rho_{k-prod} = \sum_l p_l |\Psi_{k-prod}\rangle \langle \Psi_{k-prod}|. \quad (3.3)$$

3.2 Classical and Quantum Phase Estimation

Precision measurements are often based on the detection of a weak signal which distinguishes different states of the system [8]. The most general example is the estimation of a phase shift ϑ using classical interferometry. The task of finding the best possible estimation of ϑ can be formalized as a classical optimization of the estimator ϑ from measurements x , distributed ac-

according to some probability density function $f(x; \vartheta)$. The ultimate precision achievable in a single measurement is then given by the Cramér-Rao lower bound [48]

$$(\Delta \vartheta)^2 \geq \frac{1}{F}, \quad (3.4)$$

which states that the inverse of the classical Fisher information F is a lower bound on the variance of any unbiased estimator of ϑ , with

$$F = - \left\langle \frac{\partial^2 \log(f(x; \vartheta))}{\partial \vartheta^2} \right\rangle. \quad (3.5)$$

An unbiased estimator is given when the mean value coincides with the true value of the phase shift, i.e. $\langle \vartheta \rangle = \tilde{\vartheta}$. Usually, the Cramér-Rao lower bound is sufficiently reached in the approximation of a large number of measurements when ϑ approaches $\tilde{\vartheta}$. Intuitively, we can understand (3.4) from the fact that the true parameter $\tilde{\vartheta}$ maximizes the value of the log-likelihood function

$$\frac{\partial \log(f(x; \tilde{\vartheta}))}{\partial \vartheta} = 0. \quad (3.6)$$

Since the classical Fisher information (3.5) is defined as the second derivative of the log-likelihood function, it is a measure for how variable the maximum likelihood estimation is, given the parameter ϑ .

The notion of parameter estimation can be generalized to quantum states. The transformation of a probe state

$$\rho' = e^{-i\vartheta \hat{O}} \rho e^{i\vartheta \hat{O}} \quad (3.7)$$

is characterized by the hermitian operator \hat{O} with difference 1 between the maximal and minimal eigenvalues of \hat{O} . In a typical atom interferometry experiment, the unknown phase imprint ϑ is determined from measuring ρ' . The quantum Cramér-Rao bound then gives the limit to the precision with which the phase shift ϑ can be estimated as a function of the quantum Fisher information F_Q and number of measurements M

$$(\Delta \vartheta)^2 \geq (MF_Q)^{-1}. \quad (3.8)$$

For pure states $\rho = |\Psi\rangle \langle \Psi|$, the QFI takes the simple form

$$F_Q = 4 \left(\langle \Psi | \hat{O}^2 | \Psi \rangle - \langle \Psi | \hat{O} | \Psi \rangle^2 \right). \quad (3.9)$$

For mixed states, such as a thermal ensemble $\rho = \sum_{\lambda} p_{\lambda} |\lambda\rangle \langle \lambda|$ with energy eigenbasis $|\lambda\rangle$ and occupation probabilities $p_{\lambda} = \exp(-\beta E_{\lambda}) / Z$, the QFI can be obtained from

$$F_Q = 2 \sum_{\lambda, \lambda'} \frac{(p_{\lambda} - p_{\lambda'})^2}{p_{\lambda} + p_{\lambda'}} \langle \lambda | \hat{O} | \lambda' \rangle^2, \quad (3.10)$$

where only terms with $p_{\lambda} + p_{\lambda'} > 0$ are taken into account. This formulation is considerably more complicated and, in general, requires full tomography of the state.

In quantum metrology problems with linear interferometers, which is the most relevant type of metrology considering large particle ensembles, the operator \hat{O} is a linear observable generating the interferometric transformation $\mathbf{u} \hat{\mathbf{G}}$. The interferometric direction is defined by \mathbf{u} and the collective transformation $\hat{\mathbf{G}} = \sum_i^N \hat{\mathbf{g}}^{(i)}$ is constituted from the generators $\mathbf{g}^{(i)}$ of the underlying $su(N)$ -algebra of the N -particle system.

Considering the case of a spin-1/2 systems, the operator \hat{O} can be described by a collective angular momentum component defined as

$$\hat{O} = \sum_l \hat{\mathbf{n}}_l \hat{\sigma}_l, \quad (3.11)$$

where $\hat{\sigma}_l = (\hat{\sigma}_l^x, \hat{\sigma}_l^y, \hat{\sigma}_l^z)$ are the Pauli matrices for spin l . $\hat{\mathbf{n}}_l$ correspondingly describes a unit vector on the Bloch sphere. For separable N -particle states in a linear interferometer it was shown that the quantum Fisher information is bounded by [10]

$$F_Q \leq N. \quad (3.12)$$

Any state violating this bound (3.12) with

$$\frac{F_Q}{N} > m \quad (3.13)$$

surpasses classical limits and witnesses $m + 1$ - partite entanglement. For general spin-1/2 states the upper bound is

$$F_Q \leq N^2 \quad (3.14)$$

which is called the Heisenberg-limit. The entanglement criterion (3.12) can be extended to degrees of freedom other than spin-1/2, as long as \hat{O} represents a sum of local operators with a bounded spectrum. If λ_{max} and λ_{min} are the largest and smallest eigenvalues, respectively, of the operator \hat{O} , then the right-hand side of equation (3.13) acquires the prefactor $(\lambda_{max} - \lambda_{min})^2$. Viewing the quantum Fisher information again in the context of a phase estimation problem, the

optimal phase uncertainty attainable with a m -partite entangled state is

$$\Delta\vartheta = \frac{1}{\sqrt{mN}}. \quad (3.15)$$

The uncertainty $\Delta\vartheta = 1/\sqrt{N}$ is called standard quantum limit (SQL) and gives the most precise estimation when measuring N uncorrelated particles. Thus, equation (3.15) has the physical implication that increasing the number of entangled particles yields a better estimation of the phase shift ϑ . So again, F_Q quantifies how sensitive the state is against the phase shift ϑ .

This is very similar to our intuitive understanding of the difference in phase sensitivity from the quasi-probability distributions (Figure 1.4) of a coherent and a superimposed state. Rotations $e^{i\vartheta\hat{S}_y}$ of the coherent spin state (1.13) aligned along the z -axis and characterized by $|\theta = \frac{\pi}{2}, \varphi = 0\rangle$, can be detected with best possible phase resolution

$$\Delta\vartheta = \left. \frac{\Delta\hat{S}_z}{\frac{\partial}{\partial\vartheta}\langle\hat{S}_z\rangle} \right|_{\vartheta=0} = \frac{\sqrt{S/2}}{S} = \frac{1}{\sqrt{N}}, \quad (3.16)$$

corresponding to the SQL. $\langle\hat{S}_z\rangle$ and $\Delta\hat{S}_z = \sqrt{\frac{S}{2}}$ from equation (1.15) represent the mean and standard deviation. This bound can be surpassed with the help of correlations and entanglement of the collective spin state, such as depicted in Figure 1.4b.

To conclude, under the action of the unitary transformation (3.7) with suitable operator \hat{O} , entangled states become more distinguishable (i.e. evolve more rapidly) than separable states. Hence, quantum correlations in the system can be exploited in order to enhance the sensitivity of a linear interferometer.

Part II.

Studying Multipartite Entanglement in Spin-1 BECs

4 Extracting Quantum Fisher Information from Quench Dynamics

Now that the fundamentals of spinor Bose gases, Bogoliubov theory, and quantum Fisher information (QFI) have been introduced, we combine these concepts in order to study the multipartite entanglement content of a spin-1 Bose-Einstein condensate, which is the major objective of this thesis. Part of this strategy is to present an overarching framework of extracting the QFI from quench dynamics using mean-field Bogoliubov theory, discussed in this chapter. Based on this method, we study multipartite entanglement in spin-1 BECs, first, in single-mode approximation (chapter 5) and, second, in an extended system (chapter 6).

Previous research revealed the possibility to create metrologically useful states with spinor Bose gases, thereby going beyond classical limits [4, 2, 24]. So far, however, only lower bounds to the QFI have been experimentally measured [25, 6, 5]. Extracting the QFI from equation (3.10) is in general a hard task in both theory and experiment. A comparably new, but seminal approach [12] relates the QFI to dynamic quantities, in particular, the dynamic susceptibility. After a weak quench, introducing new dynamics to the system, the dynamic susceptibility accounts for the temporal evolution of quantum fluctuations. The connection to the QFI arises from the fact that the sensitivity of a state towards a weak quench is determined by its fluctuations. Or in other words, this approach extracts the amount of entanglement by means of the dynamic susceptibility, which contains information about the generation of correlations in the system.

In order to fully recap the potential of extracting QFI through dynamic susceptibilities, mean-field Bogoliubov theory is a tool that enables us to describe the underlying physics of the system and to compute relevant observables. Therefore, this chapter not only reviews the relation between dynamic susceptibilities and QFI, but also shows how first order correlation functions after a weak quench can be computed from Bogoliubov theory. By doing so, we connect the two concepts, Bogoliubov theory and QFI, and give an overview of the methodology applied within this thesis.

4.1 Linear Response Theory

Dynamic susceptibility is a central quantity in linear response theory, describing the change of time-dependent observables after a weak perturbation to an equilibrium system. Measuring this quantity has therefore become a very effective and widely used method in condensed matter physics for studying the dynamics of driving the system out of equilibrium [51].

In thermal equilibrium, a quantum system is characterized by the density matrix

$$\rho_0 = \frac{1}{Z} e^{-\beta \hat{\mathcal{H}}_0} \quad \text{with} \quad Z = \text{Tr}\{e^{-\beta \hat{\mathcal{H}}_0}\}, \quad (4.1)$$

where Z is the partition function and β the inverse temperature, defined as $\beta = (k_B T)^{-1}$. Applying a sufficiently weak external force $f(t)$ gives rise to a linear time-dependent perturbation in the total Hamiltonian

$$\hat{\mathcal{H}} = \hat{\mathcal{H}}_0 - f(t) \hat{A}, \quad (4.2)$$

where \hat{A} is a time-independent operator. As a consequence of this perturbation, the density matrix $\rho(t)$ becomes time-dependent, and so does the ensemble average of the operator $\hat{B}(t)$

$$\hat{B}(t) = \text{Tr}\{\rho(t) \hat{B}\}. \quad (4.3)$$

The response function, through the so-called Kubo formula [52], relates the change of an ensemble-averaged physical observable $\langle \hat{B}(t) \rangle$ to an external force $f(t)$ via

$$\langle \hat{B}(t) \rangle = \langle \hat{B} \rangle + \int_{-\infty}^t dt' f(t') \chi_{BA}(t - t'), \quad (4.4)$$

where $\langle \hat{B} \rangle = \text{Tr}\{\rho_0 \hat{B}\}$ and $f(t)$ is assumed to vanish for $t \rightarrow \infty$. As indicated by its name, linear response theory requires that the differential change of $\langle \hat{B} \rangle$ is proportional to the external disturbance $f(t)$. The disturbances at different times act independently of each other, implying that the response function χ_{BA} in (4.4) may only depend on the time difference $t - t'$ and is independent of any future perturbations. This causal behavior may be incorporated in the response function by the requirement

$$\chi_{BA}(t - t') = 0 \quad \text{for} \quad t' > t. \quad (4.5)$$

Consider the special case of $f(t) = \lambda \Theta(t)$, with quench strength λ and the Heaviside step function $\Theta(t) = 0$ or 1 when $t < 0$ or $t \geq 0$, respectively (Figure 4.1). The Kubo formula (4.4) then relates the time-dependent response function up to linear order in perturbation to the operators in Heisenberg picture as follows

$$\begin{aligned} \langle \hat{B}(t) \rangle &= \langle \hat{B} \rangle + \lambda \int_0^t dt' \chi_{BA}(t') \\ \chi_{BA}(t - t') &= i \Theta(t - t') \langle [\hat{B}(t), \hat{A}(t')] \rangle. \end{aligned} \quad (4.6)$$

Since the response function χ_{BA} only depends on the time difference, it is very convenient to introduce the Fourier transform of the response function $\chi_{BA}(\omega) = \int_{-\infty}^{\infty} dt e^{i\omega t} \chi_{BA}(t)$, which is called the frequency-dependent or generalized susceptibility. It is a complex function which

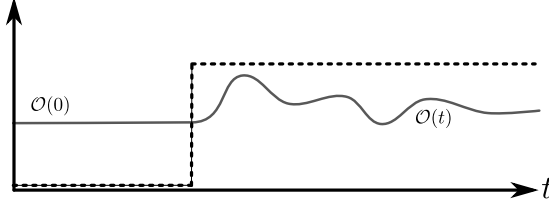


Figure 4.1.: By adding a 'step function - like' potential to the Hamiltonian (4.2) introduces dynamics to the system which can be observed in the time-dependent change of an observable $\hat{O}(t)$. Figure courtesy of Ricardo Costa de Almeida, SynQS Heidelberg.

consists of a symmetric (reactive) part χ'_{BA} and anti-symmetric (absorptive) part χ''_{BA} as follows

$$\begin{aligned}\chi'_{BA}(\omega) &= \frac{1}{2}\{\chi_{BA}(\omega) + \chi_{AB}(-\omega^*)\} \\ \chi''_{BA}(\omega) &= \frac{1}{2i}\{\chi_{BA}(\omega) - \chi_{AB}(-\omega^*)\}.\end{aligned}\quad (4.7)$$

4.2 Quantum Fisher Information through Dynamic Susceptibilities

With the use of the Kubo formula (4.6) and the absorptive part of the susceptibility χ'' (4.7), it was shown [12] that the quantum Fisher information can be computed by integrating over the frequency spectrum

$$F_Q(T) = \frac{4}{\pi} \int_0^\infty d\omega \tanh\left(\frac{\omega}{2T}\right) \chi''(\omega, T), \quad (4.8)$$

where T is the temperature. The strength of this expression is that the QFI becomes a quantity which is straightforward to measure, even for large systems, at finite temperatures and in real time.

The connection between QFI and linear response theory can be understood from the definition of the dynamic susceptibility

$$\chi(\omega, T) = i \int_0^\infty dt e^{i\omega t} \text{tr} \left(\rho \left[\hat{O}(t), \hat{O} \right] \right), \quad (4.9)$$

where we have inserted $\hat{A} = \hat{B} = \hat{O}$ into (4.6). Accordingly, the dynamic susceptibility contains information about quantum fluctuations, which determine the time evolution of \hat{O} . From these fluctuations, the QFI quantifies the sensitivity of a state towards external perturbation.

If the assumptions of a thermal initial state and a weak quench are fulfilled, the connection between QFI and dynamic susceptibility always holds. However, relating the quantum Fisher information to multipartite entanglement depends on the choice of the operator \hat{O} . A suitable \hat{O} accounts for quantum correlations which enhance the metrological sensitivity of the state and, in turn, are related to entanglement in the system. We explicitly examine this on the example of a

bosonic spin chain in section 6.2.

An equivalent formulation of equation (4.8) in the time-domain can be rigorously obtained using Fourier transformations [53]. Equation (4.8) contains essentially the integral of a product of two odd function, $\tanh\left(-\frac{\beta\omega}{2}\right)$ and $\chi''(\omega)$, such that $\tanh\left(-\frac{\beta\omega}{2}\right)\chi''(-\omega) = \tanh\left(\frac{\beta\omega}{2}\right)\chi''(\omega)$ is even. Without loss of generality, the boundary of the integral can be changed according to

$$\Rightarrow F = \frac{2}{\pi} \int_{-\infty}^{\infty} d\omega \tanh\left(\frac{\beta\omega}{2}\right) \chi''(\omega). \quad (4.10)$$

Furthermore, we rewrite (4.6) as follows

$$\chi(t) = \frac{d}{dt} \frac{\langle \hat{\mathcal{O}}(t) \rangle}{\lambda} = \frac{d}{dt} \frac{\langle \hat{\mathcal{O}}(t) \rangle - \langle \hat{\mathcal{O}} \rangle}{\lambda}. \quad (4.11)$$

Performing the Fourier transform with the use of

$$\begin{aligned} \chi''(\omega) &= \int_{-\infty}^{\infty} dt e^{i\omega t} \chi''(t) \\ \chi''(t) &= \frac{1}{2i} \{\chi(t) - \chi(-t)\} = \begin{cases} \frac{\chi(t)}{2i} & , \quad t \geq 0 \\ -\frac{\chi(-t)}{2i} & , \quad t < 0 \end{cases}, \end{aligned} \quad (4.12)$$

leads to the quantum Fisher information [53]

$$F_Q(T) = 4\pi T^2 \int_0^{\infty} dt \frac{\eta(t)}{\sinh(\pi t T) \tanh(\pi t T)}. \quad (4.13)$$

Here, we introduce the short form $\eta(t)$ of the time-dependent change of $\hat{\mathcal{O}}$, normalized with respect to the quench strength

$$\eta(t) := \frac{\langle \hat{\mathcal{O}}(t) \rangle - \langle \hat{\mathcal{O}} \rangle}{\lambda}. \quad (4.14)$$

We will make extensive use of (4.13) for the computation of the entanglement content in an extended spin-1 BEC, as demonstrated in Figure 4.2.

To conclude, multipartite entanglement can be deduced from many-body correlations contained in experimentally accessible dynamic susceptibilities of a quantum system. Those can be, for example, extracted after a weak quench introducing new dynamics to the system. We also recall that in the case of a pure state at zero temperature, the quantum Fisher information becomes considerably easier and can be computed from the variance of an observable (3.9).

4.3 Correlation Functions from Bogoliubov Theory

In either way, it is essential to calculate first and second order correlation functions in order to determine the quantum Fisher information. To this end, this section presents a detailed description

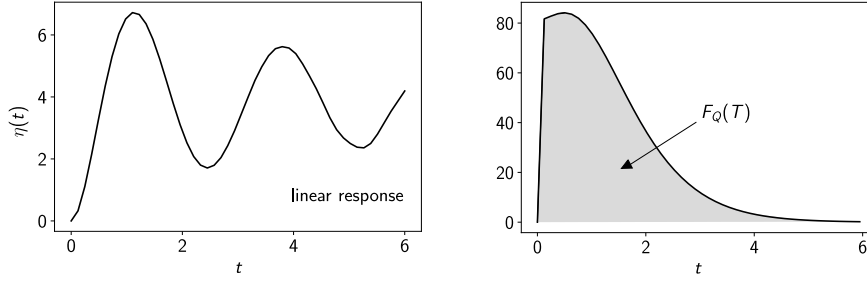


Figure 4.2.: Schematical extraction of the quantum Fisher information from simulated data: First, a quench introduces dynamics to the system and leads to a time-dependent change in the observable which can be observed in a linear response measurement (left panel). Second, the QFI is computed from the temperature-dependent integral (4.13). The QFI is thus given by the shaded area of the right panel.

of how correlation functions can be computed from Bogoliubov theory in thermal equilibrium and after a weak quench, including time evolution.

4.3.1 Thermal Equilibrium

As outlined before, thermal equilibrium is generally characterized by an equilibrium density matrix ρ_0 within the meaning of equation (4.1). Diagonalization of a bosonic Hamiltonian with the help of Bogoliubov transformation (2.13) yields the quasi-particle spectrum $\omega = (\omega_1, \dots, \omega_n, \omega_1, \dots, \omega_n)$ and the quasi-particle modes \mathbf{b}^\dagger and \mathbf{b} , as described in section 2.1. We define the entries of the so-called the correlation matrix $\Gamma = \langle \mathbf{b}\mathbf{b}^\dagger \rangle$, containing all first order correlation functions, as follows

$$\Gamma_{ij} = \text{Tr} \left\{ \rho_0 b_i b_j^\dagger \right\} = \langle b_i b_j^\dagger \rangle. \quad (4.15)$$

For the sake of simplicity, the hat ‘^’ on the operators is omitted within this section. Since the quasi-particle basis corresponds to the eigenbasis of the problem with eigenenergies ω_i , the population of modes in thermal equilibrium is given by

$$\langle \beta_i^\dagger(z) \beta_i(z) \rangle = (\exp(\beta \hbar \omega_i) - 1)^{-1}. \quad (4.16)$$

Performing the Bogoliubov transformations of the state $\mathbf{a} = \mathcal{T} \mathbf{b}$, as outlined in section 2.1, the correlation matrix $\Gamma_{\mathbf{a}}$ in the initial modes (here denoted by the subscript \mathbf{a}) reads

$$\Gamma_{\mathbf{a}} = \langle \mathbf{a}\mathbf{a}^\dagger \rangle = \mathcal{T} \langle \mathbf{b}\mathbf{b}^\dagger \rangle \mathcal{T}^\dagger = \mathcal{T} \Gamma \mathcal{T}^\dagger. \quad (4.17)$$

As a consequence, first order correlation functions in the initial frame can be read off from the elements of the correlation matrix $\Gamma_{\mathbf{a}}$. This procedure will become considerably more complicated if the problem is not diagonal anymore, as for example, after a weak quench. We derive the correlation matrix and its time-evolution for this specific case in what follows.

4.3.2 Time-Evolution Following a Weak Quench

Assuming a Hamiltonian of the form $\mathcal{H}(\lambda) = \mathbf{a}^\dagger \mathcal{M}(\lambda) \mathbf{a}$, which is described by the matrix \mathcal{M} depending on a quench parameter λ , we find two distinct Bogoliubov transformations diagonalizing the Hamiltonian $\mathcal{H}(\lambda_0)$ and $\mathcal{H}(\lambda)$ before and after the quench $\lambda_0 \rightarrow \lambda$, respectively. From here on, operators and matrices in the initial basis are denoted by "tilde", as, for instance, $\tilde{\mathbf{b}}$. Accordingly, the Bogoliubov transformation $\tilde{\mathcal{T}}$ diagonalizes the Hamiltonian $\mathcal{H}(\lambda_0)$ and, the same does \mathcal{T} for $\mathcal{H}(\lambda)$ as depicted in Figure 4.3. Both quasi-particle states $\tilde{\mathbf{b}}$ and \mathbf{b} are related to the same initial state \mathbf{a} via $\tilde{\mathcal{T}}$ and \mathcal{T} , respectively.

$$\begin{aligned} \mathcal{H}(\lambda_0) &= \tilde{\mathbf{b}}^\dagger (\tilde{\mathcal{T}}^\dagger \mathcal{M}(\lambda_0) \tilde{\mathcal{T}}) \tilde{\mathbf{b}} = \tilde{\mathbf{b}}^\dagger \tilde{\mathcal{D}} \tilde{\mathbf{b}}, & \tilde{\mathbf{b}} &= \tilde{\mathcal{T}}^{-1} \mathbf{a} \\ \mathcal{H}(\lambda) &= \mathbf{b}^\dagger (\mathcal{T}^\dagger \mathcal{M}(\lambda) \mathcal{T}) \mathbf{b} = \mathbf{b}^\dagger \mathcal{D} \mathbf{b}, & \mathbf{b} &= \mathcal{T}^{-1} \mathbf{a}. \end{aligned} \quad (4.18)$$

Combining these two equations, the new quasi-particle operator can be expressed in terms of the initial ones, $\mathbf{b} = \mathcal{T}^{-1} \tilde{\mathcal{T}} \tilde{\mathbf{b}}$, such that the Hamiltonian becomes

$$\mathcal{H}(\lambda) = \tilde{\mathbf{b}}^\dagger \tilde{\mathcal{T}}^\dagger \underbrace{\mathcal{T}^{-1\dagger} \mathcal{T}^\dagger}_{\mathbb{I}} \mathcal{M}(\lambda) \underbrace{\mathcal{T} \mathcal{T}^{-1}}_{\mathbb{I}} \tilde{\mathcal{T}} \tilde{\mathbf{b}} = \tilde{\mathbf{b}}^\dagger \tilde{\mathcal{T}}^\dagger \mathcal{M}(\lambda) \tilde{\mathcal{T}} \tilde{\mathbf{b}}. \quad (4.19)$$

Here, it is important to note that $\tilde{\mathcal{T}}^\dagger \mathcal{M}(\lambda) \tilde{\mathcal{T}}$ is not diagonal any more. This reflects the fact that the quench introduces new dynamics to the system, which is encoded in the off-diagonal elements, thereby accounting for the redistribution of the occupation of modes.

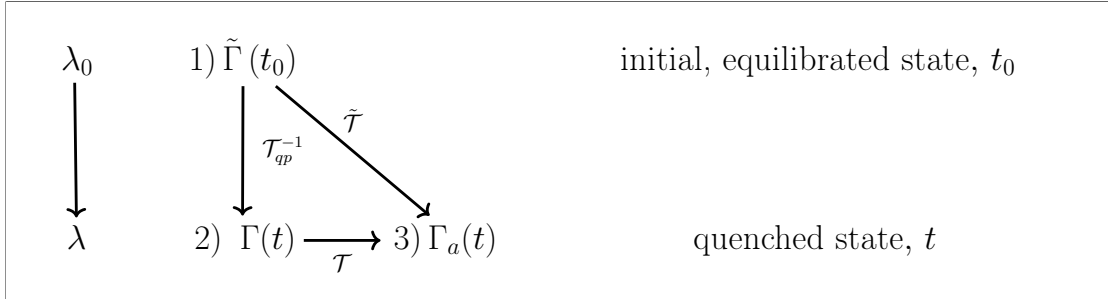


Figure 4.3.: Bogoliubov transformation form a group. That is why the transformation $\mathcal{T}_{qp} = \tilde{\mathcal{T}}^{-1} \mathcal{T}$ between the two quasi-particle modes $\tilde{\mathbf{b}} = \mathcal{T}_{qp} \mathbf{b}$ can be calculated from the transformations diagonalizing the Hamiltonian before and after the quench. We will use this in order to populate the modes in the initial basis and perform the time-evolution in the quenched state as outlined in Figure 4.4.

We are interested in the time evolution of an observable $\mathcal{O}(t)$ under the quench $\lambda_0 \rightarrow \lambda$. In general, time-dependent expectation values of observables can be computed from the partition function Z and the density matrix ρ_0 in the Heisenberg picture via $\langle \hat{\mathcal{O}}(t) \rangle = \text{Tr} \{ \rho(t) \mathcal{O} \}$. Making use of the invariance of the trace under cyclic permutations and inserting the expression $\mathcal{O} =$

$\mathbf{b}\mathbf{b}^\dagger$, yields the time evolution of the correlation matrix Γ

$$\Gamma(t) = \text{Tr} \left\{ \rho_0 e^{i\mathcal{H}(\lambda)t} \mathbf{b}\mathbf{b}^\dagger e^{-i\mathcal{H}(\lambda)t} \right\} = \langle \mathbf{b}\mathbf{b}^\dagger(t) \rangle. \quad (4.20)$$

$\Gamma = \langle \mathbf{b}\mathbf{b}^\dagger \rangle$ contains combinations of quasi-particle operators $\beta_i^\circ \beta_j^\diamond$, whereby \diamond and \circ denote whether the hermitian conjugate is applied to β . The term $\beta_i^\circ \beta_j^\diamond(t) = e^{i\mathcal{H}(\lambda)t} \beta_i^\circ \beta_j^\diamond e^{-i\mathcal{H}(\lambda)t}$ can be computed from the commutator with the Bogoliubov Hamiltonian (4.19) according to the Heisenberg equation of motion

$$\frac{d}{dt} \beta_i^\circ \beta_j^\diamond(t) = i [\mathcal{H}, \beta_i^\circ \beta_j^\diamond] - \frac{\partial}{\partial t} (\beta_i^\circ \beta_j^\diamond). \quad (4.21)$$

The last term is zero because $\beta_i^\circ \beta_j^\diamond$ is not explicitly time-dependent, such that the equations of motion become

$$\frac{d}{dt} \beta_i^\circ \beta_j^\diamond(t) = i [\mathcal{H}, \beta_i^\circ \beta_j^\diamond] = i \left[\sum_{k=1}^n \hbar\omega_k \{ \hat{\beta}_k^\dagger \hat{\beta}_k + \hat{\beta}_k \hat{\beta}_k^\dagger \}, \beta_i^\circ \beta_j^\diamond \right]. \quad (4.22)$$

An exponential ansatz solves the time evolution, which can be formalized by a matrix product using the unitary matrix $\mathcal{E}(t)$

$$\Gamma(t) = \mathcal{E}(t) \Gamma \mathcal{E}^\dagger(t). \quad (4.23)$$

$\mathcal{E}(t)$ is a diagonal matrix resembling the form $\text{diag} (e^{-i\hbar\omega_1 t}, \dots, e^{-i\hbar\omega_n t}, e^{i\hbar\omega_1 t}, \dots, e^{i\hbar\omega_n t})$ in the quench-basis. The exact form is specific to the equations of motion (4.22) and commutation relations, which can be also seen from the example given in Appendix A.5.

Now that we have described the time-evolution and the transformations between quasi-particle modes before and after a weak quench $\lambda_0 \rightarrow \lambda$, we put all the pieces together and compute the correlation matrix $\Gamma_{\mathbf{a}}(t)$ at time t after the quench

$$\Gamma_{\mathbf{a}}(t) = \mathcal{T} \underbrace{\mathcal{E}(t) \mathcal{T}_{qp}^{-1} \tilde{\Gamma}(t_0) \mathcal{T}_{qp}^{-1 \dagger} \mathcal{E}^\dagger(t)}_{\Gamma(t)} \mathcal{T}^\dagger. \quad (4.24)$$

Given an initial population of quasi-particle modes in thermal equilibrium $\tilde{\Gamma}(t_0) = \langle \tilde{\mathbf{b}}\tilde{\mathbf{b}}^\dagger \rangle$, we use the eigenenergies of the quenched Hamiltonian in order to perform the time evolution with $\mathcal{E}(t)$ in the quench basis. The obtained correlation matrix is then rotated back into the initial modes by means of the compound Bogoliubov transformation $\mathcal{T}_{qp} = \tilde{\mathcal{T}}^{-1} \mathcal{T}$ (Figure 4.3). Finally, the correlation functions can be read off from the matrix elements of $\Gamma_{\mathbf{a}}$. This scheme of calculating $\Gamma_{\mathbf{a}}$ from equation (4.24) is also summarized in Figure 4.4.

To conclude, observables relevant to the calculation of the quantum Fisher information can be

obtained from the correlation matrix $\Gamma_{\mathbf{a}}(t)$, which is given by the initial population of the quasi-particle modes in thermal equilibrium, the Bogoliubov transformations \mathcal{T} , $\tilde{\mathcal{T}}$, and the eigenvalues ω_i in the quenched system, as outlined in Figure 4.4.

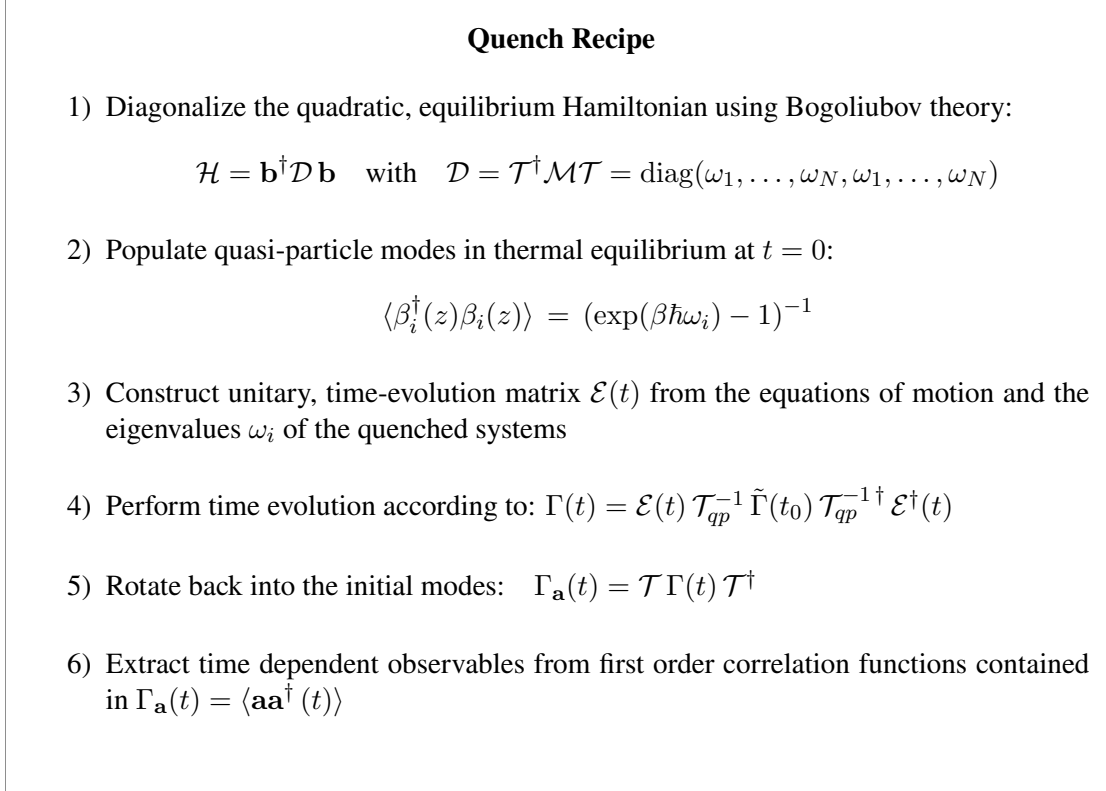


Figure 4.4.: Methodology as applied within this thesis for extracting first order correlation function after a weak quench using Bogoliubov theory.

5 Quantum Fisher Information of a Spin-1 BEC in Single-Mode Approximation

As outlined in the previous sections, Bogoliubov theory can be exploited to compute the quantum Fisher information from the variance of a pure state at zero temperature. Due to the underlying assumptions of Bogoliubov theory, which significantly decrease computational efforts, it is possible to study large many-particle systems such as spinor Bose gases. By employing the scheme from section 4.3, we numerically investigate the QFI for a single-mode spin-1 BEC with $N = 12000$ particles in the Broken-Axisymmetry (BA) phase in this section. We choose the BA phase because a large many-particle entanglement can be expected due to a strong presence of spin-changing collisions [21]. In addition to that, we compare the results to calculations based on exact diagonalization of a system with $N = 500$ particles.

5.1 Single-Mode Approximation

The single-mode approximation [28, 7] assumes that the wave function for each spin component retains the same spatial atomic distribution and, further, that this density profile is not affected by spin dynamics. When interactions are weak and well below the critical temperature, almost all particles are found in the zero momentum mode ($k = 0$). Additionally, a length scale separation is provided by the different interaction strengths λ_s and λ_a in the main Hamiltonian (1.5)-(1.7), which allows one to treat spatial and spin internal modes independently¹. These assumptions are valid in the limit where the spatial extension of the condensate is comparable to or smaller than the spin-healing length. It thus justifies the approximation of the field operator by a product of the ground state solution $\phi(\mathbf{r})$ of the Gross-Pitaevskii equation [26, 27] and the bosonic operator \hat{a}_m

$$\hat{\psi}_m \approx \hat{a}_m \phi(\mathbf{r}). \quad (5.1)$$

In this context, we use \hat{a}_m (\hat{a}_m^\dagger) as the operator annihilating (creating) a bosonic particle in the $m_F = m$ hyperfine state. Integrating out the spatially dependent part, the second quantized form

¹for bosons such as ^{87}Rb and ^{23}Na , one typically finds $|\lambda_s| \gg |\lambda_a|$ [23].

of the Hamiltonian (1.5) - (1.7) reads

$$\begin{aligned}
 \hat{\mathcal{H}}_S &= -\bar{\lambda}_s \hat{N}(\hat{N} - 1) - \mu \hat{N} \\
 \hat{\mathcal{H}}_A &= \bar{\lambda}_a \{ \hat{a}_1^\dagger \hat{a}_1^\dagger \hat{a}_1 \hat{a}_1 + \hat{a}_{-1}^\dagger \hat{a}_{-1}^\dagger \hat{a}_{-1} \hat{a}_{-1} + 2\hat{a}_1^\dagger \hat{a}_0^\dagger \hat{a}_1 \hat{a}_0 + 2\hat{a}_{-1}^\dagger \hat{a}_0^\dagger \hat{a}_{-1} \hat{a}_0 \\
 &\quad - 2\hat{a}_1^\dagger \hat{a}_{-1}^\dagger \hat{a}_1 \hat{a}_{-1} + \underbrace{2\hat{a}_0^\dagger \hat{a}_0^\dagger \hat{a}_1 \hat{a}_{-1} + 2\hat{a}_1^\dagger \hat{a}_{-1}^\dagger \hat{a}_0 \hat{a}_0}_{\text{SCC}} \} \\
 \hat{\mathcal{H}}_B &= p(\hat{N}_1 - \hat{N}_{-1}) + q(\hat{N}_1 + \hat{N}_{-1}).
 \end{aligned}$$

The spatially integrated interaction strengths are given by $2\bar{\lambda}_i = \lambda_i \int d\mathbf{r} |\phi(\mathbf{r})|^4$ and $\hat{N} = \hat{N}_0 + \hat{N}_1 + \hat{N}_{-1}$ denotes the total number of atoms in the condensate with $\hat{N}_0 = \hat{a}_0^\dagger \hat{a}_0$ and $\hat{N}_{\pm 1} = \hat{a}_{\pm 1}^\dagger \hat{a}_{\pm 1}$. Hence, $\hat{\mathcal{H}}_S$ is a constant as long as there is no atom loss or change in the trapping potential and $\hat{\mathcal{H}}_A$ determines the non-trivial dynamics involving spin-changing collisions. The Zeeman energies are taken into account by $\hat{\mathcal{H}}_B$.

A vanishing linear Zeeman effect ($p = 0$) is assumed in this thesis which can be taken care of experimentally by a rotating frame approximation [54, 55]. The second quantized form of the single-mode approximation Hamiltonian (5.2) reads

$$\begin{aligned}
 \hat{\mathcal{H}}_{SMA} &= \left(2\lambda \hat{N}_0 + q - \lambda \right) \left(\hat{N}_1 + \hat{N}_{-1} \right) + \lambda \left(\hat{N}_1 - \hat{N}_{-1} \right)^2 \\
 &\quad + 2\lambda \underbrace{\left(\hat{a}_1^\dagger \hat{a}_{-1}^\dagger \hat{a}_0 \hat{a}_0 + \hat{a}_0^\dagger \hat{a}_0^\dagger \hat{a}_1 \hat{a}_{-1} \right)}_{\text{SCC}} - \mu \hat{N},
 \end{aligned} \tag{5.2}$$

where $\bar{\lambda}_a$ is simply denoted by λ from here on. We keep explicitly track of the total magnetization $\hat{M} = \hat{N}_1 - \hat{N}_{-1}$, which, in the absence of a linear Zeeman shift, becomes zero at the mean-field level. Its fluctuations, however, can contribute to the dynamics. The Hamiltonian (5.2) operates on a Fock basis represented by $|N_1; N_0; N_{-1}\rangle$ where N_i is the number of particles in the $m_F = i$ state [21]. By direct computation, one finds that the spin mixing dynamics through spin changing collisions (SCC) conserves both the total atom number and the magnetization. The first term comprises density-density interactions, with a negative interaction constant $\lambda < 0$ for ferromagnetic interactions and the quadratic Zeeman shift proportional to the magnetic field parameter q . The chemical potential $\mu < 0$ (for bosons) was introduced in order to fix the total amount of particles in number-conserving Bogoliubov theory. Changing the value of the chemical potential adjusts the total number of bosons in the condensate. Depending upon the physical conditions, a given system can either be constrained to be at a fixed chemical potential (the grand canonical ensemble) or have a fixed total number of bosons (the canonical ensemble). We will revisit the important role of the chemical potential when considering numerical calculations of observables in subsection 5.3.2.

The spin-1 BEC in single-mode approximation gives rise to two quantum phase transitions (QPTs)

with the critical values $q = \pm q_c$ and $q_c = 4|\lambda|N$. The phase diagram is depicted in Figure 5.1a in terms of the occupation of the hyperfine spin states $m_F = -1, 0, 1$. For a specific ratio of interaction and Zeeman energies, we find the Broken-Axisymmetry phase in the regime where $|q| < q_c$. This phase is characterized by an occupation of all modes and, as can be seen from Figure 5.1b, facilitating spin-changing collisions due to the comparably small energy difference between the Zeeman sublevels.

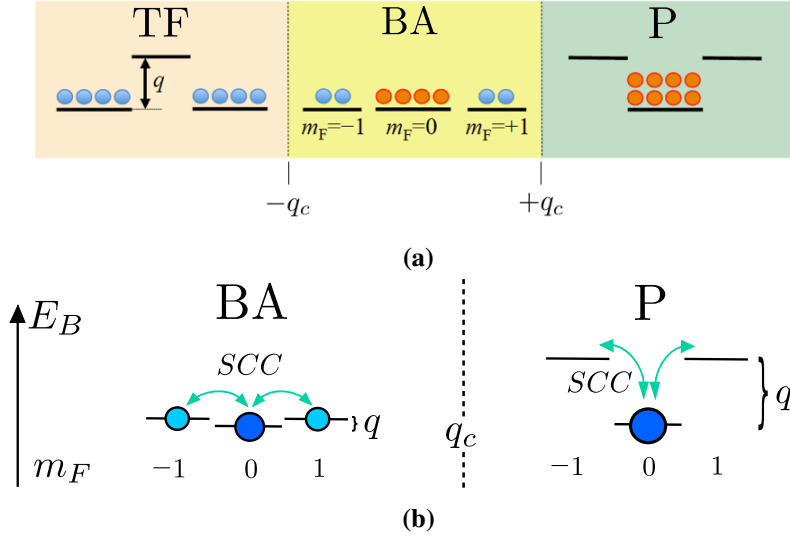


Figure 5.1.: (a) The phase diagram of a spin-1 BEC in single-mode approximation consists of three quantum phases. We focus on the Broken-Axisymmetry (BA) phase which is the only phase exhibiting a population of all three modes in the mean-field ground state. (b) The interchange of hyperfine states among the m_F -components is driven by spin-changing collisions. Experimentally, the energy difference between the side modes ($m_F = \pm 1$) and the central mode ($m_F = 0$) can be tuned by the magnetic field parameter q . The closer the energy levels, the more likely are spin-changing collisions, leading to dynamical redistribution of the occupations. Because of this, we expect strong presence of spin-changing collisions and therefore a large amount of entanglement in the BA phase.

5.2 Lipkin-Meshkov-Glick Representation

The SMA Hamiltonian (5.2) from above can be studied in the more intuitive picture of Lipkin-Meshkov-Glick (LMG) models [56]. The LMG model belongs to a class of spin models first introduced by H. J. Lipkin, N. Meshkov and A. J. Glick [57]. The LMG Hamiltonian is of the form $\hat{\mathcal{H}}_{LMG} = -\frac{g}{N}(\hat{S}_x^2 + \gamma\hat{S}_y^2) - h\hat{S}_z$ which corresponds to a fully connected Ising Hamiltonian of spin-1/2 particles where each spin interacts with all the other spins and the parameters g, γ and h account for the interaction, anisotropy and external field strength, respectively [1, 49]. Within this representation, the SMA Hamiltonian (5.2) becomes a sum of two non-commuting Lipkin-Meshkov-Glick Hamiltonians [1, 21] for the operators \hat{S} and \hat{A} from equation (1.11),

when neglecting constant terms

$$\hat{\mathcal{H}} = 2 \left(\lambda \hat{S}_x^2 - \frac{q}{3} \hat{S}_z \right) + 2 \left(\lambda \hat{A}_y^2 - \frac{q}{3} \hat{A}_z \right). \quad (5.3)$$

For $q = 0$ and $\lambda < 0$, the ground state of the first and second term in (5.3) can be represented by a N00N state aligned along the \hat{S}_x and \hat{A}_y axis. A N00N state is a coherent superposition of all particles in the maximum and all particles in the minimum eigenstate of the corresponding operator

$$|\text{N00N}\rangle = \frac{|N\rangle_a |0\rangle_b + e^{i\phi} |0\rangle_a |N\rangle_b}{\sqrt{2}}, \quad (5.4)$$

where ϕ is an arbitrary phase. Figure 5.2 showcases an example of a state with a and b being states that are fully polarized in the \hat{S}_x and $-\hat{S}_x$ direction, respectively. The N00N state belongs to the same class of highly-entangled states such as the Schrödinger cat [58, 59] or Greenberger-Horne-Zeilinger state [60]. The subtle difference is that the term N00N state is specific to indistinguishable bosonic particles [61].

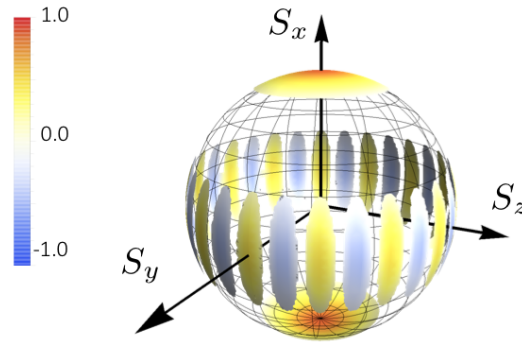


Figure 5.2.: The Wigner function of a N00N states (here, we use $N = 14$) reveals the structure of the state on the Bloch sphere. The quasi-distribution exhibits an interference pattern along the equator with positive and negative values. The pattern can be attributed to the entanglement of this state and makes it metrologically more distinguishable compared to a coherent state (Figure 1.4a), which gives already an intuition about the optimal rotation axis [35].

5.3 Self-Consistent Mean-Field Bogoliubov Theory

As outlined in section 2.1, Bogoliubov transformations can be used to diagonalize quadratic Hamiltonians. However, our target Hamiltonian (5.3) is not of quadratic form. Hence, further assumptions are needed in order to apply the suggested scheme from section 4.3 to the calculation of quantum Fisher information for a spin-1 BEC within single-mode approximation.

One possible simplification arises from the framework of mean-field theory which is a very common approach to describe quantum many-body systems with small quantum statistical fluctua-

tions compared to classical statistical fluctuations. It allows one to expand the Hamiltonian in terms of fluctuations around the expectation value of the field

$$\hat{\Psi} \approx \langle \hat{\Psi} \rangle + \delta \hat{\Psi}. \quad (5.5)$$

In Bose-Einstein condensates, this assumption is valid in the limit of large particle numbers, weak interactions and sufficiently low temperatures when the depletion of the condensate by quantum and thermal fluctuations can be neglected. The classical complex field $\langle \hat{\Psi} \rangle$ is then macroscopically occupied and commonly referred to as the ground state wave function of the condensate, given by the Gross-Pitaevskii equation [26, 27].

By keeping track of all fluctuations $\delta \hat{\Psi}$ up to second order, an effective Hamiltonian of quadratic form can be derived. Accordingly, the diagonalized Bogoliubov Hamiltonian then describes the system by its characteristic quasi-particle excitations, which are closely related to the fluctuations around the mean-field solution via Bogoliubov transformations. However, this approximation is only valid as the number of particles remains large since the expectation values of the fields $\langle \hat{\Psi} \rangle$ are normalized to the number of particles in the system, which becomes problematic in case of increased fluctuations: The more excitations, the less particles can be found in the mean-field ground state of the condensate. In subsection 5.3.2 we therefore introduce a self-consistent way to fix the total particle number in numerical calculations.

5.3.1 Mean-Field Description

As outlines above, the quantum fields in the Hamiltonian (5.3) can be replaced by bosonic creation/annihilation operators. Because of the normalization of the wavefunction, the mean-field substitution is then characterized by the atomic occupations $\langle \hat{a}_i \rangle \approx \sqrt{\langle \hat{a}_i^\dagger \hat{a}_i \rangle}$. We choose the following semi-classical approximation

$$\hat{a}_m^\dagger \rightarrow \sqrt{N} \zeta_m, \quad \hat{a}_m \rightarrow \sqrt{N} \zeta_m^* \quad \text{with} \quad \zeta_m = |\zeta_m| e^{i\theta_m}, \quad (5.6)$$

where the complex vector $\zeta = (\zeta_1, \zeta_0, \zeta_{-1})$ represents the amplitude and phase of the classical field of the m_F -mode. We search for the mean field solution ζ which minimizes the ground state energy E_0 . Inserting the above ansatz (5.6) into (5.2) yields the following equations

$$\begin{aligned} E_0 &= 2(q - \lambda)|\zeta_1|^2 N + 4\lambda N^2 |\zeta_0|^2 |\zeta_1|^2 \{1 + \cos(\theta_1 + \theta_{-1} - 2\theta_0)\} \\ \frac{\delta E_0}{\delta \theta_0} &= 8\lambda N^2 |\zeta_0|^2 |\zeta_1|^2 \sin(\theta_1 + \theta_{-1} - 2\theta_0) \stackrel{!}{=} 0 \\ \frac{\delta E_0}{\delta |\zeta_0|^2} &= 4\lambda N^2 |\zeta_1|^2 \{1 + \cos(\theta_1 + \theta_{-1} - 2\theta_0)\} - \mu N \stackrel{!}{=} 0 \\ \frac{\delta E_0}{\delta |\zeta_1|^2} &= 2(q - \lambda)N + 4\lambda N^2 |\zeta_0|^2 \{1 + \cos(\theta_1 + \theta_{-1} - 2\theta_0)\} - 2\mu N \stackrel{!}{=} 0. \end{aligned} \quad (5.7)$$

We assume equal mean-field populations of the side modes ($|\zeta_1| = |\zeta_{-1}|$), since the Hamiltonian (5.2) is invariant under the exchange $m_F = 1 \leftrightarrow m_F = -1$ up to a global phase shift. The chemical potential μ acts as a Lagrange multiplier $-\mu N(\sum_{0,\pm 1} |\zeta_m|^2 - 1)$, thereby enforcing the constraint of particle number conservation. The second equation from (5.7) implies that the so-called spinor phase is fixed: $\theta_s = \theta_1 + \theta_{-1} - 2\theta_0 = 0, \pm\pi, \pm 2\pi, \dots$ [16]. In the same manner, the third equation determines the chemical potential $\mu = 8\lambda N |\zeta_1|^2$. Solving for the third equation under the constraint $\sum_{0,\pm 1} |\zeta_m|^2 = 1$ yields two solutions for $\cos(\theta_s) = \pm 1$:

$$\cos(\theta_s) = +1 \quad \Rightarrow \quad |\zeta_0|^2 = \frac{1}{2} - \frac{q}{8\lambda N} \quad \text{and} \quad \cos(\theta_s) = -1 \quad \Rightarrow \quad -qN = 0. \quad (5.8)$$

The second solution ($\cos(\theta_s) = -1$) implies that the energy minimum sits at the boundary ($|\zeta_0| = 0$ or 1) for $\lambda < 0$ and is therefore an unstable solution. On the contrary, the first solution ($\cos(\theta_s) = 1$) implies an energy minimum since the second derivative becomes negative. The occupation of the $m_F = 0$ -mode is therefore parameterized in the BA phase by

$$|\zeta_0| = \sqrt{\frac{1}{2} - \frac{q}{8\lambda N}}, \quad |\zeta_1| = \frac{1}{\sqrt{2}} \sqrt{\frac{1}{2} + \frac{q}{8\lambda N}}, \quad (5.9)$$

and shown in Figure 5.3. Furthermore, we introduce $\rho_0 = |\zeta_0|^2 = N_0/N$ as the fractional population of the $m_F = 0$ -component. A convenient parametrization [30] of the order parameter is then given by

$$\begin{aligned} \zeta_1 &= \sqrt{\frac{1-\rho_0}{2}} e^{i(\theta_S/2 + \phi_L)}, \\ \zeta_0 &= \sqrt{\rho_0}, \\ \zeta_{-1} &= \sqrt{\frac{1-\rho_0}{2}} e^{i(\theta_S/2 - \phi_L)}. \end{aligned} \quad (5.10)$$

Here, θ_S is the spinor phase $\theta_S = \theta_1 + \theta_{-1} - 2\theta_0$, capturing the relative phase between the so-called side modes ($m_F = \pm 1$) and the central mode ($m_F = 0$). The Larmor precession phase $\phi_L = (\theta_1 - \theta_{-1})/2$ corresponds to the phase difference between the $m_F = 1$ and $m_F = -1$ component. However, ϕ_L does not appear in the energy functional (5.7) and is therefore a random phase $\phi_L \in [0, 2\pi]$ which is typically not controlled in experiments with spin-1 BECs [16]. It performs rotations along the \hat{S}_z axis, thereby mapping the dynamics from one $su(2)$ -subspace to the other (compare to section 1.2 and the mapping $\{\hat{S}_x, \hat{S}_y, \hat{S}_z\} \rightarrow \{\hat{Q}_{yz}, \hat{Q}_{xz}, \hat{S}_z\}$). Without loss of generality, it is not necessary to track the Larmor precession in most of our numerical calculations and is therefore set to $\phi_L = 0$, if not otherwise stated.

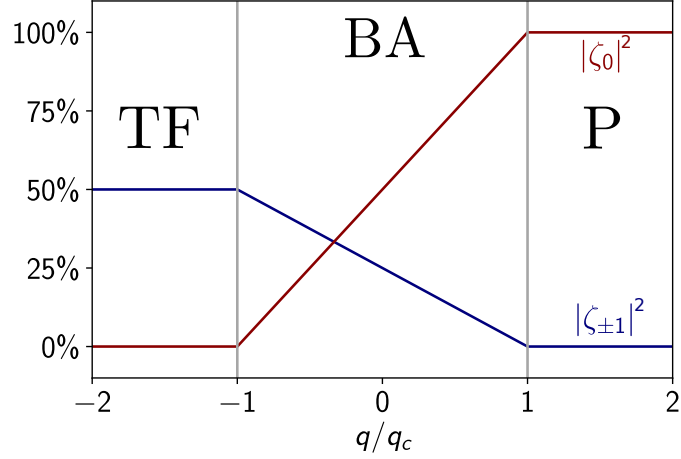


Figure 5.3.: The magnetic field parameter q changes the mean-field occupation of the m_F -modes, thereby yielding a separation into the Twin-Fock (TF), Broken-Axisymmetry (BA) and Polar (P) phase according to their magnetic order. We observe that close to the BA-P transition the occupation of the side modes vanishes, whereas the population of the central mode decreases towards the BA-TF transition.

5.3.2 Quadratic Form of the SMA Hamiltonian

Expanding the Hamiltonian (5.2) up to second order in fluctuation $\delta\hat{a}_i$ according to $\hat{a}_i = \sqrt{N}\zeta_i + \delta\hat{a}_i$, yields the effective, quadratic Hamiltonian

$$\mathcal{H}_{eff}^{(2)} = \begin{pmatrix} \delta\hat{\mathbf{a}}^\dagger & \delta\hat{\mathbf{a}} \end{pmatrix} \begin{pmatrix} \mathcal{A} & \mathcal{B} \\ \overline{\mathcal{B}} & \overline{\mathcal{A}} \end{pmatrix} \begin{pmatrix} \delta\hat{\mathbf{a}} \\ \delta\hat{\mathbf{a}}^\dagger \end{pmatrix}, \quad (5.11)$$

where the mode $\delta\hat{\mathbf{a}}$ comprises the entries $\delta\hat{\mathbf{a}} = (\delta\hat{a}_1, \delta\hat{a}_0, \delta\hat{a}_{-1})$. The matrices \mathcal{A} and \mathcal{B} are given by

$$\mathcal{A} = \lambda N_c \begin{pmatrix} \frac{q-\lambda-\mu}{2\lambda N_c} + (\zeta_0^2 + |\zeta_1|^2) & 3\zeta_0\zeta_1 & -\zeta_1^2 \\ 3\zeta_0\zeta_{-1} & -\frac{\mu}{2} + 2|\zeta_1|^2 & 3\zeta_0\zeta_1 \\ -\zeta_{-1}^2 & 3\zeta_0\zeta_{-1} & \frac{q-\lambda-\mu}{2\lambda N_c} + (\zeta_0^2 + |\zeta_1|^2) \end{pmatrix}$$

and

$$\mathcal{B} = \lambda N_c \begin{pmatrix} \zeta_1^2 & \zeta_0\zeta_1 & (\zeta_0^2 - |\zeta_1|^2) \\ \zeta_0\zeta_1 & 2|\zeta_1|^2 & \zeta_0\zeta_{-1} \\ (\zeta_0^2 - |\zeta_1|^2) & \zeta_0\zeta_{-1} & \zeta_{-1}^2 \end{pmatrix}.$$

$\overline{\mathcal{A}}$, respectively $\overline{\mathcal{B}}$ denote the conjugated matrix, providing that the Hamiltonian is of the desired hermitian form (2.5). We thus follow the diagonalization scheme as described in section 2.1 and

find the Bogoliubov transformations diagonalizing the Hamiltonian via

$$\mathcal{D} = \mathcal{T}^\dagger \begin{pmatrix} \mathcal{A} & \mathcal{B} \\ \overline{\mathcal{B}} & \overline{\mathcal{A}} \end{pmatrix} \mathcal{T}. \quad (5.12)$$

After thermally populating the quasi-particle modes according to (4.16), the correlation matrix (4.17) can be calculated using Bogoliubov transformation as outlined in the scheme from Figure 4.4. This gives access to all first order correlation functions. Consistent with the treatment of the annihilation/creation operators in the Hamiltonian, however, the correlation functions need to be expanded as well

$$\langle \hat{a}_i^\diamond \hat{a}_j^\circ \rangle = \langle \{ \langle \hat{a}_i^\diamond \rangle + \delta \hat{a}_i^\diamond \} \{ \langle \hat{a}_j^\circ \rangle + \delta \hat{a}_j^\circ \} \rangle. \quad (5.13)$$

Since the statistical quantum fluctuation around the mean-field ground state are assumed to be Gaussian distributed with $\langle \delta \hat{a}_i \rangle = 0$, equation (5.13) simplifies to

$$\langle \hat{a}_i^\diamond \hat{a}_j^\circ \rangle = \langle \hat{a}_i^\diamond \rangle \langle \hat{a}_j^\circ \rangle + \langle \delta \hat{a}_i^\diamond \delta \hat{a}_j^\circ \rangle. \quad (5.14)$$

Here, we use again \diamond , \circ , $\#$ and \star in order to denote whether the hermitian conjugate is applied to the operator. The first term is given by the mean-field parametrization (5.6) and the second term can be read off from the correlation matrix. Second order correlation functions $\langle \hat{a}_i^\diamond \hat{a}_j^\circ \hat{a}_k^\# \hat{a}_l^\star \rangle$ were computed by expanding (5.13) up to second order in fluctuations and applying Wick's theorem (section 2.3).

5.3.3 Numerical Implementation

Regarding numerical parameterization, we consider the typical values: $q_c/\hbar = 1\text{Hz}$ and, correspondingly, $\lambda = -1/(4N)$ [62, 30, 63]. As outlined above, the total number of condensed particles N can be adjusted, by changing the chemical potential μ , which sets an energy threshold for the quasi-particle excitations. If fluctuations increase, the underlying mean-field ansatz becomes invalid, such that the constraint on the number of condensed particles N_0 and the fluctuation of the total particle number $\sum_i \langle \delta \hat{N}_i \rangle = \sum_i \langle \delta \hat{a}_i^\dagger \delta \hat{a}_i \rangle$

$$N = N_0 - \sum_i \langle \delta \hat{N}_i \rangle, \quad (5.15)$$

is not necessarily fulfilled anymore. Within our numerical calculations, we take care of this constraint by self-consistently adapting the chemical potential μ , such that (5.15) is satisfied. This approach can be implemented to explore the thermal phase diagram relying on the extraction of the mean-field occupation at finite temperatures, as outlined in Appendix A.2. Moreover, we derive analytical expressions for the Bogoliubov modes, given in Appendix A.3, as a benchmark to our numerical results. All calculations were performed numerically and cross-checked with

the analytical expressions. Although the analytical approach requires further assumptions, it qualitatively confirms the numerical results as demonstrated in Figure A.17 and Figure A.19. Here, we will focus on the discussion of the numerical results, providing a clearer description of the investigated quantities.

5.4 Quantum Fisher Information at Zero Temperature

As a first study, we compute the quantum Fisher information for a single-mode spin-1 BEC in Broken-Axisymmetry phase at zero temperature from the variance of an operator \hat{O} according to $F_Q = 4(\Delta \hat{O})^2 = 4(\langle \hat{O}^2 \rangle - \langle \hat{O} \rangle^2)$. A good choice for \hat{O} is the key component to witness multipartite entanglement, since the QFI formulates the sensitivity of a quantum state towards a suitable rotation $\hat{O} = \mathbf{u} \cdot \hat{\mathbf{G}}$ (3.7). This reflects the fact that not all classes of entangled states are appropriate for quantum interferometry measurements [11, 1]. We further require that \hat{O} is a local operator of experimental relevance which can be represented within the underlying $su(n)$ algebra, here $su(3)$. As described in section 1.2, we therefore refer back to the pseudospin-1 representation in terms of the collective Gell-Mann operators [21].

Since the Hamiltonian (5.3) is invariant under the exchange $\hat{\mathbf{S}} \leftrightarrow \hat{\mathbf{A}}$, it is sufficient to focus on only one of these subspaces in order to find a suitable operator. In the subspace $\{\hat{S}_x, \hat{S}_y, \hat{S}_z\}$ the operators \hat{S}_x and \hat{S}_y contain spin-interaction terms (1.11), which are expected to play a crucial role in the creation of entanglement and are therefore our operators of choice for the computation of the quantum Fisher information. Rotations around the \hat{S}_z axis, which are inherent to the system due to the free precession at the Larmor frequency, map the \hat{S}_y axis into the measurement basis of \hat{S}_x and vice versa. Consequently, it is expected that studying either of them already extracts relevant physical information for bounding the amount of entanglement in the system [21]. In fact, we have checked that numerical calculations show the same outcome for $\hat{S}_x, \hat{S}_y, \hat{A}_x,$ and \hat{A}_y when considering a corresponding shift in the Larmor phase and, for this reason, only showcase the results for \hat{S}_x in Figure 5.4.

The graph on the left panel demonstrates that the Fisher information density F_Q/N takes the value 1 in the middle of the phase and increases when approaching the critical points $\pm q_c$. Hence, there is no entanglement witnessed at $q = 0$ but the same builds up as soon as the absolute value of q increases. How can we interpret this finding amid our expectation from section 5.2 of a large entanglement content at the center of the phase?

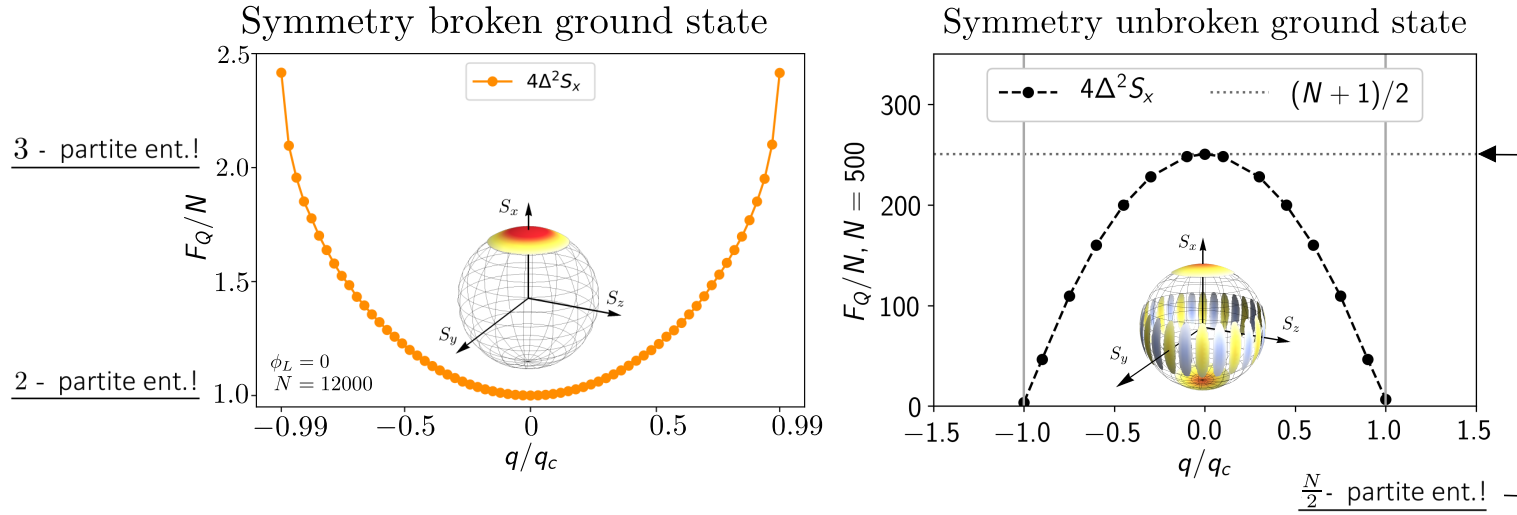


Figure 5.4.: Quantum Fisher information for a single-mode spin-1 BEC in Broken-Axisymmetry phase described by $\hat{\mathcal{H}} = 2(\lambda\hat{S}_x^2 - \frac{q}{3}\hat{S}_z) + 2(\lambda\hat{A}_y^2 - \frac{q}{3}\hat{A}_z)$, with regard to spontaneous symmetry breaking of the ground state. Left panel: Numerical calculations based on mean-field Bogoliubov theory suggest that in the limit of large system sizes ($N = 12000$) the symmetry broken ground state shows no entanglement at $q = 0$. We observe, that the quantum Fisher information increases towards the critical points which could be attributed to increased quantum fluctuations, thereby witnessing up to tri-partite entanglement. Using exact diagonalization [20] for $N = 500$ particles (right panel), the quantum Fisher information shows Heisenberg scaling of the entanglement which is attributable to the symmetry unbroken N00N state and in very good agreement with results from [21]. We explicitly note that both curves are independent of the particle number since the interaction parameter is normalized in such a way that the critical value remains the same $q_c = 4|\lambda|N = 1$.

5.4.1 Spontaneous Symmetry Breaking of the Ground State

Similar investigations were done by Feldmann et al [21], showing a contrary result for the QFI. In their analytical calculation, the QFI approaches the Heisenberg limit with $F_Q = N(N+1)/2$ in the center of the BA phase ($q = 0$). With the use of exact diagonalization [20], we reproduce these result for a system of $N = 500$ particles, shown in the right pannel of Figure 5.4. The ground state of the system resembles a N00N state, as described in section 5.2. A look at the Wigner distribution from equation (1.14) and Figure 5.2 reveals substructures of the state [36], thereby giving a better intuition about the metrologically favored rotational axis. Due to the emerging interference pattern in the quasi-probability distribution around the equator, rotations along the \hat{S}_x axis become more distinguishable when compared to a pure, coherent state. This sensitivity towards rotation of the state is captured by the QFI, saturating the Heisenberg limit.

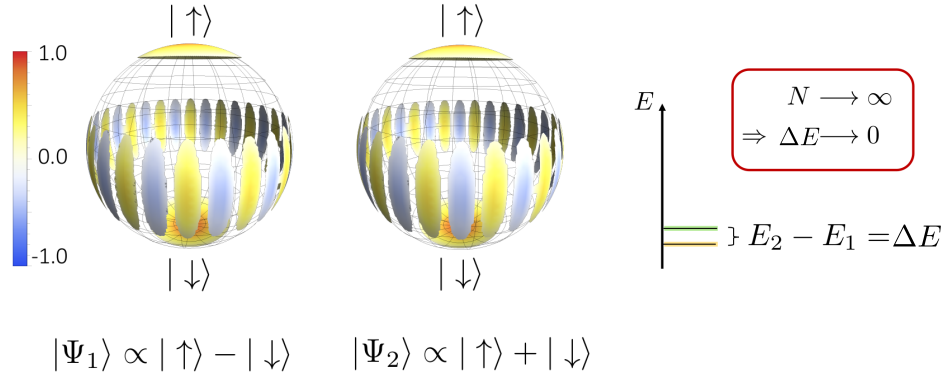


Figure 5.5.: Visualization of the analogy to spontaneous symmetry breaking of the Ising model in 2D. The energy gap $\Delta E = E_2 - E_1$ between the two cat states $|\Psi_1\rangle$ and $|\Psi_2\rangle$ closes in the thermodynamic limit $N \rightarrow \infty$ which leads to increased instability of the ground state towards fluctuations.

However, the N00N ground state is also highly unstable against perturbations. This can be understood from Figure 5.5, providing an analogy to the Ising model in two dimensions. The energetically lowest lying state $|\Psi\rangle \propto (|\uparrow\rangle - |\downarrow\rangle)$ is only a small energy ΔE apart from the first excited state $|\Psi\rangle \propto (|\uparrow\rangle + |\downarrow\rangle)$. As the energy gap closes in the thermodynamic limit (Figure 5.6), infinitesimally small fluctuations will break the symmetry of the system, resulting in a state with all particles pointing either $|\uparrow\rangle$ or $|\downarrow\rangle$. Hence, spontaneous symmetry breaking transforms the ground state from a highly entangled superposition state to a non-entangled state [49].

The concept of spontaneous symmetry breaking applies also to our studies. Choosing a finite expectation value of the spin in one direction by applying the mean-field substitutions, explicitly breaks the symmetry of the system, thus explaining why the results are characterized by the quantum Fisher information of a non-entangled state at $q = 0$ (left panel of Figure 5.4). The mean-field ground state is best described at the center of the phase whereas the relative fluctua-

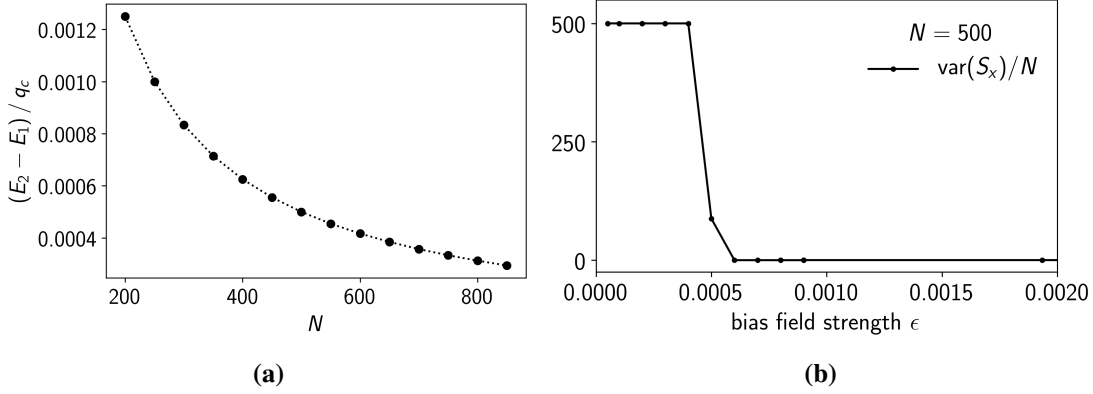


Figure 5.6.: (a) With the use of exact numerical diagonalization, we observe the strong decay of the energy gap $\Delta E = E_2 - E_1$ at $q = 0$ between the ground state and first excited state for large particle numbers ($N = 200, \dots, 850$). (b) Adding a bias field $\epsilon \hat{S}_x$ to the Hamiltonian explicitly breaks the symmetry and changes the variance of the operator \hat{S}_x from its maximal to its minimal value. The symmetry breaking happens when the bias field strength is comparable to the energy gap, here $\epsilon \approx 0.0005$ for $N = 500$ particles.

tions increase with $q \rightarrow \pm q_c$. When approaching the critical points, the order parameter \hat{S}_x of the QPTs changes continuously according to the decreasing occupation of the side modes and the central mode towards the Twin-Fock and Polar phase, respectively (Figure 5.3). It was shown that the QFI can be generally exploited as a signature for quantum phase transitions [12]. Its increasing value towards the critical points is therefore in agreement with the expectation of a scaling growth of the QFI for second-order phase transitions (left panel of Figure 5.4). This in turn can be attributed to the growth of correlations, captured by the order parameter \hat{S}_x , when approaching the QPT. A quantum Fisher information density of $F_Q/N = 1$ in the center of the phase, however, corresponds to a non-entangled state.

According to the properties of a coherent spin state aligned along \hat{S}_x , we would expect that the variance $(\Delta \hat{S}_x)^2$ and, thus, the quantum Fisher information, vanishes in the middle of the phase, as also revealed by exact numerical calculations in Figure 5.6 (b). We might attribute this discrepancy to limitations of the mean-field approach which manifest themselves in neglecting phase fluctuations, since $\hat{a}_i \rightarrow \sqrt{N} \zeta_i + \delta \hat{a}_i$. Another possibility to semi-classically expand the field operator $\hat{\Psi}_i \approx \langle \hat{\Psi}_i \rangle + \delta \hat{\Psi}_i$ arises from the phase–density representation $\hat{\Psi}_i \cong e^{i\hat{\theta}_i} \sqrt{\hat{n}_i}$, as we will explain in chapter 6. Here, the field operator can be approximated by density and phase fluctuations around the corresponding mean-field expectation value: $\sqrt{\hat{n}_i(z)} \rightarrow \sqrt{n_i(z)} + \frac{1}{2} \frac{\delta \hat{n}_i(z)}{\sqrt{n_i(z)}} - \frac{1}{8} \frac{\delta \hat{n}_i^2(z)}{\sqrt{n_i(z)^3}}$ and $e^{\pm i\hat{\theta}_i} \rightarrow e^{\pm i\theta_i} (1 \pm i\delta \hat{\theta}_i - \frac{\delta \hat{\theta}_i^2}{2})$.

Using this expansion hints at a qualitatively different quantum Fisher information in the center of the phase, as demonstrated in Figure 5.7. In order to mimic our results from above and to obtain a positive-definite Hamiltonian, as required for the Bogoliubov transformation of the state,

we add a chemical potential to the Bogoliubov modes B_i (6.20) of the quadratic Hamiltonian, i.e. $\mathcal{H} + \mu \sum_{i=\pm 1,0} B_i^\dagger B_i$. This is motivated by the notion of adding a bias field $h\hat{S}_x$ which stabilizes the fluctuations [64] and likewise contains the terms $(\sum_{\pm 1} \sqrt{\frac{n_0}{8n_1}} B_i^\dagger B_i + \sqrt{\frac{n_1}{2n_1}} B_0^\dagger B_0)$. We further compare these results to the symmetry broken state from Figure 5.4 using exact diagonalization. As shown in Figure 5.7, the variance from exact diagonalization and phase–density representation becomes zero in the center of the phase, as expected for a coherent spin state in \hat{S}_x -direction. More importantly, however, Figure 5.7 hints at a better match between mean-field and exact numerical calculations when using the phase–density representation. That is why the following studies of an one-dimensional spin-1 BEC (chapter 6) are based upon this expansion. We will see that the fluctuations in the spatially extended BEC are stabilized by the coupling via a kinetic term, with the advantage of not requiring a self-consistent treatment of the chemical potential and particle number. Already at this stage, we can therefore anticipate the strong enhancement of quantum fluctuation in the zero-dimensional (i.e. single-mode) spin-1 BEC compared to the one-dimensional, extended system as expected for low-dimensional quantum many-body systems [65].

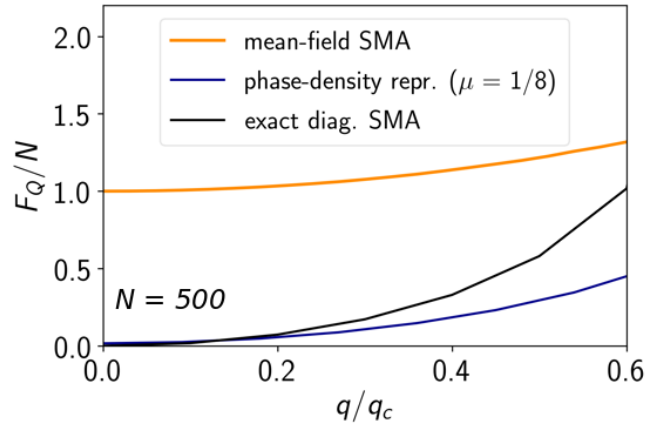


Figure 5.7.: The comparison of the quantum Fisher information from the variance of a pure state at $q = 0$, obtained from different mean-field descriptions and exact diagonalization, shows a qualitatively similar behavior with different onsets at $q = 0$. In particular, the results from the mean-field expansion of the modes ($\hat{a}_i \rightarrow \sqrt{N}\zeta_i + \delta\hat{a}_i$) differs from exact numerical calculations. However, the results from the phase–density approach is in good agreement with the exact diagonalization. Resolving the remaining discrepancies and investigating the influence of different mean-field expansions on the estimation of the QFI is a task of ongoing research.

Referring back to the results outlined in Figure 5.5, we finally elucidate whether the symmetry broken or unbroken ground state corresponds best to the physical nature of a spin-1 BEC in single-mode approximation. From our point of view, the fragile stability of the symmetry unbroken ground state will collapse at finite temperature and in the limit of large particle numbers as described above and shown in Figure 5.6. Although having established themselves as a versatile and well-controlled experimental platform, spin-1 BECs are usually not fully decoupled from the environment. They are therefore subject to fluctuations in the optical and magnetic fields which

could explicitly break the underlying symmetry. In addition to that, experiments performed so far were able to witness only a small amount of entanglement, particularly bi- and tri-partite entanglement [25, 55]. All together, we are confident that our picture of a symmetry broken ground state therefore suits experiments with spin-1 BECs in single-mode approximation rather well.

Regarding the limitations of single-mode approximation, it could be argued that it often does not reflect the experiment in the best possible way since motional and spin degrees of freedom are not fully decoupled. Furthermore, it is doubtful whether, in the context of the Eigenstate Thermalization Hypothesis [66], these systems can experience thermal relaxation. However, thermal equilibrium is a major requirement for our computation of the QFI. Besides, we did not apply the outlined quench recipe (Figure 4.4) to the single-mode approximation since the zero temperature result for the symmetry broken ground state is already an upper bound on the quantum Fisher information at finite temperatures. Thus, the already relatively weak entanglement can only further decrease for $T \geq 0$. Further efforts are therefore needed in order to fully describe multipartite entanglement in spin-1 systems beyond single-mode approximation. One natural way to overcome these limitations is by introducing spatial degrees of freedom. For the remaining part of this thesis, we will therefore study the quantum Fisher information in an one-dimensional spin-1 BEC using an extended Bogoliubov theory for quasi-condensates [13]. Therein, the above introduced phase–density representation allows one to treat the spin-1 BEC in a comprehensive description by systematic expansions in powers of the density fluctuations and of the spatial gradient of phase fluctuations.

6 Multipartite Entanglement in Spin-1 Quasi-Condensate (1D)

Low-dimensional quantum systems play a central role in the understanding of quantum matter. They show very characteristic properties associated with their geometry [65], as, for example, the enhancement of thermal and quantum fluctuations. In this way, the effective dimension has strong implications on transport properties or relaxation dynamics in quantum many-body systems. In low-dimensional Bose gases, that is with the atomic motion frozen in one or two directions, large phase fluctuations restrict the coherence length of the bosonic field to a finite value. This prohibits the forming of a condensate at finite temperature as demonstrated by D. Mermin, H. Wagner and P. Hohenberg [67, 68]. In presence of weak interactions and an anisotropic trapping potential, however, quasi lower-dimensional condensates can occur and were experimentally demonstrated [69]. They are good candidates for studying phenomena characteristic to low-dimensional quantum systems, including multipartite entanglement which is the subject to this thesis. In the following, we extend the studies from chapter 5 to the more involved one-dimensional spin-1 BEC in the Easy-Plane (EP) phase, using an extended Bogoliubov theory for quasi-condensates. We compute the amount of entanglement at finite temperatures through dynamic susceptibilities following a weak quench (4.13) as described by P. Hauke [12] and in chapter 4. Furthermore, we derive entanglement bounds relating the quantum Fisher information to k -partite entanglement for generic spin states. These bounds generalize the results of [11] to include systems of spins with non-uniform length.

6.1 Extension of Bogoliubov Theory to Spin-1 Quasi-Condensates

A powerful extension of Bogoliubov theory to quasi-condensates was derived by C. Mora and Y. Castin [13] and is based on a phase–density formalism which describes the quasi-condensate in the limit of weak interactions and low density fluctuations. It relies on the often well-founded assumption that the density fluctuations of the Bose gas are strongly reduced in presence of repulsive interactions [70, 71]. A spatial discretization is introduced in order to achieve a precise definition of the phase operator. The global phase is not necessarily conserved but phase variations are assumed to vary smoothly between two neighboring points of the lattice model. This enables a well-defined description of the underlying physics of Bose-Einstein quasi-condensates in one dimension. A major part of this thesis is to adapt the general, extended Bogoliubov theory for quasi-condensates to the special case of a spin-1 BEC, exhibiting additional spin degrees of freedom compared to single-component BECs.

6.1.1 Effective Interaction in One Dimension

We consider a spin-1 BEC as described in chapter 1 and focus for the remaining part of the thesis on an one-dimensional, elongated geometry (Figure 6.1). This geometry can be experi-

mentally accessed by using a highly anisotropic trapping potential $V(\mathbf{r}) = \frac{1}{2}(\omega_{\parallel}^2 z^2 + \omega_{\perp}^2 r_{\perp}^2)$ with much smaller longitudinal than transversal trapping frequency $\omega_{\parallel} \ll \omega_{\perp}$ [69] (Figure 6.1). Here, we choose $\omega_{\parallel} = \omega_z$ and $\omega_{\perp} = \omega_x = \omega_y$, and we may assume the ground-state wave function to be approximately separable, factorizing into a longitudinal and transversal part $\hat{\Psi}_m = \hat{\Psi}_m(z)\hat{\Psi}_{\perp}(x, y)$. The transversal wave function $\hat{\Psi}_{\perp}$ is the same for all three components and has a weak time and z -dependence. Therefore, the corresponding transversal mode energy $E_{\perp} = \int d\mathbf{r}_{\perp} \hat{\Psi}_{\perp}^{\dagger} \left[-\frac{\hbar^2}{2m} \nabla_{\perp}^2 + \frac{1}{2}m\omega_{\perp}^2 r_{\perp}^2 \right] \hat{\Psi}_{\perp}$ adds only a constant term to the Hamiltonian, which does not affect the dynamics [72] and is omitted in what follows.

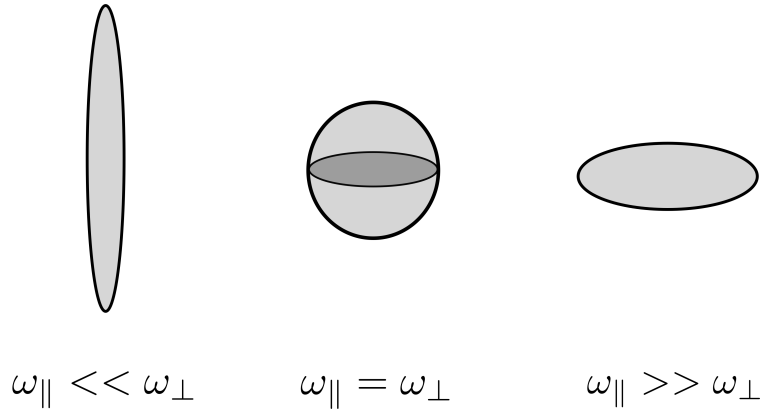


Figure 6.1.: Elongated, circular, and so-called pancake shaped trapping potential can be experimentally generated by tuning the ratio of the trapping frequencies ω_{\parallel} and ω_{\perp} . In this thesis we focus on the elongated trapping geometry which can be achieved by $\omega_{\parallel} \ll \omega_{\perp}$.

Besides, we still have to specify the interaction strength describing density-density (1.5) and spin-spin (1.6) interactions. For dilute and weakly interacting spinor Bose gases, they relate to the s-wave scattering length of the total spin- \mathcal{F} channel, $a_{\mathcal{F}}$, via $g_{\mathcal{F}} = \frac{4\pi\hbar^2}{M}a_{\mathcal{F}}$ (see also equation (1.3) and the review by Y. Kawaguchi and M. Ueda [15]). In three dimensions, the coupling constants c_0 and c_1 , which account for spin-independent and spin-dependent collisions, respectively [73] read

$$c_0^{3D} = \frac{g_0 + 2g_2}{3} \quad , \quad c_1^{3D} = \frac{g_2 - g_0}{3} . \quad (6.1)$$

The anisotropy of the one-dimensional quasi-condensate, however, changes the effective interaction strengths. The rescaled quantities used within this thesis become

$$c_i = \frac{c_i^{3D}}{2\pi a_{\perp}^2} \quad \text{with} \quad a_{\perp} = \sqrt{\frac{\hbar}{M\omega_{\perp}}} \quad \text{for } i = 0, 1 . \quad (6.2)$$

6.1.2 Discretization of Space

Following [13], we formulate the Hamiltonian (1.5)-(1.7) in terms of a discrete lattice model, that is we put the particles into small boxes with equal length l and central position z

$$\begin{aligned} \mathcal{H} = \sum_z l \left\{ \sum_m \hat{\Psi}_m^\dagger(z) \left[-\frac{\hbar^2 \nabla^2}{2m} + V(z) - \mu + q(f_z)_{mm} \right] \hat{\Psi}_m(z) \right. \\ + \frac{c_0}{2} \sum_{m,m'=-1}^1 \hat{n}_m(z) [\hat{n}_{m'}(z) - \frac{1}{l}] \\ + \frac{c_1}{2} \left([\hat{n}_1(z) - \hat{n}_{-1}(z)]^2 + [2\hat{n}_0(z) - \frac{1}{l}] [\hat{n}_1(z) + \hat{n}_{-1}(z)] \right. \\ \left. \left. + 2 \hat{\Psi}_1^\dagger(z) \hat{\Psi}_{-1}^\dagger(z) \hat{\Psi}_0(z) \hat{\Psi}_0(z) + 2 \hat{\Psi}_0^\dagger(z) \hat{\Psi}_0^\dagger(z) \hat{\Psi}_1(z) \hat{\Psi}_{-1}(z) \right) \right\}. \end{aligned} \quad (6.3)$$

The kinetic, trapping and Zeeman energy can be identified from the first row in (6.3). The term which is proportional to c_0 denotes density-density interactions, whereas spin-dependent interactions are proportional to c_1 , including spin-changing collision and terms accounting for the imbalance between the side-modes, i.e. the magnetization of the system. The field operator in phase–density representation reads

$$\hat{\psi}_i(z) \cong e^{i\hat{\theta}_i(z)} \sqrt{\hat{n}_i(z)} \quad (6.4)$$

and fulfills the commutation relations

$$\begin{aligned} [\hat{\Psi}_i(z), \hat{\Psi}_j(z)] &= \frac{i\delta_{zz'}\delta_{ij}}{l}, & [\hat{n}_i(z), \hat{\theta}_j(z)] &= \frac{i\delta_{zz'}\delta_{ij}}{l}, \\ [\hat{n}_i(z), \hat{n}_j(z)] &= 0 \quad \text{and} \quad [\hat{\theta}_i(z), \hat{\theta}_j(z)] &= 0. \end{aligned} \quad (6.5)$$

l denotes the grid spacing, $\hat{\theta}_i(z)$ the phase and $\hat{n}_i(z)$ the density of the $m_F = i$ component of the field operator at position z .

The possibility to treat space in a discretized way requires physical justification. We focus here on the restrictions relevant to a highly degenerate and weakly interacting Bose gas: Sufficiently large boxes of size l are needed in order to ensure low density fluctuations. The condition for a large mean number of particles in a box and small relative particle number fluctuations is reached [13] when

$$n_i(z) l \gg 1. \quad (6.6)$$

Furthermore, performing a coarse-grained average over all physical quantities within the grid spacing l requires l to be smaller than the characteristic length scales in order to extract the relevant physics of the system. By comparing the interaction energies from the main Hamiltonian (6.3), we can identify the characteristic length scales: The density healing length $\xi_D = \frac{\hbar}{\sqrt{2mnc_0}}$,

associated with the typical density-density interaction energy $\propto nc_0$, gives the length scale in which the density fluctuations in the BEC are removed by the interaction between condensed particles. Correspondingly, we find the spin healing length $\xi_S = \frac{\hbar}{\sqrt{2mnc_1}}$, associated with spin-spin interactions $\propto nc_1$. It describes the length scale over which the condensate heals from local defects such as vortices in 2D. Another characteristic length scale is given by the thermal de Broglie wave length $\lambda_T = \sqrt{\frac{2\pi\hbar^2}{mk_B T}}$ which describes the regime of quantum degeneracy occurring at sufficiently low temperatures. According to above, the grid spacing l is therefor subject to the following the constraints

$$l < \xi_D, \quad l < \xi_s \quad \text{and} \quad l < \lambda_T. \quad (6.7)$$

Combining the restrictions (6.6) and (6.7) imposes

$$n_i(z)\xi_D \gg 1, \quad (6.8)$$

thereby enabling the mean-field ansatz, based on sufficiently large particle number and low density fluctuations. Spinor BECs with ^{87}Rb typically feature a much smaller spin-healing length compared to the density healing length $\xi_D \ll \xi_S$ since $|c_1| \ll c_0$ [16], such that one immediately finds equation (6.8) fulfilled for the spin healing length as well. Further combining (6.6) and (6.7) imposes the validity of the discrete model in the presence of quantum degeneracy and therefore a condensate fraction in the weakly interacting dilute Bose gas

$$n_i(z)\lambda_T \gg 1. \quad (6.9)$$

6.1.3 Dimensionless Formulation

Explicit numerical calculations in this thesis are performed for a homogeneous system, which allows for considerable simplifications and is expected to contain most of the physical effects [74, 75]. We focus on a box potential with fixed boundary conditions, comparing rather well to state-of-the art experiments with spin-1 BECs as demonstrated in Figure 1.3. In general, it is very convenient to write a dimensionless description by rescaling times and lengths according to

$$\tilde{t} = \frac{t}{t_s}, \quad \tilde{x} = \frac{x}{x_s}. \quad (6.10)$$

Quantities with a tilde $\tilde{}$ are dimensionless. The choice of the scaling parameter x_s yields a corresponding time unit $t_s = \frac{mx_s^2}{\hbar}$. As a consequence, the characteristic energy unit reads $E_s = \frac{\hbar}{t_s} = \frac{\hbar^2}{mx_s^2}$. The fields rescale according to $\tilde{\Psi}_m = x_s^{d/2} \Psi_m$, where d is the spatial dimension. A typical length scale inherent to an one-dimensional Box potential ($V(z < L) = 0$) is its extension L . That is why we refer to the choice for the scaling parameters $x_s = L$ and $t_s = mL^2/\hbar$.

The above Hamiltonian (6.21) contains two types of terms. The first one, which we will refer to as E_{kin} , contains the Laplacian operator ∇^2 . The second type, denoted by E_{int} , describes either density-density or spin-spin interaction and is proportional to nc_0 or nc_1 , respectively. We straightforwardly obtain a non-dimensional form of the Hamiltonian, by rescaling the terms corresponding to the following scheme:

$$E_{\text{kin}} \rightarrow \tilde{E}_{\text{kin}} \propto -\frac{\tilde{l}}{2} \tilde{B}_m^\dagger(\tilde{z}) \tilde{\nabla}^2 \tilde{B}_m(\tilde{z}) \quad (6.11)$$

$$E_{\text{int}} \rightarrow \tilde{E}_{\text{int}} \propto \tilde{l} \tilde{n} \tilde{c}_i \tilde{B}_m^\dagger(\tilde{z}) \tilde{B}_m(\tilde{z}). \quad (6.12)$$

The dimensionless quantities are given by

$$\tilde{c}_i = \frac{c_i}{\hbar x_s / t_s}, \quad \tilde{l} = \frac{l}{x_s} \quad \text{and} \quad \tilde{n} = n x_s. \quad (6.13)$$

There is only a small range of parameters fulfilling the following two restrictions on the numerical grid spacing \tilde{l} : On one hand side, \tilde{l} should be large enough such that the phase operator still remains well-defined, which is not given in the continuous limit [13]. On the other hand, \tilde{l} should be small enough in order to resolve the density healing length. Considering computational efforts [72] and experimental realizability, we find that both constraints are best satisfied for $\tilde{l} = 1/200$ (i.e. #boxes = 200) when choosing the remaining free parameters for the particle number and interaction parameters as $N = 20000$ and $\tilde{c}_0 + \tilde{c}_1 = 1$, respectively. In addition to that, we use $\tilde{c}_0/\tilde{c}_1 = 200$, which is a typical ratio for experiments with ^{87}Rb spin-1 BECs [16]. Higher particle numbers ($N \approx 80000$ [55]), leading to smaller \tilde{l} , are desirable in order to improve the comparability with experiments, which is further discussed in subsection 6.3.1. Within the scope of this thesis, however, we do not consider smaller \tilde{l} due to a lack of computational efficiency and capacity. Nevertheless, higher particle numbers could in principle be employed in future studies. All results outlined in this chapter are therefore performed using the above set of parameters.

6.1.4 Mean-Field Description

In order to derive the mean-field ground state and thus a parametrization of the mean densities $n_i(z) = \zeta_i(z)\sqrt{n}$, we assume that all particles occupy the same single-particle state in both coordinate and spin spaces. The semi-classical expansion $\zeta_i(z)\sqrt{n}$ replaces the field operator $\hat{\Psi}_i(z)$ of the Hamiltonian (6.3) and the expectation value of the latter defines an energy functional. Minimizing this functional with respect to the condensate wave function $\zeta_m(z)\sqrt{n}$ under the normalization constraint $\sum_z \sum_m l |\zeta_m(z)\sqrt{n}|^2 = N$ allows one to deduce the order parameters $\zeta(z) = (\zeta_1(z), \zeta_0(z), \zeta_{-1}(z))^T$.

The mean-field phase diagram, defined by the magnetic order parameters ζ , is presented in Figure 6.2. In analogy to the Broken-Axisymmetry phase of a single-mode BEC, all modes are occupied in the Easy-Plane (EP) phase of the extended system. There is a first-order quantum

phase transition (QPT) towards the Easy-Axis (EA) phase, involving a discontinuous change in the mean-field parameter and therefore the density (Figure 6.3). In contrast, there is a second-order phase transitions between the Easy-Plane (EP) and Polar (P) phase, with the continuous order parameter of the side-mode population.

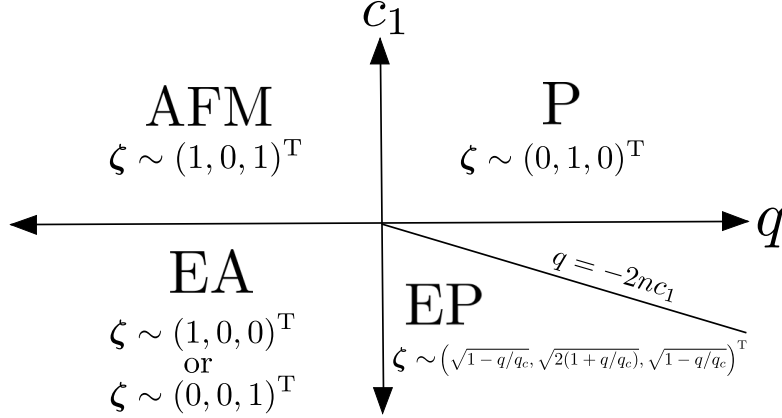


Figure 6.2.: Mean-field phase diagram of a spin-1 BEC in the (q, c_1) -plane. The mean-field ground states in the respective phases are given by $\Psi = \sqrt{n} \zeta$. The acronyms AFM, P, EA and EP denote the Anti-Ferromagnetic, Polar, Easy-Axis and Easy-Plane phase, respectively. We particularly focus on the EP phase, which is the analogue to the BA phase in the single-mode approximation (see Figure 5.1a) and which is therefore expected to exhibit a large amount of entanglement.

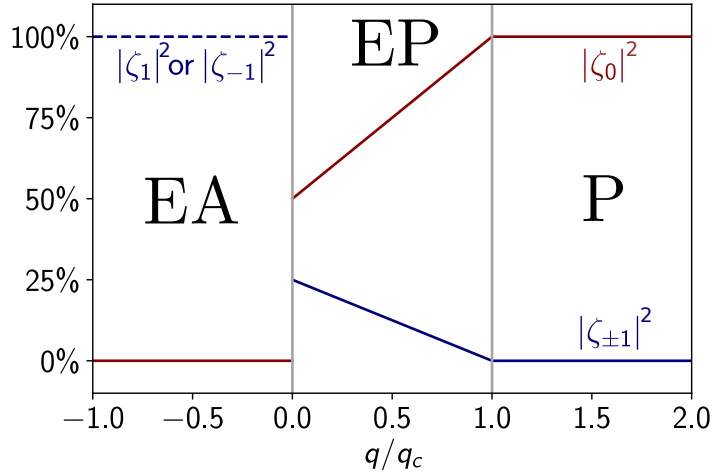


Figure 6.3.: Mean-field occupations $|\zeta_m|^2$ of the $m_F = m$ hyperfine states as a function of the magnetic field q . We observe that the density of the side modes continuously vanishes in the limit $q \rightarrow q_c$, yielding a second-order phase transition towards the Polar (P) phase. In contrast, there is a first-order phase transitions between the Easy-Plan (EP) and Easy-Axis (EA) phase, involving a discontinuous change of the mean-field occupations.

In the special case of a uniform system ($V_T(z) = 0$), the classical fields are spatially-independent and can be analytically calculated in analogy to chapter 5. For the Easy-Plane phase (Figure 6.2),

studied in this thesis, the mean-field solution is given by

$$\zeta = \frac{1}{\sqrt{2}} \begin{pmatrix} e^{-i\phi} \sqrt{\frac{1}{2} \left(1 - \frac{q}{2|c_1|n}\right)} \\ \sqrt{1 + \frac{q}{2|c_1|n}} \\ e^{i\phi} \sqrt{\frac{1}{2} \left(1 - \frac{q}{2|c_1|n}\right)} \end{pmatrix}. \quad (6.14)$$

$\phi = \theta_1 - \theta_{-1} = 2\phi_L$, with ϕ_L being the Larmor frequency, specifies the azimuthal angle of the transversal spin \hat{F}_\perp , and, thus, the direction of magnetization in the xy -plane. The mean-field values, corresponding to the occupation of the m_F -modes, is visualized in Figure 6.3.

6.1.5 Characteristic Properties

In order to benchmark the numerical calculations and gain a better understanding of the underlying physics, we briefly discuss characteristic observables within the mean-field description of an extended spin-1 BEC in the EP phase, with particular regard to correlations in the vicinity of quantum phase transitions. We first examine the transversal magnetization \hat{F}_\perp of the spin-1

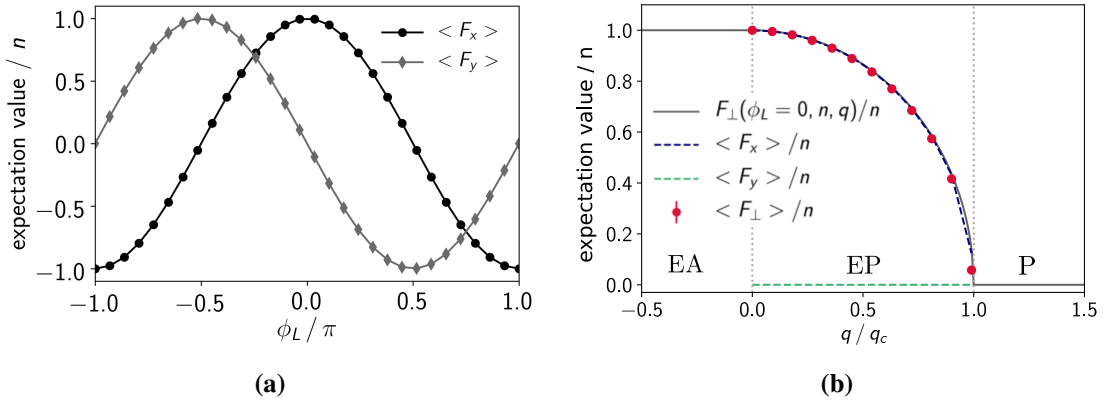


Figure 6.4.: (a) Transversal magnetization in EP phase with spinor phase $\theta_s = 0$ and Larmor phase $\phi_L = 0$, such that it is fully described by \hat{F}_x and agrees with the theoretically predicted curve from (6.15), given by the gray line in (a). As $\hat{F}_\perp = \hat{F}_x + i\hat{F}_y$, the expectation value of \hat{F}_y vanishes. \hat{F}_x therefore corresponds to the mean-field order parameter of the second-order QPT towards the Polar phase. (b) Expectation value of spin operators as a function of the Larmor phase ϕ_L . One clearly sees that the expectation values vanish when averaging over the Larmor phase (i.e. integrating from $\phi_L = -\pi$ to $\phi_L = \pi$). The dashed lines are computed from Bogoliubov theory, leading to slight deviations from the mean-field expectation value for $q \rightarrow q_c$.

BEC. According to [76], the mean-field expectation value of \hat{F}_\perp is given as a function of the magnetic field parameter q

$$\langle \hat{F}_\perp(\phi_L, n, q) \rangle = n e^{i\phi_L} \sqrt{1 - (q/q_c)^2}. \quad (6.15)$$

The Larmor phase ϕ_L rotates the direction of magnetization in the xy -plane which can be seen from Figure 6.4a. For $\phi_L = \theta_S = 0$, it follows that \hat{F}_\perp is fully determined by \hat{F}_x and attains the maximal value $\langle \hat{F}_x(q=0) \rangle = n$, reached in the EA phase, and minimal value $\langle \hat{F}_x(q=q_c) \rangle = 0$, reached in the P phase, as can be seen from Figure 6.4b.

\hat{F}_x is the order parameter of the second-order EP-P phase transition, and so is \hat{S}_x , being the analogue of \hat{F}_x in the $su(3)$ representation (1.12). As outlined above (chapter 5), extracting the QFI with respect to the order parameter is of special interest because of its scaling growth of correlations [12]. For these reasons, we use \hat{S}_x for computing the QFI in the zero temperature ground state and from the dynamics following a weak quench $\hat{\mathcal{H}} \rightarrow \hat{\mathcal{H}}_0 + \lambda \sum_z \hat{S}_x(z)$ in section 6.3

6.1.6 Bogoliubov Hamiltonian

In order to achieve a quadratic description, we first expand the Hamiltonian up to second order in fluctuations around the z -dependent mean-field solution $\zeta(z)$ for the density $n_i(z) = \zeta_i(z) n$ and the mean phase $\theta_i(z)$ according to

$$\begin{aligned} \sqrt{\hat{n}_i(z)} &\rightarrow \sqrt{n_i(z)} + \frac{1}{2} \frac{\delta \hat{n}_i(z)}{\sqrt{n_i(z)}} - \frac{1}{8} \frac{\delta \hat{n}_i^2(z)}{\sqrt{n_i(z)}^3} \\ e^{\pm i \hat{\theta}_i} &\rightarrow e^{\pm i \theta_i} \left(1 \pm i \delta \hat{\theta}_i - \frac{\delta \hat{\theta}_i^2}{2} \right) \quad \forall \quad i \in \{-1, 0, 1\}. \end{aligned} \quad (6.16)$$

One restriction characterizing this expansion is that it requires density fluctuations $\langle \delta \hat{n}_i^2(z) \rangle$ to be small in relative values. In the same manner, on-site phase fluctuations $\langle \delta \hat{\theta}_i^2(z) \rangle$ need to be small as well

$$\frac{\langle \delta \hat{n}_i^2 \rangle}{n_i^2} \ll 1 \quad , \quad \langle \delta \hat{\theta}_i^2 \rangle \ll \pi. \quad (6.17)$$

The parameter range at which these constraints are fulfilled is thoroughly studied by means of numerical calculations for the extended spin-1 BEC in subsection 6.1.7. Provided that the grid spacing l is small enough, the exponential function of the type $e^{i(\delta \hat{\theta}_i(z+l) - \delta \hat{\theta}_i(z))}$ can be expanded according to

$$e^{i(\delta \hat{\theta}_i(z+l) - \delta \hat{\theta}_i(z))} \approx 1 + i\{\delta \hat{\theta}_i(z+l) - \delta \hat{\theta}_i(z)\} - \frac{1}{2}\{\delta \hat{\theta}_i(z+l) - \delta \hat{\theta}_i(z)\}^2. \quad (6.18)$$

This means, that the phase fluctuations are allowed to vary smoothly between neighboring points. Without loss of generality, we set the mean-field phases to zero, corresponding to a vanishing spinor and Larmor phase, $\theta_s = 0$ and $\phi_L = 0$ in equation (6.14), respectively. In a second step,

we normalize the operators with respect to the density

$$\hat{X}_i(z) = \frac{\delta \hat{n}_i(z)}{2\sqrt{n_i(z)}} \quad , \quad \hat{P}_i(z) = \sqrt{n_i(z)} \delta \hat{\theta}_i(z) \quad (6.19)$$

and define the Bogoliubov modes

$$\hat{B}_i(z) = \hat{X}_i(z) + i\hat{P}_i(z) \quad \text{with} \quad \left[\hat{B}_i(z), \hat{B}_j^\dagger(z') \right] = \frac{\delta_{ij} \delta_{zz'}}{l}. \quad (6.20)$$

Using this notation, we derive the quadratic Bogoliubov Hamiltonian in a similar way as outlined in [13, 77, 75]. Omitting the operator symbols ‘‘’, the Bogoliubov Hamiltonian reads

$$\begin{aligned} \mathcal{H}^{(2)} = & \sum_z \frac{l}{2} \left(B_j^\dagger(z) \left(-\frac{\hbar^2}{2m} \nabla^2 \right) B_j(z) + \text{h.c.} \right) \\ & + \sum_z \frac{l}{2} \left\{ c_0 \sum_{i,j} \sqrt{n_i(z)n_j(z)} \left(B_i^\dagger(z) B_j(z) + B_i(z) B_j(z) + \text{h.c.} \right) \right. \\ & \quad + c_1 \sum_{i=\pm 1} n_i(z) \left(B_i^\dagger(z) B_i(z) + B_i(z) B_i(z) + \text{h.c.} \right) \\ & \quad - c_1 \sum_{\substack{i=\pm 1 \\ i \neq j}} n_i(z) \left(B_i^\dagger(z) B_j(z) + B_i(z) B_j(z) + \text{h.c.} \right) \\ & \quad \left. + 2c_1 \sum_{j=\pm 1} \sqrt{n_0(z)n_j(z)} \left(B_0^\dagger(z) B_j(z) + B_0(z) B_j(z) + \text{h.c.} \right) \right\} \\ & + \sum_z \frac{l}{2} \left\{ -c_1 n_0(z) \sum_{i=\pm 1} \left(B_i^\dagger(z) B_i(z) + \text{h.c.} \right) - 4c_1 n_1(z) \left(B_0^\dagger(z) B_0(z) + \text{h.c.} \right) \right. \\ & \quad + 2c_1 \sum_{j=\pm 1} \sqrt{n_0(z)n_j(z)} \left(B_0^\dagger(z) B_j(z) + B_0(z) B_j(z) + \text{h.c.} \right) \\ & \quad + 2c_1 \sum_{j=\pm 1} \sqrt{n_0(z)n_j(z)} \left(B_0^\dagger(z) B_j(z) + B_0(z) B_j^\dagger(z) - B_0(z) B_j(z) - B_0^\dagger(z) B_j^\dagger(z) \right) \\ & \quad \left. + 2c_1 n_0 \left(B_1^\dagger(z) B_{-1}^\dagger(z) + \text{h.c.} \right) \right\}. \quad (6.21) \end{aligned}$$

The discrete Laplacian is a symmetric operator that couples different neighboring boxes through the kinetic term

$$\nabla^2 B(z) = \frac{1}{l^2} [B_i(z+l) + B_i(z-l) - 2B_i(z)]. \quad (6.22)$$

6.1.7 Density and Phase Fluctuations

The validity of the extended Bogoliubov theory performed in this thesis is ensured by permitting only small fluctuations on top of the mean-field ground state, as defined in (6.17). However, the fluctuations also depend on the number of grid points. This is due to the fact that the phase operator does not remain well-defined in the continuous limit $l \rightarrow 0$ [13], which is revealed by

the divergence in Figure 6.5. $1/l = 0.005$ corresponds to the parameter we are using. There, the constraint $\langle \delta\hat{\theta}_i^2 \rangle \ll \pi$ is still fulfilled for a broad range of quadratic Zeeman shifts q .

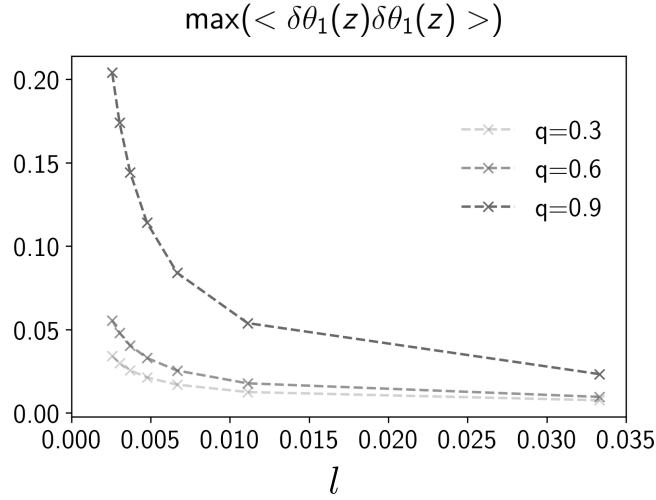


Figure 6.5.: The scaling of phase fluctuations is highly sensitive on the choice of the grid spacing l and diverges in the continuous limit $l \rightarrow 0$. We choose $l = 0.005$ for our computations, which remains well-defined for most magnetic field parameter values.

With this, we thoroughly study the behavior of density and phase fluctuations as a function of the magnetic field parameters in Figure 6.6. In the limit of small densities, the mean-field assumptions generally break down and give rise to large relative fluctuations. Approaching the Polar phase ($q \rightarrow q_c$), the population of the side modes ($n_1 = n_{-1}$) continuously decreases to zero as depicted in Figure 6.3. Correspondingly, the phase and density fluctuations of the side modes increase, as shown in Figure 6.6. We have checked that the inter-component and density-phase fluctuations are much smaller than the density and phase fluctuations of the same hyperfine state. The scaling of the relative density fluctuations when approaching the EP-P phase transition on the right pannel of Figure 6.6 indicates, that the relative density fluctuations become larger than 10% for $q/q_c \geq 0.8$, thereby violating the constraint (6.17). That is why we define the regime at which the mean-field assumptions are still well-founded as $0 \leq q/q_c \leq 0.8$.

A very similar behavior is observed for the spatial correlations of the density and phase fluctuations, depicted in Figure 6.7 and Figure 6.8, respectively. Here, we examine the correlations between the density/phase fluctuations at the center of the trap and the rest. We observe that the density correlations decay at shorter distances compared to the phase correlations. This is due to the fact that the box length is of the order of the density healing length. On the contrary, by applying the characteristic expansion in small neighboring phase fluctuations (6.18), we allow the fluctuations to vary smoothly from one lattice point to another.

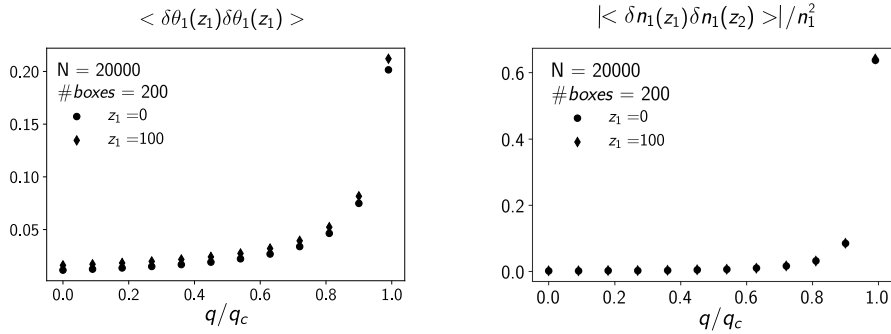


Figure 6.6.: Fluctuations increase with decreasing density. Since the side-mode populations strongly decrease upon approaching the QPT towards the Polar phase, both density and phase fluctuations strongly increase with the magnetic field parameter $q \rightarrow q_c$. This hints at a break-down of the extended Bogoliubov theory in this regime.

At this stage, it is also important to mention that the outlined extended Bogoliubov theory [13] allows the correlations of the phase fluctuations to vanish at long distances, as can be seen in Figure 6.8. Accordingly, phases far apart from each other can arbitrarily fluctuate. This does not necessarily match the phase properties of an elongated spinor BEC, where the trapping geometry stabilizes the phases, being tightly related to each other via the spinor phase. In principle, a full three-dimensional treatment of the elongated BEC would be necessary in order to model this behavior. However, we consider the fluctuations around the phase difference (given by the spinor phase), to vary smoothly along the trap, and therefore, the extended Bogoliubov theory to describe the underlying physics of spinor BECs in the low-dimensional limit rather well. Moreover, it allows for a comprehensive description through the expansions in density fluctuations and the spatial gradient of phase fluctuations. That is why it is still highly preferred to treat the spin-1 BEC in the extended Bogoliubov theory.

To summarize, we have analyzed the mean-field phase diagram and introduced an extended Bogoliubov theory in order to make ourselves familiar with the underlying physics of a spin-1 quasi-condensate and derive an appropriate mathematical description. Furthermore, we have discussed a numerical implementation of the system and studied characteristic quantities as a benchmark. Finally, we have looked at the behavior of phase and density fluctuations in order to assess the validity of the method and to describe the physics in the EP phase. We have estimated the regime $0 \leq q/q_c \leq 0.8$ at which the mean-field assumptions are well-founded. With this, we have built a framework to determine the amount of entanglement in a spin-1 BEC, which is the final goal of this thesis. To this end, we first derive entanglement bounds relating the quantum Fisher information to the entanglement content of a spatially discretized spin configuration in the upcoming section. This approach is then extended to a spin-1 BEC on a spatial grid as described above. In this way, we finally extract the multipartite entanglement content of the system at both zero and finite temperature in section 6.3.

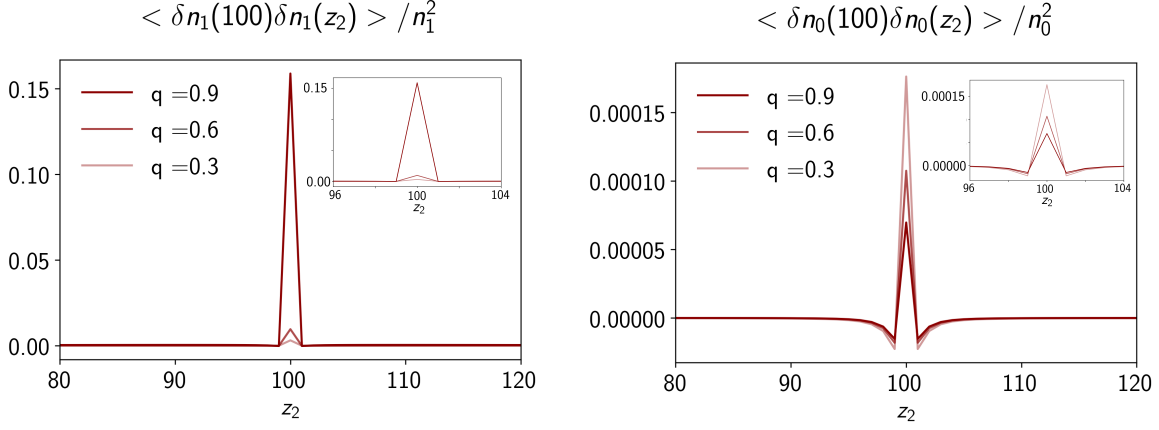


Figure 6.7.: Density fluctuations are uncorrelated everywhere except at very short distances, which is consistent with our parametrization, choosing the density healing length of the order of the grid spacing. Since the relative fluctuations increase with decreasing occupation of the modes, we observe stronger correlations of the side-mode density fluctuations when approaching the Polar phase, i.e. $q \rightarrow q_c$ on the right panel. The same holds for the correlations of the central mode density fluctuations when $q \rightarrow 0^+$.

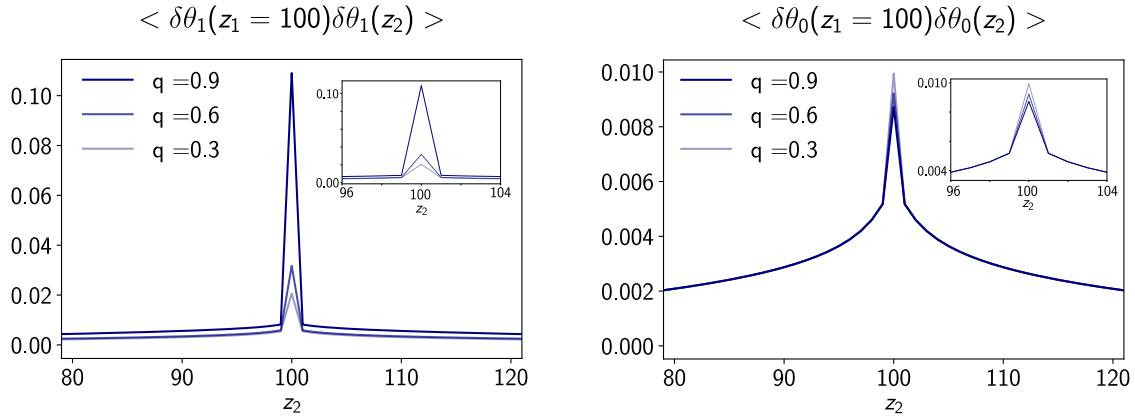


Figure 6.8.: The spatial correlations of phase fluctuations are required to vary smoothly between neighboring points, and thus show increased correlations as compared to the density fluctuations. However, at large distance they become approximately uncorrelated. In line with the arguments from Figure 6.7, we observe stronger phase correlations of the $m_F = \pm 1$ and $m_F = 0$ mode when approaching $q \rightarrow q_c$ and $q \rightarrow 0^+$, respectively.

6.2 Entanglement Bounds for Spin Systems

Treating the spin-1 BEC in a discrete way amounts to grouping spinful bosons together into small boxes. Thereby, the number of bosons and the orientations of their spins might vary between different boxes. Neglecting the spatial substructure within each box, the system can be described as a state of collective spins of different length, coupled to each other. So far, only bounds for the entanglement among uniform spins has been derived [11]. One question that therefore naturally arises is, how entanglement bounds for generic states of distinct spins can be derived? And even further, how can this in turn be applied to a distribution of spinful bosons on a spatial grid?

In order to answer this question, we first derive a generic bound for k -partite entanglement among N_s different spins. Second, we use this result to compute entanglement bounds of a spinor BEC for any desired particle distribution on an one-dimensional spatial grid.

6.2.1 Generic Configuration of Quantum-Mechanical Spins

As outlined in section 3.2, the best possible interferometric phase estimation using a linear, hermitian operator \hat{O} is given by the largest spread in eigenvalues λ according to

$$\left(\Delta\hat{O}\right)^2 \leq \frac{[\lambda_{\max} - \lambda_{\min}]^2}{4}. \quad (6.23)$$

If \hat{O} is a spin operator of a spin- s system¹, the largest and smallest eigenvalue is given by $+s$ (*all spins up*) and $-s$ (*all spins down*), respectively, which maximizes the quantum Fisher information for a pure state $F_Q = 4(\Delta\hat{O})^2$. According to that, it has been shown that $k + 1$ -partite entanglement is witnessed in a system of N_s spins of equal length s by

$$F_Q/N_s > 4 k s^2 \quad (6.24)$$

apart from corrections for commensurability [11]. In the following, we investigate how this entanglement bound generalizes to systems of N_l distinct spins with $l = 1 \dots N_s$ as sketched in Figure 6.9.

Applying the notion of k -producible states from section 3.1 to a state of N_s spins of different length (Figure 6.9), the system can be partitioned in many ways by merging different spins together. We define the partition $\mathcal{G} = \{g_i\}$ containing the groups g_i with $|g_i| < k$ spins, as shown in Figure 6.9. The cardinality of the partition $|\mathcal{G}| = G$ gives the number of groups. In this

¹In this case, the operator \hat{O} needs to be constructed from the underlying $su(n)$ algebra. The Gell-Mann operators from the $su(2)$ subspaces of the $su(3)$ algebra (1.11) fulfill these properties despite with the exception of G_8 which requires the correct normalization.



Figure 6.9.: Configuration of N_s distinct spins, which can be partitioned in different groups (here shown is the example of one group, labeled g_1). For the sake of simplicity, all spins in this sketch are pointing in the same direction. This picture can be straightforwardly expanded to the below discussion of spinful bosons on a spatial grid (subsection 6.2.2), where the spins s_1, s_2, \dots simply refer to the collective spin of the particles within a box.

manner, the generic spin state can be written as a product state

$$|\Psi\rangle = \bigotimes_{i=1}^G |\Psi_i\rangle. \quad (6.25)$$

Assuming a local spin operator \hat{O}_i acting on the individual spin s_i of a spin- s system in analogy to (3.11), the QFI with respect to the i -th group is given by

$$F_Q \left[|\Psi_i\rangle, \hat{O}_i \right] = 4 \left(\underbrace{\sum_{l \in g_i} s_l}_{S_i} \right)^2. \quad (6.26)$$

We call $S_i = \sum_{l \in g_i} s_l$ the accumulated spin of the i -th group. Optimizing over all possible choices of partitions with $g_i \in \mathcal{G}$, the bound for the QFI reads

$$F_Q \leq \max_{\{\mathcal{G}\}} \left(\sum_{i=1}^G F_Q \left[|\Psi_i\rangle, \hat{O}_i \right] \right) = \max_{\{\mathcal{G}\}} \left[4 \sum_{i=1}^G \left(\underbrace{\sum_{l \in g_i} s_l}_{S_i} \right)^2 \right]. \quad (6.27)$$

But what is the optimal configuration of groups that maximizes F_Q ?

A glance at Figure 6.10 provides an intuitive picture for the guideline towards answering this question. Consider the following imagined procedure: We start with an arbitrary initial configuration of N_s spins and cluster them in $G - 1$ groups of k spins and one group with the remaining r spins, so $N_s = k \lfloor \frac{N_s}{G-1} \rfloor + r$. The next step is to pick two of the groups, S_1 and S_2 with $S_1 \geq S_2$, and optimize (6.27) in order to achieve the maximal possible QFI of the k -producible state by interchanging spins among the two groups. This is illustrated on the example of panel i.) in Figure 6.10: Without loss of generality the groups are ordered according to the size of their accumulated spin, i.e. $S_1 \geq S_2 \cdots \geq S_G$. Step ① takes the largest spin of the second group, denoted by s_{long} , and interchanges it with the smallest spin of the first group, called s_{short} , thereby modifying the accumulated spin according to $S_1 \rightarrow \tilde{S}_1$ and $S_2 \rightarrow \tilde{S}_2$. The optimization imme-

diately follows from.

$$\begin{aligned}\tilde{S}_1^2 + \tilde{S}_2^2 &= (S_1 - s_{\text{short}} + s_{\text{long}})^2 + (S_2 - s_{\text{long}} + s_{\text{short}})^2 \\ &= S_1^2 + S_2^2 + 2(s_{\text{long}} - s_{\text{short}})^2 + 2(S_1 - S_2)(s_{\text{long}} - s_{\text{short}}) \geq S_1^2 + S_2^2\end{aligned}\quad (6.28)$$

In a similar manner, S_{G-1}^2 is optimized by filling the group g_{G-1} up with the largest spin from the group g_G , as described by step ②. Panel ii.) shows the new spin configuration which is going to be iteratively optimized from here on by repeating the interchange of spins as, for instance, shown in step ③. Since the optimization procedure does not depend on the initial configuration of the spins, it always converges to the optimal configuration $\tilde{S}_1^{\text{opt}} \geq \tilde{S}_2^{\text{opt}} \geq \dots \geq \tilde{S}_G^{\text{opt}}$ given in panel iii.) of Figure 6.10. By ordering also the individual spins according to their lengths $s_1 \geq s_2 \dots \geq s_{N_s}$, the optimal partition $\mathcal{G}^{\text{opt}} = \{g_i^{\text{opt}}\}$ is given by

$$g_i^{\text{opt}} = \{s_{k(i-1)+1}, \dots, s_{ki}\}, \quad (6.29)$$

for at most k spins within each group, i.e. $|g_i^{\text{opt}}| \leq k$. Thus, the first group g_1 contains the k largest spins, g_2 the next k largest spins, and so on. The last group g_G contains the r smallest spins. A heuristic explanation, why precisely this is the optimal spin configuration, is given by the quadratic scaling of the quantum Fisher information with the spin length. Rewriting (6.26) for the optimal grouping yields the maximal quantum Fisher information achievable

$$F_Q \leq \left[4 \sum_{i=1}^G \left(\underbrace{\sum_{l \in g_i^{\text{opt}}} s_l}_{\tilde{S}_i^{\text{opt}}} \right)^2 \right] \quad (6.30)$$

and k -partite entanglement is witnessed by²

$$F_Q > 4 \sum_{i=1}^G \left(\sum_{l=1}^k s_{k(i-1)+l} \right)^2 \quad \longrightarrow \quad \text{at least } k+1 \text{-partite entangled.} \quad (6.31)$$

Thus, optimizing for the accumulated spin within each group also maximizes the quantum Fisher information. Taking $G = N_s/k$ for $r = 0$, we immediately identify the bound (6.24) for $k+1$ -partite entanglement in a system of N_s equal spins from $F_Q > 4(N_s/k)(ks)^2 \iff F_Q/N_s > 4ks^2$.

²If the last group contains only r spins, we simply add $k-r$ spins of length 0 to the group, such that the second sum in (6.31) remains well-defined.

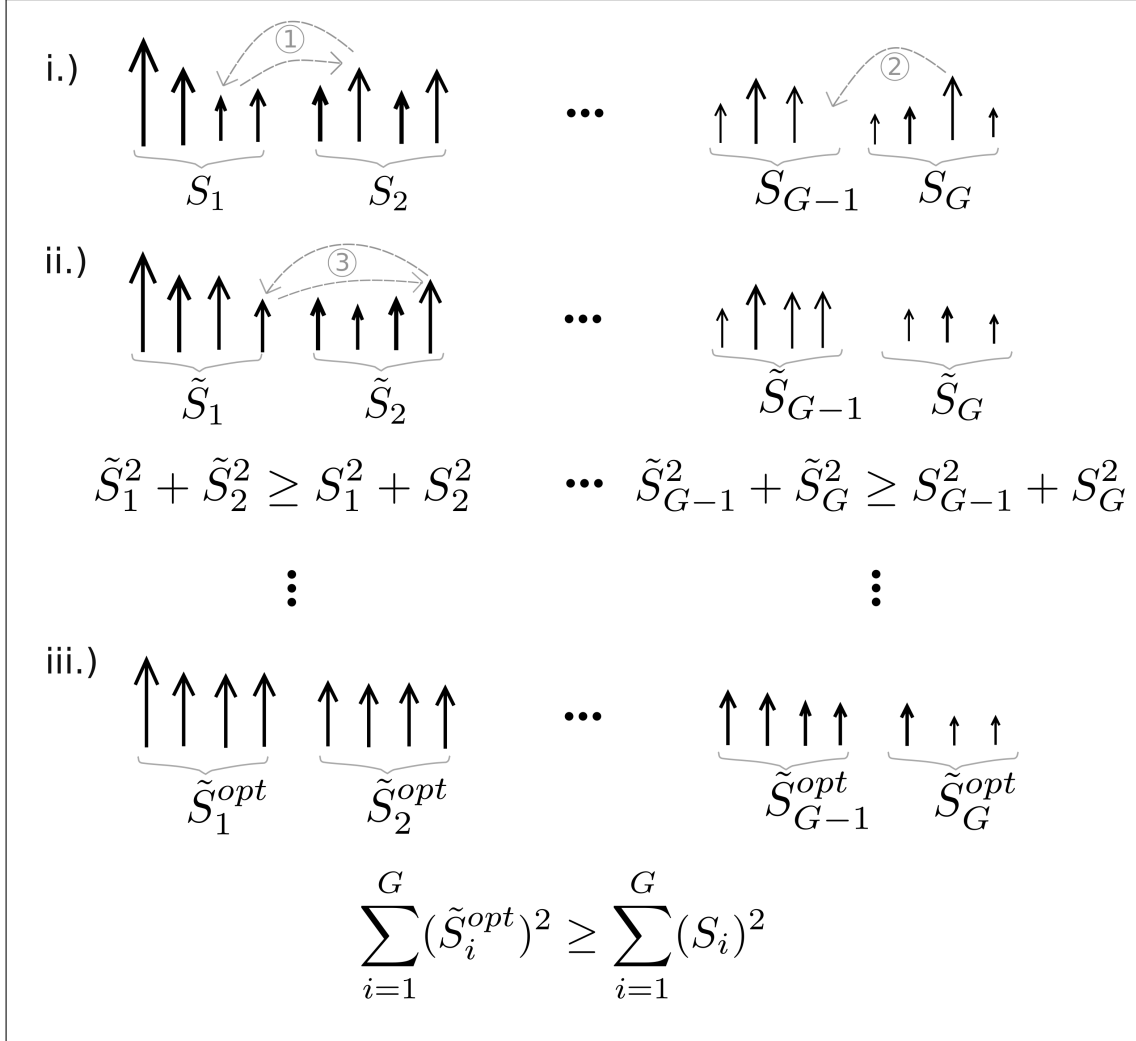


Figure 6.10.: Outline for finding the spin configuration that maximizes the quantum Fisher information. This procedure essentially optimizes the collective spin length of each group by the interchange of spins. The optimal configuration for k -partite entanglement (6.29) corresponds to a state where the k largest spins are contained in the first group, the next k largest spins in the second group and so on. The meaning of the optimization steps i.) - iii.) is explained in detail in the main text.

6.2.2 Spinor BEC on a Spatial Grid

It is straightforward to extend this analysis to a spatial distribution of spinful bosons, which is especially relevant in view of experiments with spinor BECs. As outlined in section 6.1, the mathematical approach for describing these systems is based on putting the BEC on a discrete lattice model, where N particles are grouped within N_B boxes (Figure 6.11). In experiments, one-dimensional geometries are typically achieved with an elongated, harmonic trapping potential such that the density is largest at the center and smallest at the edge of the trap. Time-of-flight absorption imaging maps the density distribution onto the pixel grid of a CCD camera, where the observables and correlations are averaged within a the single pixel. This is in analogy to our approach of putting the BEC onto small boxes, thereby assuming that the spatial substructure within each box is irrelevant³ and therefore best described by a collective spin akin to the single-mode approximation. In comparison to experiments⁴, the grid spacing can be seen as the resolution of the imaging process. In this case, the outlined approach can be straightforwardly employed to find experimentally relevant bounds on the quantum Fisher information. In simple terms, it boils down to the question of how many boxes are entangled with each other given a specific distribution of spinful bosons.

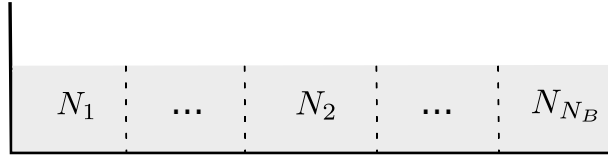


Figure 6.11.: The spin-1 BEC can be partitioned in N_B boxes of unit length such that the l -th box contains N_l particles.

The largest bandwidth in eigenvalues, so to say the spin length of each box, is simply given by the number of particles contained in this box. We can therefore exchange s_l by the number of particles N_l in (6.31). For the sake of simplicity, we assume again that the particle numbers N_l with $l = 1 \dots N_B$ are ordered according to their size

$$N_1 \geq N_2 \geq \dots \geq N_{N_B}, \quad (6.32)$$

such that N_i corresponds to the i -th largest particle number. In total, there are G groups g_i^{opt} , acquiring the same structure from above, such that g_1^{opt} contains the k largest particle numbers. By straightforwardly mapping the particle number of the spinful bosons to the collective spin of

³This is due to the fact that the density healing length was chosen on the order of the grid spacing.

⁴Considering for example an atom cloud of $200 \mu\text{m}$, 200 boxes and a resolution below $1 \mu\text{m}$ [55].

each box, the quantum Fisher information from above (6.31) becomes

$$F_Q > 4 \sum_{i=1}^G \left(\sum_{l=1}^k N_{k(i-1)+l} \right)^2 \longrightarrow \text{at least } k+1 \text{ - partite entangled.} \quad (6.33)$$

Homogeneous Limit

In the case of a box potential, which can be approximately met in experiments (Figure 1.3), the homogeneous density distribution is characterized by $N_i = \bar{N} = \frac{N}{N_B} \forall 1 \leq i \leq N_B$. The Fisher information for a spin-1 system is then bounded by

$$F_Q \leq \max \left[4 \bar{N}^2 \sum_i |g_i|^2 \right], \quad (6.34)$$

where $|g_i|$ is the cardinality of the i -th group of boxes. For a k -producible state, $\sum_i |g_i|^2$ is bounded as well

$$\sum_G |g_i|^2 \leq dk^2 + r^2, \quad (6.35)$$

where $d = \lfloor \frac{N_B}{k} \rfloor$ is the integer divisor of N_B by k and $r = N_B - dk$ is the rest [11]. Equation (6.35) can be optimized by having as many $|g_i| = k$ as possible. For simplicity, we assume $r = 0$. However, calculations can be straightforwardly extended to $r \neq 0$. Inserting (6.35) into (6.34) and using $\bar{N} = N/N_B$, the following rule is obtained

$$\frac{F_Q}{N_B} > 4 \bar{N}^2 k \implies k+1 \text{ - partite entanglement.} \quad (6.36)$$

This is a generic bound, which can be straightforwardly expanded to $k+1$ - partite entanglement of a spin- s systems if $F_Q/N_B > 4 \bar{N}^2 s^2 k$. We identify the analogy to the bound for uniform spins (6.24) by comparing the mean spin length per box $\bar{N}s$ with the spin s and the number of boxes N_B to the number of spins N_s .

According to above, m -partite entanglement corresponds to a partition as suggested in (6.32), where the first group contains the k largest particle numbers and the last group contains the k smallest particle numbers. Examples for the spin-1 BEC are:

$$k = 1 : \quad \text{separable state, no entanglement} \implies F_Q \leq 4 (\bar{N})^2 N_B$$

$$k = 2 : \quad \text{at least bipartite entangled} \implies F_Q > 4 (\bar{N})^2 N_B \quad (6.37)$$

$$k = 3 : \quad \text{at least tripartite entangled} \implies F_Q > 8 (\bar{N})^2 N_B \quad (6.38)$$

⋮

$$k = N_B : \quad N_B \text{ -partite and maximally entangled} \implies F_Q = 4 (\bar{N})^2 N_B^2 = 4N^2$$

As one can see, the Heisenberg limit is reached and the upper bound (6.23) is met in the case of a fully entangled state. This corresponds to a state where all boxes are entangled with each other. One minor limitation of this approach is that it does not take the entanglement among the particles within a box into account, however, this resembles the coarse-graining process of typical experimental measurements based on absorption imaging.

To conclude, the physical implication of (6.31) is that the largest value of the Fisher information for an arbitrary configuration of spins of different length is achieved by successively maximizing the spin length for each group within the partition. By putting the BEC into small boxes in accordance with the outlined extended Bogoliubov theory [13], the system can be described within the notion of collective spin states. The bounds for an arbitrary configuration of spins is then extended to bounds for a general distribution of spinful bosons on a spatial grid. In this way, we derived experimentally relevant bounds relating the quantum Fisher information to the multipartite entanglement content of a spin-1 BEC for both homogeneous and inhomogeneous particle distributions. Along with the extraction of the QFI from quench dynamics and the calculation of correlation functions using Bogoliubov theory, it completes the set of requirements that we need in order to connect the quantum Fisher information with the amount of entanglement in the spin-1 system. Using the derived bounds for a homogeneous density distribution (6.36), we compute the QFI for a pure state at $T = 0\text{K}$ and for a mixed state at finite temperatures through dynamical susceptibility using (4.13) in the following section.

6.3 Signatures of Multipartite Entanglement in spin-1 BECs

We start out with computing the quantum Fisher Information at zero temperature from the variance of the global operator $\sum_z \hat{S}_x(z)$, which is the order parameter of the second-order EP-P quantum phase transition (Figure 6.4b)

$$F_Q = 4 \left\{ \Delta \left(\sum_z \hat{S}_x(z) \right) \right\}^2 = 4 \left\{ \left\langle \sum_z \hat{S}_x(z) \sum_{z'} \hat{S}_x(z') \right\rangle - \left\langle \sum_z \hat{S}_x(z) \right\rangle^2 \right\}. \quad (6.39)$$

In a second step, we compute the quantum Fisher information through dynamic susceptibilities after a weak, global quench $\hat{\mathcal{H}} \rightarrow \hat{\mathcal{H}}_0 + \lambda \sum_z \hat{S}_x(z)$ as outlined in section 4.2. The time-dependent observable $\langle \sum_z \hat{S}_x(z)(t) \rangle$ corresponds to the linear response from which the QFI is calculated by integrating over temperature-dependent functions as given by equation (4.13) and depicted in Figure 4.2. For both ways of calculating the QFI with respect to the operator $\sum_z \hat{S}_x(z)$, the latter is expanded up to second order in fluctuations in analogy to equation (6.16) and chapter 5.

After having computed the QFI, we apply the entanglement bounds (6.36) in order to relate the variance (6.39) to k -partite entanglement. The results are presented in Figure 6.12 and Figure 6.13 and can be summarized as follows: There is a growth of entanglement witnessed by the

QFI with respect to \hat{S}_x when approaching the Polar phase as we would expect for this second-order quantum phase transition [12]. In the same manner, there is no entanglement witnessed close to the EA-EP transition, which agrees with our expectations for a first-order QPT with discontinuous change in the density at zero magnetic field $q = 0$. The amount of entanglement grows continuously with increasing field strength q up to 50-partite entanglement for $q/q_c \approx 0.8$. In addition to that, it is important to note that the mean-field Bogoliubov approximation is valid at $q \rightarrow 0^+$, but breaks-down when $q \rightarrow q_c$.

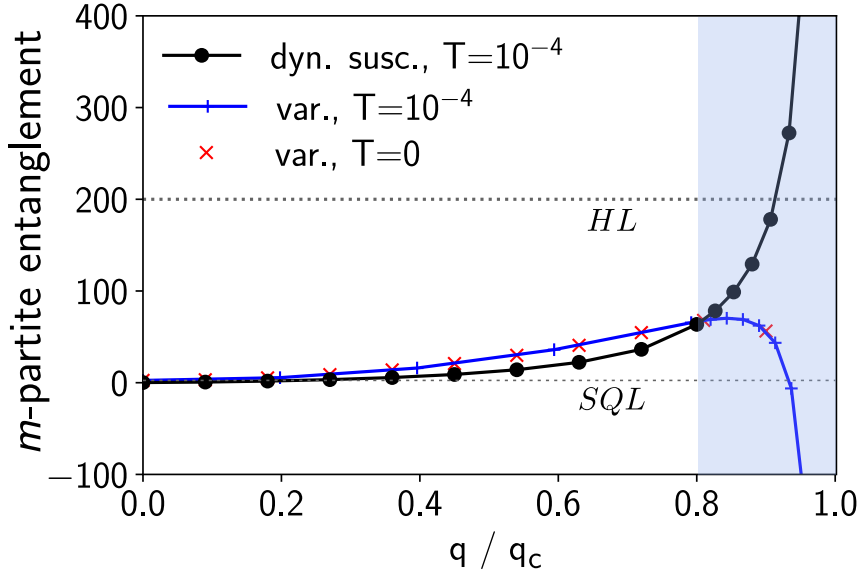


Figure 6.12.: Zero temperature limit of multipartite entanglement computed from quantum Fisher information of spin-1 BEC in EP phase through dynamical susceptibilities (dyn. susc.) and the variance (var.) of a pure state at $T \rightarrow 0$. SQL denotes the standard quantum limit and HL the Heisenberg limit, giving the lower and upper bound for multipartite entanglement in the system. The graph therefore shows an increased multipartite entanglement between the boxes for $0 \leq q/q_c \leq 0.8$. Due to a strong presence of density fluctuations (Figure 6.6), the underlying assumptions of the extended mean-field Bogoliubov theory are considered to be violated in the shaded region.

For a more detailed discussion, we first focus on the zero temperature limit of the QFI given in Figure 6.12. In general, the multipartite entanglement calculated from dynamic susceptibilities and the variance shows a similar behavior in the limit of $T \rightarrow 0$ for moderate magnetic field parameters. For $q/q_c > 0.8$, however, the curves strongly diverge. It is highly doubtful whether the underlying physics can be still described within our framework of extended mean-field Bogoliubov theory in the shaded region of Figure 6.12. Diverging fluctuations (Figure 6.6) arise naturally due to the vanishing density of the side modes (Figure 6.3) close to the EP-P quantum phase transition. The essential assumptions, namely small density fluctuations in relative values ($\langle \delta \hat{n}_i^2 \rangle / n_i^2 \ll 1$) and a sufficient mean-field density compared to the grid spacing (6.6)- (6.8), are violated. Furthermore, higher-order correlations were not incorporated into the calculation

of the variance via Wick's theorem. That is why the negative variance shows that these correlations can not be neglected anymore and, thus, that the mean-field assumption becomes invalid⁵. All in all, this may explain why the quantum Fisher information takes unreasonable values for $q/q_c > 0.9$ in Figure 6.12.

However, there remains also a small difference between the QFI from quench dynamics at small temperatures and the variance of the pure state at intermediate q values which we would expect to vanish in the limit of zero temperature. At the present time, we do not have a conclusive explanation for this discrepancy. Although having performed broad numerical checks we can not fully excluded subtle differences between the numerical integration of the time-evolved state and the calculation of the variance. Moreover, the computation of higher-order correlation functions could be improved in future studies by using the cumulant expansion outlined in A.6.

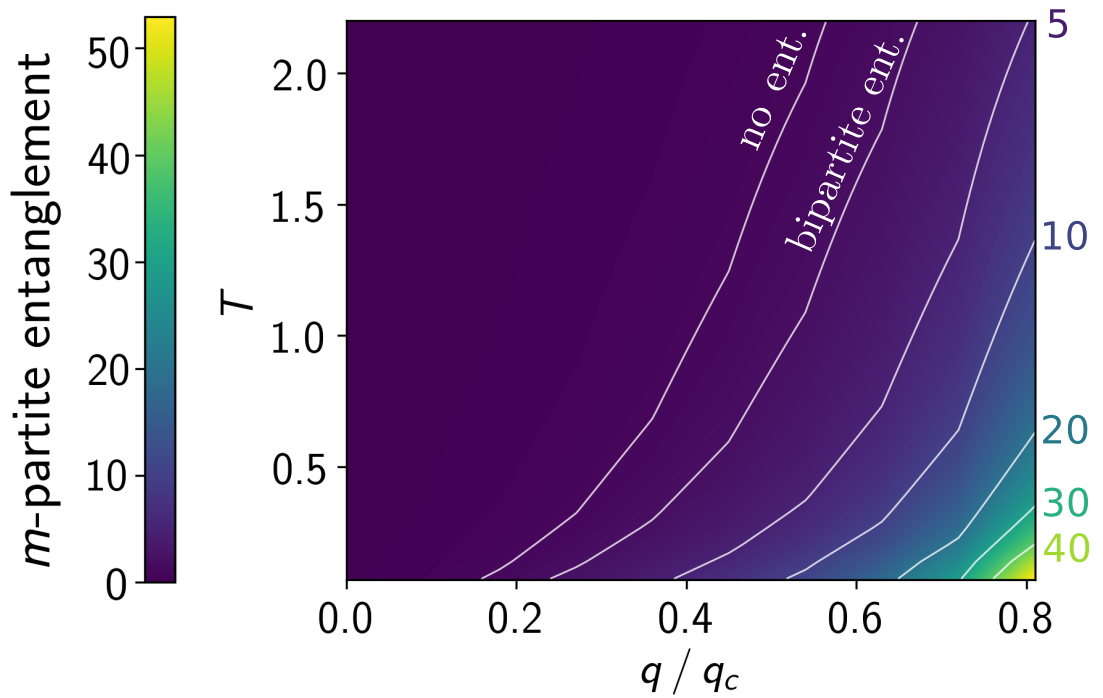


Figure 6.13.: Presence of multipartite entanglement in EP phase of spin-1 BEC at finite temperature. The amount of entanglement was computed from the quantum Fisher information with respect to the operator $\sum_z \hat{S}_x(z)$ through dynamical susceptibilities following a weak quench $\hat{\mathcal{H}} + \lambda \sum_z \hat{S}_x(z)$. At least bipartite entanglement is witnessed in large parts of the phase diagram. Stronger, up to 50-partite entanglement, is found for low temperatures and large magnetic field parameters. The entanglement vanishes for temperatures on the order of the characteristic energy scale due to increased thermal fluctuations.

⁵To be precise, the negativity arises from the fact that 4-th order fluctuations of the form $\langle \delta \hat{O} \delta \hat{O} \delta \hat{O} \delta \hat{O} \rangle$ were neglected compared to the term $\langle \delta \hat{O} \delta \hat{O} \rangle^2$ which is subtracted through the squared expectations value in the computation of the variance.

The heatmap in Figure 6.13 extends the analysis of multipartite entanglement to finite temperatures. The finite temperature QFI shows a very similar dependence on the magnetic field parameter q . There is multipartite entanglement witnessed in a large part of the phase diagram. As expected, the amount of entanglement decreases with the temperature until vanishing at temperatures on the order of the characteristic energy⁶ of the system. This is a typical finding [53, 12], since at this temperature scale large thermal fluctuations destroy the correlations in the system which can be readily seen from expanding (3.10) for large temperatures. Regardless finite temperature effects, one limitation of this approach is the extraction of the entanglement content for larger q -values. It suffers from the same limitations associated with the break-down of the mean-field assumption due to diverging quantum fluctuations. The latter invalidates the method in the regime $q/q_c > 0.8$, but we observe an increased multipartite entanglement between the boxes for $0 \leq q/q_c \leq 0.8$ in Figure 6.13.

Last but not least, one major question that naturally arises from our results is, how the simulated data compares to the experiment.

6.3.1 Experimental Considerations

First, it is important to note a difference between the numerical calculation of the variance and a typical experimental measurement, where the Larmor Phase $\phi_L = (\theta_1 - \theta_{-1})/2$ between the $m_F = -1$ and $m_F = 1$ component cannot be controlled [55, 22]. In this regard, the repetitive measurement of the observable averages over ϕ_L , which takes a random value between $-\pi$ and π . Consequently, the expectation value from many measurements vanishes $\int d\phi_L \langle \hat{S}_x(\phi_L) \rangle = 0$ as can be seen from Figure 6.4a. One has therefore to clearly distinguish between the typically measured variance $(\Delta \sum_z \hat{S}_x(z))^2 = \sum_{zz'} \int \frac{d\phi_L}{2\pi} \langle \sum_z \hat{S}_x(z) \sum_{z'} \hat{S}_x(z') \rangle - (\sum_z \int \frac{d\phi_L}{2\pi} \langle \hat{S}_x(z) \rangle)^2$, presented in Figure 6.14, and the quantum Fisher information from equation (6.39). Although, correlations up to N^2 could in principle be experimentally observed [55], they do not necessarily witness a large amount of entanglement. For these reasons it is important to take care of this subtle difference when evaluating experimental data. Since the correspondence of the variance and the QFI is only valid for pure states at $T = 0K$, we focus here on the discussion of the experimentally more interesting case of extracting the QFI for a thermal state through dynamic susceptibilities.

In order to thoroughly study the general applicability of a measurement protocol based on dynamical susceptibilities, we connect the dimensionless parameters used in this thesis with experimental parameters. The length scale x_s , corresponding to the extension of the box potential, fixes all other scales. Energies and temperatures are therefore given in terms of $E_s = \frac{\hbar}{t_s} = \frac{\hbar^2}{mx_s^2}$

⁶Here, we normalize the temperature according to the energy scale $E_s = 1/L^2$, where L is the system size (subsection 6.1.3).

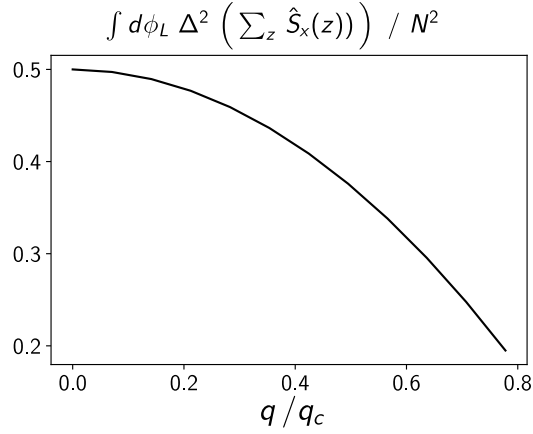


Figure 6.14.: Variance as possibly observed in a repetitive experiment, where every measurement of the observable $S_x(z)$ is attained with random Larmor phase ϕ_L . These correlations do not describe the quantum Fisher information.

and times in $t_s = \frac{mx_s^2}{\hbar}$. The energy scale for experiments with spin-1 BEC, however, is usually given by $\hbar\text{Hz}$. The conversion table 6.1 relates the two energy scales to each other for reasonable extensions x_s of the trapping potential⁷.

In contrast to experiments, where one typically finds an almost constant spin-changing collision rate [78], it is important to note that we consider the same particle number $N = 20000$ for all three scenarios outlined in Table 6.1, yielding different critical values $q_c = 2nc_1$. This gives a first mismatch with typical one-dimensional spinor BECs, where larger particle numbers ($N \approx 80000$) are desired in order to decrease experimental noise, for example on the quadratic Zeeman shift q . However, this is no fundamental limitation of our method since the simulations can be straightforwardly extended to larger system when taking care of the constraints on the spatial discretization (6.6) - (6.8). Due to a lack of computational capacity and time, we have not performed computations for larger systems so far.

L [μm]	E_s [$\hbar\text{Hz}$]	t_s [s]	$q_c = 2nc_1$ [$\hbar\text{Hz}$]
100	0.07302	13.69	14.604
200	0.01853	54.78	3.651
300	0.00811	123.25	1.622

Table 6.1.: Conversion of the energy and time scales used within this thesis to the experimentally relevant scale of $\hbar\text{Hz}$ for different extensions x_s of the trapping potential and $N = 20000$ particles.

Having a look at Table 6.1, we observe that the second row $x_s = 200\mu\text{m}$ fits best to today's experiments at SynQS, Heidelberg. Furthermore, the choice of partition sizes corresponding to a few micrometers is in good agreement with experimental values, thereby reducing the influ-

⁷The discussion of the comparability and applicability of our method is done in view of state-of-the-art experiments located at the SynQS collaboration, Heidelberg.

ence of classical correlations [55]. The critical value $q_c \approx 4\hbar\text{Hz}$ and temperature scales in the millihertz, i.e. sub-nanokelvin⁸ regime is what one would expect from the spin temperature [78] (although reliable methods to rigorously measure the spin temperature are still missing). Regarding the time-scales, our simulations suggest measurement times of the order of t_s , required in order to faithfully extract the QFI through the quench dynamics, as depicted in Figure 4.2. Especially for lower temperatures and small q -values coherence times of $\approx 10 t_s$ lie far away from experimentally feasible values. However, one could think of extrapolating the exponential decay of the integrand (4.13) for larger q values and temperatures, where our simulations suggest that $1 - 5 t_s$ could be sufficient to estimate the quantum Fisher information. We expect that shorter coherence times will rather underestimate than overestimate the integral of (4.13), such that already measurements on shorter time-scales could extract a finite multipartite entanglement content. To conclude, there are no fundamental limitations for experimentally implementing the work of this thesis.

⁸In our considerations, $20 \hbar\text{Hz}$ relates to approximately 1nK.

Conclusion and Outlook

The course of this Master's thesis allowed us to venture into the field of quantum many-body theory. One reason that makes this field so fascinating is the thrilling phenomenon of many-particle entanglement and the strong connection of theoretical and experimental studies. In this regard, our investigations combine the two versatile concepts of spinor Bose gases and quantum Fisher information and constitute a contribution towards a measurement protocol for the investigation of multipartite entanglement through quench dynamics in spin-1 Bose-Einstein condensates.

Following a summary of basic concepts in Part I, we have presented our main results in Part II of this thesis. Therein, chapter 4 has started out with deriving a detailed calculation scheme for extracting the quantum Fisher information from quench dynamics using mean-field Bogoliubov theory. In a first study, we have analyzed the quantum Fisher information of a pure state at zero temperature for a spin-1 BEC in single-mode approximation (chapter 5). Diagonalizing the Hamiltonian by means of both exact numerical calculations [20] and Bogoliubov transformations, we have elucidated the crucial influence of spontaneous symmetry breaking in determining the amount of entanglement in the system. In Chapter 6 we have extended the investigation of multipartite entanglement to one-dimensional spin-1 quasi-condensates [13] in a box potential. The quantum Fisher information has been first computed at zero temperature for a pure state and, second, through dynamic susceptibilities [12] at finite temperature after a weak quench (Figure 6.13). After having derived analytic bounds for generic spin states, the amount of multipartite entanglement has been related to the QFI. This has led us to conjecture that there could be indeed multiparticle entanglement witnessed in spin-1 BECs, especially in the vicinity of the continuous phase transition between the Easy-Axis and the Polar phase.

There are many possibilities for conducting subsequent studies which could also clarify outstanding questions and unresolved problems, regarding theoretical and experimental considerations. In first place, the studies allow for a straightforward expansion to other operators and quantum phases relevant to spinor BECs. One important open question is whether the growth of the quantum Fisher information can be fully attributed to underlying microscopic mechanisms such as the varying strength of the spin-mixing dynamics. Although having performed benchmark studies, it remains unclear in how far artifacts of the breakdown of the mean-field assumption can be excluded. For these reasons, it would be very helpful to systematically verify the outlined results with methods other than mean-field Bogoliubov theory, for example, Matrix-Product states [79]. Furthermore, the time evolution could be benchmarked using classical statistical simulation [80], based on the Gross-Pitaevskii equation [27] for Bose gases. Resolving the small difference of the quantum Fisher information in the zero temperature limit (Figure 6.12) represents another

important task for future studies. One possible starting point for an improved estimation of the variance could be the implementation of the cumulant expansion (Appendix A.6) and Wick's theorem (Appendix 2.3) for higher-order correlation functions.

It is very appealing to implement this work in a measurement protocol for spin-1 BECs. State-of-the-art experiments can in principle meet the requirements regarding optical resolution, trapping potentials, and read-out schemes outlined in chapter 6, which is already an indication for the applicability of the method. First steps have been already taken in this direction. However, longer coherence times would be desirable to fully extract the quantum Fisher information. Furthermore, a thermal state is a necessary requirement for our considerations. However, it is still an open question of research whether the spin-1 BEC in one dimension can experience thermal relaxation under its own dynamics and, if yes, how to probe it. Additionally, the choice of partition size might influence the effects of classical correlations due to the limited resolution of absorption imaging [55]. Last but not least, the generic mathematical description of the extended system outlined in this thesis allows one to readily extend the calculations to inhomogeneous density distributions in one dimension. In this context, an additional analysis of the influence of the trapping potential on the mean-field ground state [81] would be required. Besides, one could think of studying different phase domains within a trap coupled via the kinetic term. To conclude, there are still many possibilities to deepen our investigations and address further pertinent questions to it.

All in all, our studies suggest the presence of multipartite entanglement in spin-1 BECs, which could possibly be measured using an experimental protocol based on this work.

Appendices

A.1 Wick's Theorem

In this thesis, we use Wick's theorem [47] in order to compute higher-order correlation functions. Before discussing the main aspects of this theorem, we introduce the concept of normal ordering as, for instance, explained in [82]. For the sake of simplicity, we omit the operator symbol " $\hat{}$ ", and write $a_i = \hat{a}_i$ and $\mathcal{O} = \hat{\mathcal{O}}$ from here on. An operator \mathcal{O} is called normal-ordered if all creation/annihilation operators appear on the left/right. In particular, a product of operators of the same type, is normally ordered. For such \mathcal{O} we write $:\mathcal{O}:$, for example

$$\begin{aligned} :a_2 a_1^\dagger a_2^\dagger: &= a_1^\dagger a_2^\dagger a_2 = a_2^\dagger a_1^\dagger a_2 \quad \text{for } a_i, a_i^\dagger \hat{=} \text{ bosonic creation/annihilation operator} \\ :c_2 c_1^\dagger c_2^\dagger: &= c_1^\dagger c_2^\dagger c_2 = -c_2^\dagger c_1^\dagger c_2 \quad \text{for } c_i, c_i^\dagger \hat{=} \text{ fermionic creation/annihilation operator} . \end{aligned}$$

The very usefulness of the definition is the property that the expectation value on the ground state $|0\rangle$ of a normally ordered operator is always zero

$$\langle 0 | : \mathcal{O} : | 0 \rangle = 0. \quad (\text{A.40})$$

The contraction $\overline{\mathcal{O}_1 \mathcal{O}_2}$ of two operators \mathcal{O}_1 and \mathcal{O}_2 is defined as the difference between the time-ordered product (denoted by T) and the normal-ordered product

$$\overline{\mathcal{O}_1 \mathcal{O}_2} = T(\mathcal{O}_1 \mathcal{O}_2) - : \mathcal{O}_1 \mathcal{O}_2 : . \quad (\text{A.41})$$

Here, time-ordering refers to the ordering a product of operators, where each operator is defined at one time, such that every operator has only later operators to the left and earlier operators to the right. One can show by direct computation that

$$T(\mathcal{O}_1 \mathcal{O}_2 \mathcal{O}_3) = : \mathcal{O}_1 \mathcal{O}_2 \mathcal{O}_3 : + : \overline{\mathcal{O}_1 \mathcal{O}_2} \mathcal{O}_3 : + : \overline{\mathcal{O}_1 \mathcal{O}_2} \mathcal{O}_3 : + : \overline{\mathcal{O}_1 \mathcal{O}_2} \overline{\mathcal{O}_3} : \quad (\text{A.42})$$

$$= : \mathcal{O}_1 : \overline{\mathcal{O}_2 \mathcal{O}_3} + : \mathcal{O}_3 : \overline{\mathcal{O}_1 \mathcal{O}_2} + : \mathcal{O}_2 : \overline{\mathcal{O}_1 \mathcal{O}_3} . \quad (\text{A.43})$$

Wick's theorem generalizes this to N operators as

$$T(\mathcal{O}_1 \mathcal{O}_2 \dots \mathcal{O}_N) = : \mathcal{O}_1 \mathcal{O}_2 \dots \mathcal{O}_N : + \text{ : all contractions of distinct pairs : } . \quad (\text{A.44})$$

Since the ground state expectation value of a normal ordered operator is zero, we define the time-ordered contraction as $\overline{\mathcal{O}_1 \mathcal{O}_2} = \langle 0 | T \mathcal{O}_1 \mathcal{O}_2 | 0 \rangle$. There are two important consequences arising

from Wick's theorem (A.44) and the constraint (A.40) for N being an even number

$$\begin{aligned} \langle 0 | T \mathcal{O}_1 \mathcal{O}_2 \dots \mathcal{O}_{N+1} | 0 \rangle &= 0 \\ \langle 0 | T \mathcal{O}_1 \mathcal{O}_2 \dots \mathcal{O}_N | 0 \rangle &= \langle 0 | T \mathcal{O}_1 \mathcal{O}_2 | 0 \rangle \dots \langle 0 | T \mathcal{O}_{N-1} \mathcal{O}_N | 0 \rangle + \text{all other contractions.} \end{aligned} \quad (\text{A.45})$$

The first term contains a single unpaired operators and therefore vanishes. From the second equation, we identify the general rule that the non-vanishing expectation value of all even-ordered N -point correlation functions can be determined by the first order correlation function. In particular, Wick's theorem for bosonic (+1) and fermionic (-1) creation and annihilation operators becomes

$$\langle \hat{a}_1 \hat{a}_2 \dots \hat{a}_N \rangle = \sum_{\text{partitions } \mathcal{P}} (\pm 1)^{\mathcal{P}} \langle \hat{a}_{i_1} \hat{a}_{i_2} \rangle \dots \langle \hat{a}_{i_{N-1}} \hat{a}_{i_N} \rangle. \quad (\text{A.46})$$

A.2 Thermal Phase Diagram in Single-Mode Approximation

In this extension to section 5.3, we examine the thermal phase diagram of the single-mode system using the above self-consistent mean-field Bogoliubov formalism. To this end, we are searching for the temperature and magnetic field parameter regime at which the mean-field approximation is still valid. Therefore, the quasi-particle modes are thermally populated and the number of condensed atoms is self-consistently adjusted according to equation (5.15). The occupation of the mean-field mode is presented as a function of the temperature and quadratic Zeeman shift in Figure A.15 and the corresponding chemical potential can be read off from Figure A.16.

As expected, the mean-field assumption breaks down in the limit of high temperatures where thermal fluctuations are strongly enhanced. This happens at much lower temperature for q close to the critical point q_c than in the middle of the phase. This can be understood from the growth of fluctuations when approaching the quantum phase transition. Since many-particle excitations are needed in order to destroy the mean-field ground state, it is plausible to obtain larger temperatures compared to the typical energy per particle. A particularly interesting finding of this map is that the state is more unstable towards the Twin-Fock phase ($q \rightarrow -q_c$) than towards the Polar phase ($q \rightarrow +q_c$). This can be understood from the fact that on the Twin-Fock side two modes ($m_F = \pm 1$) are still occupied while all particles sit in the central mode ($m_F = 0$) in the Polar phase. Since the relative fluctuations of the two modes are stronger compared to the ones of the central mode, this gives a reasoning for an earlier break-down of the mean-field assumption. The thermal phase diagram therefore provides an insight into the growth of correlations and a better understanding for the reliability of the method at finite temperatures.

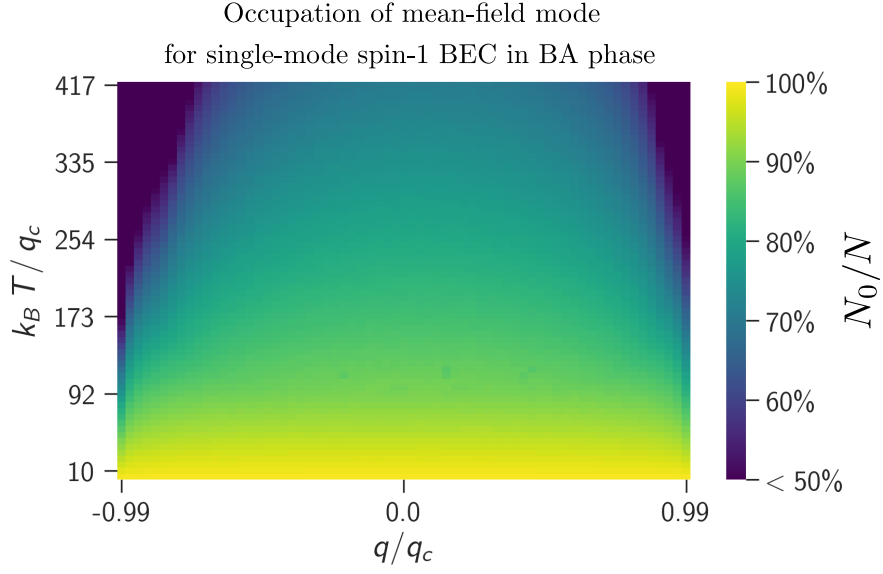


Figure A.15.: Numerical simulation of the relative occupation of the mean-field mode in the BA phase at finite temperature. We observe the break-down of the mean-field assumption through the growth of thermal and quantum fluctuations, especially close to the quantum phase transitions. Interestingly, the ground state is less stable towards the Twin-Fock phase ($q \rightarrow -q_c$) than towards the Polar phase ($q \rightarrow +q_c$), which could be attributable to the fact, that on the Twin-Fock side two modes ($m_F = \pm 1$) are still occupied while all particles sit in the central mode ($m_F = 0$) in the Polar phase. The temperature is expressed in units of critical magnetic field parameter $q_c = 1\hbar\text{Hz}$.

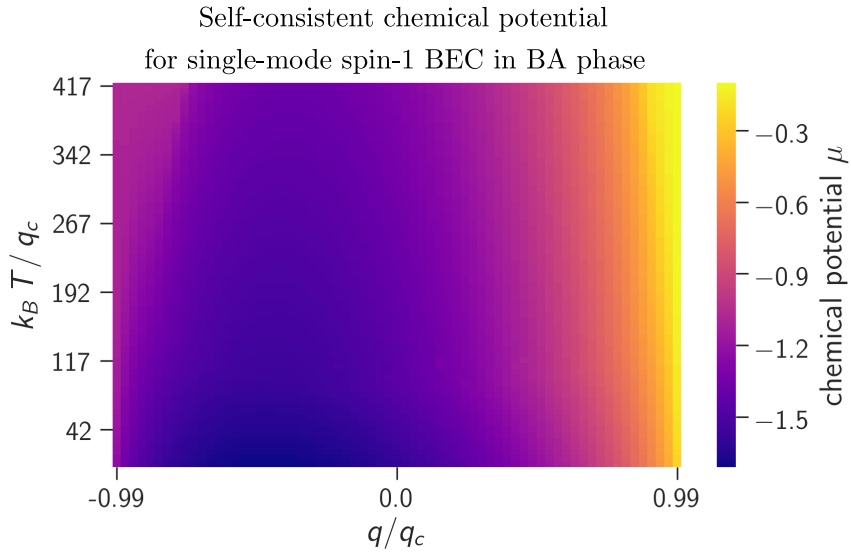


Figure A.16.: Chemical potential in the BA phase at finite temperature from self-consistent numerical calculations. The heatmap resembles the structure of the mean-field diagram, thereby underlining the close connection between the chemical potential and the conservation of the number of particles in the system.

A.3 Analytical Approach towards SMA Bogoliubov Transformations

In this supplementary analysis to section 5.3, we analytically derive Bogoliubov transformations of the state which diagonalize the Hamiltonian (5.2) within the single-mode approximation (SMA). Ideally, one finds one highly occupied and two empty modes, thereby reducing the parameter space to two modes. In this case, the basis transformation can be represented in terms of 2×2 matrices and easily solved analytically, as shown on the examples in subsection 2.2.2.

We start out with choosing the following ansatz for Bogoliubov transformation \mathcal{T} with $\hat{\beta} = \mathcal{T}\hat{\alpha}$

$$\begin{pmatrix} \hat{\beta} \\ \hat{\beta}^\dagger \end{pmatrix} = \underbrace{\begin{pmatrix} \mathcal{U} & 0 \\ 0 & \mathcal{U}^\dagger \end{pmatrix}}_{\mathcal{T}} \begin{pmatrix} \hat{\alpha} \\ \hat{\alpha}^\dagger \end{pmatrix}. \quad (\text{A.47})$$

The quasi-particle modes $\hat{\beta}$ and $\hat{\beta}^\dagger$ should obey bosonic commutation relations ($\mathcal{T}\mathcal{T}^\dagger = \mathcal{I}$) and fulfill the normalization condition

$$\mathcal{U}^{-1} = \mathcal{U}^\dagger \quad \text{and} \quad \sum_{j=1,2,3} \mathcal{U}_{ij}^2 = 1 \quad \text{for } i = 1, 2, 3. \quad (\text{A.48})$$

Additionally, the fluctuations in linear order should vanish in the new basis. Plugging this mean-field ansatz into the Hamiltonian (5.2) yields the linear part

$$\begin{aligned} \hat{\mathcal{H}}_{\text{lin}} = & \left(4\lambda N^{\frac{3}{2}} \zeta_0^2 + N^{\frac{3}{2}}(q - \lambda) - \mu\sqrt{N} \right) \left(\zeta_{-1}\hat{\alpha}_1 + \zeta_1\hat{\alpha}_{-1} + \zeta_1\hat{\alpha}_1^\dagger + \zeta_{-1}\hat{\alpha}_{-1}^\dagger \right) \\ & + \left(8\lambda N^{\frac{3}{2}} |\zeta_1|^2 \zeta_0 - \mu\sqrt{N}\zeta_0 \right) \left(\hat{\alpha}_0 + \hat{\alpha}_0^\dagger \right), \end{aligned}$$

which can be rewritten in matrix form

$$\begin{pmatrix} \Lambda_1 \zeta_{-1} \\ \Lambda_0 \zeta_0 \\ \Lambda_1 \zeta_1 \end{pmatrix} \begin{pmatrix} \zeta_1 & \mathcal{U}_{12} & \mathcal{U}_{13} \\ \zeta_0 & \mathcal{U}_{22} & \mathcal{U}_{23} \\ \zeta_1 & \mathcal{U}_{32} & \mathcal{U}_{33} \end{pmatrix} \begin{pmatrix} \hat{\beta}_d \\ \hat{\beta}_{f_z} \\ \hat{\beta}_\theta \end{pmatrix} \stackrel{!}{=} \text{const.} \quad (\text{A.49})$$

with $\Lambda_1 = 4\lambda N^{\frac{3}{2}} \zeta_0^2 + \sqrt{N}q$ and $\Lambda_0 = 8\lambda N^{\frac{3}{2}} \zeta_1^2$. The expressions $\hat{\beta} = (\hat{\beta}_d, \hat{\beta}_{f_z}, \hat{\beta}_\theta)$ was chosen in analogy to [83], where $\hat{\beta}_d$ represents the highly occupied, so-called density-mode. Solving for (A.49) under the constraints (A.48), the final transformation becomes

$$\begin{pmatrix} \hat{\beta}_d \\ \hat{\beta}_{f_z} \\ \hat{\beta}_\theta \end{pmatrix} = \underbrace{\begin{pmatrix} \frac{\sin(\phi)}{\sqrt{2}} & \cos(\phi) & \frac{\sin(\phi)}{\sqrt{2}} \\ \frac{1}{\sqrt{2}} & 0 & -\frac{1}{\sqrt{2}} \\ \frac{\cos(\phi)}{\sqrt{2}} & -\sin(\phi) & \frac{\cos(\phi)}{\sqrt{2}} \end{pmatrix}}_{\mathcal{U}} \begin{pmatrix} \hat{\alpha}_1 \\ \hat{\alpha}_0 \\ \hat{\alpha}_{-1} \end{pmatrix}, \quad (\text{A.50})$$

using the parametrization $\sin(\phi) = \sqrt{\frac{1-q/2q_c}{2}} = \sqrt{2}|\zeta_1|$ and $\cos(\phi) = \sqrt{\frac{1+q/2q_c}{2}} = |\zeta_0|$. These transformations correspond to the result from [83] and the Bogoliubov Hamiltonian reads

$$\hat{\mathcal{H}}^{(2)} \approx \begin{pmatrix} \hat{\beta}_\theta & \hat{\beta}_\theta^\dagger & \hat{\beta}_{f_z} & \hat{\beta}_{f_z}^\dagger \end{pmatrix} \begin{pmatrix} \mathcal{C} & \mathcal{D} & 0 & 0 \\ \mathcal{D} & \mathcal{C} & 0 & 0 \\ 0 & 0 & \mathcal{E} & \mathcal{F} \\ 0 & 0 & \mathcal{F} & \mathcal{E} \end{pmatrix} \begin{pmatrix} \hat{\beta}_\theta^\dagger \\ \hat{\beta}_\theta \\ \hat{\beta}_{f_z}^\dagger \\ \hat{\beta}_{f_z} \end{pmatrix}, \quad (\text{A.51})$$

with matrix entries

$$\begin{aligned} \mathcal{C} &= -6\lambda N \sin^2(\phi) \cos^2(\phi) + \lambda N [\sin^4(\phi) + \cos^4(\phi)] + \frac{1}{2} [(q - \lambda) \cos^2(\phi) - \mu] \\ \mathcal{D} &= \lambda N (\sin^2(\phi) - \cos^2(\phi))^2 \\ \mathcal{E} &= \frac{1}{2} [q - \lambda - \mu + 2\lambda N \cos^2(\phi)] \\ \mathcal{F} &= -\lambda N \cos^2(\phi). \end{aligned} \quad (\text{A.52})$$

Thus, we obtain a Bogoliubov transformation with orthogonal modes that can be mapped onto a polar state with one highly occupied mode. Computing the quantum Fisher information with respect to the operator \hat{S}_x from these transformation (Figure A.17) compares very well to the results outlined in Figure 5.4. The same holds for the occupations of the mean-field mode and the self-consistently adjusted chemical potential in Figure A.19a and Figure A.17. The small discrepancy between the analytical benchmarks and the exact numerical implementations could be attributed to the fact that the mapping onto two empty and one highly occupied mode neglects fluctuations on top of the highly occupied mode which limits the analytical approach. Thus, the latter appears to be less robust when approaching the quantum phase transitions, especially in the region close to the Twin-Fock phase where fluctuations are expected to be stronger (Figure A.19a). The same holds for the high temperature limit. Neglecting fluctuations on top of the highly occupied mode is still a good approximation for small temperatures according to the expansion of the occupations from Bose-Einstein statistics in this limit $\langle \hat{\beta}_d^\dagger \hat{\beta}_d \rangle \propto (\exp(E/(k_B T)) - 1)^{-1} \approx k_B T / E$. However, the occupation scale linearly with the temperature as demonstrated in Figure A.18. Hence, the comparison to the analytical studies is only valid in the limit of $T \rightarrow 0$, underlying the conclusions drawn from the numerical results.

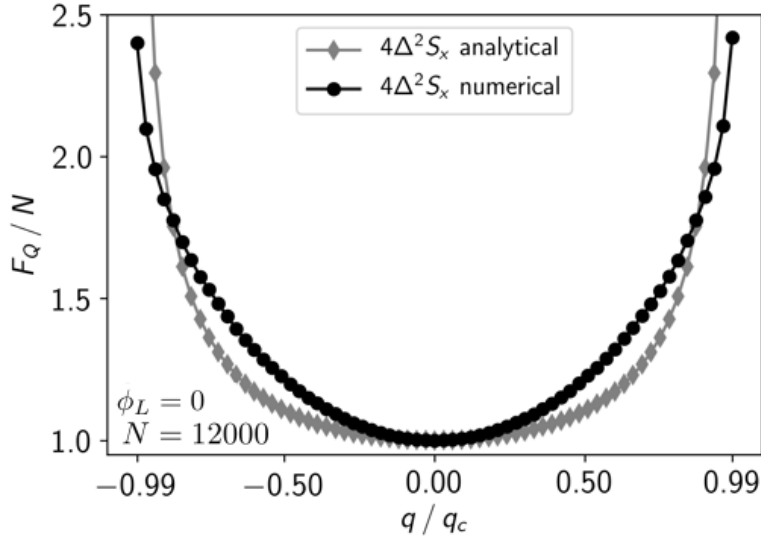


Figure A.17.: The analytical calculation of the quantum Fisher information with respect to operator \hat{S}_x for the SMA Hamiltonian $H = 2(\lambda\hat{S}_x^2 - \frac{q}{3}\hat{S}_z) + 2(\lambda\hat{A}_y^2 - \frac{q}{3}\hat{A}_z)$ compares very well to the numerical results presented in Figure 5.4. There is no entanglement witnessed at the center of the BA phase, but the same builds up as soon as the absolute value of q increases.

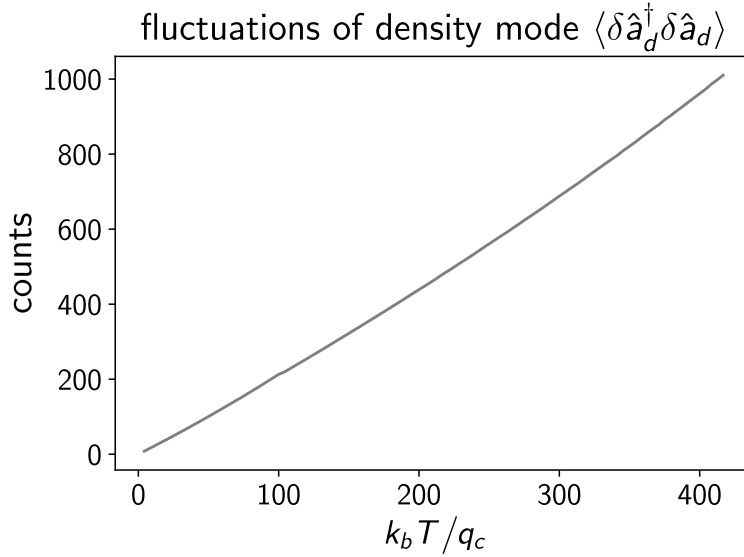


Figure A.18.: Fluctuations on top of the mean-field mode scale linearly with the temperature. Thus, neglecting these fluctuations is only valid at low temperatures and introduces systematical errors at larger temperatures.

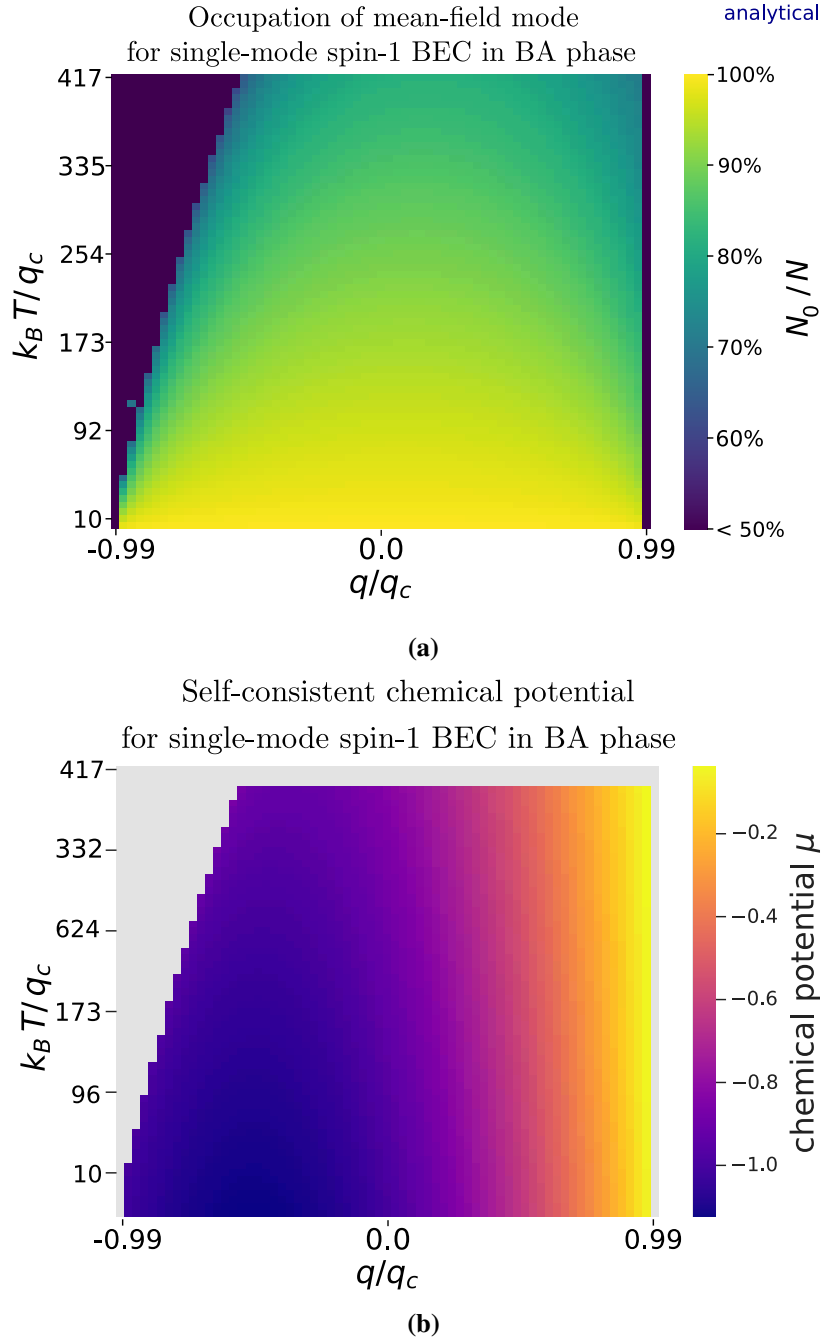


Figure A.19.: Analytical benchmark of the occupation of mean-field mode (a) and the chemical potential (b) in the Broken-Axis symmetry phase at finite temperature. The blue (a) and gray (b) areas mark regions in the phase diagram where the mean-field assumption can not be self-consistently fulfilled anymore. The results resembles the ones from numerical calculations (Figure A.15 and Figure A.16) but show an earlier break-down close to quantum phase transitions at lower temperatures, which can be attributed to neglecting fluctuations on top of the mean-field mode.

A.4 Energy Spectrum of spin-1 BEC in SMA from Exact Diagonalization

For further discussions on spontaneous symmetry breaking in the single-mode spin-1 BEC, especially in view of the comparability of different mean-field methods and exact diagonalization (Figure 5.7), we study the eigenenergies of the system in this supplementary analysis. The structure of the spectrum in Figure A.20 reveals a substantial change at $q/q_c \approx 0.7$, thereby hinting at a shift of the quantum critical point due to large fluctuations in the system.

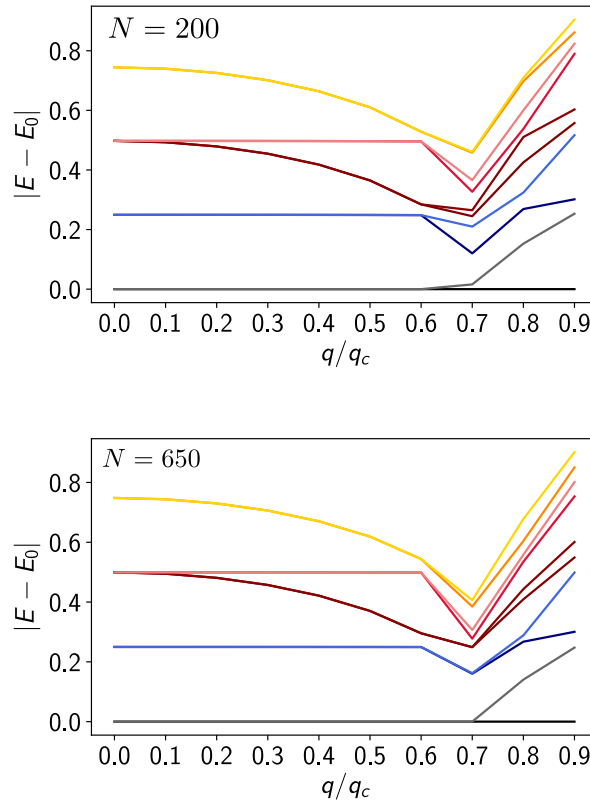


Figure A.20.: The energy spectrum obtained from exact diagonalization of the SMA Hamiltonian (5.3) reveals a degeneracy of the ground state energy E_0 for $q/q_c < 0.7$. Moreover, a large gap between the energy of the degenerate ground state and the next excited state can be observed. This supports the conclusion of a spontaneous symmetry breaking of the fragile, superimposed ground state. However, for larger q -values the notion of spontaneous symmetry breaking can not be applied. At $q/q_c \approx 0.7$ the structure of the eigenenergy spectrum substantially changes and removes the degeneracy. This is an indication of a shift of the quantum phase transition due to large fluctuations in the system. Moreover, it could explain the growth of fluctuations for magnetic field parameters $q/q_c \geq 0.7$, which was generally observed throughout our studies. It therefore also verifies the choice of the regime $0 \leq q/q_c \leq 0.8$ at which the mean-field assumption is considered to be valid in the extended system. Last but not least, the two plots for different particle numbers ($N = 200$ above and $N = 650$ below) do not indicate a significant shift of the quantum critical point, however, the suspicion of a finite size scaling could be addressed in future studies.

A.5 Equations of Motion in Extended Spin-1 BEC

As outlined in chapter 4, the time-evolution of the correlation matrix is obtained from the Heisenberg equations of motion (4.21). Therefore, the commutator of the quasi-particle modes and the Bogoliubov Hamiltonian needs to be computed. We explicitly perform these calculations on the example of the mean-field Bogoliubov description in the extended system (chapter 6), thereby omitting the operator symbol $'\sim'$

$$\begin{aligned} \frac{d}{dt}\gamma(t, z') &= i [\mathcal{H}, \gamma(z')] = i [\mathcal{H}, \beta_k^\circ(z') \beta_l^\circ(z'')] \\ &= i \left[\sum_z \sum_j E_j(z) \{ \beta_j^\dagger(z) \beta_j(z) + \beta_j \beta_j^\dagger(z) \}, \beta_k^\circ(z') \beta_l^\circ(z'') \right] \end{aligned} \quad (\text{A.53})$$

Using the commutation relation $[\beta_i(z), \beta_j^\dagger(z')] = \frac{1}{l} \delta_{zz'} \delta_{ij}$ and identity $[AB, CD] = A[B, C]D + CA[B, D] + [A, C]BD + C[A, D]B$, we derive the following equations of motions for any combination of two quasi-particle operators up to second order

$$\begin{aligned} \frac{d}{dt} \beta_k^\dagger(z') \beta_l(z'')(t) &= \frac{2i}{l} \{ E_k(z') - E_l(z'') \} \beta_k^\dagger(z') \beta_l(z'') \\ \frac{d}{dt} \beta_k(z') \beta_l^\dagger(z'')(t) &= -\frac{2i}{l} \{ E_k(z') - E_l(z'') \} \beta_k(z') \beta_l^\dagger(z'') \\ \frac{d}{dt} \beta_k(z') \beta_l(z'')(t) &= -\frac{2i}{l} \{ E_k(z') + E_l(z'') \} \beta_k(z') \beta_l(z'') \\ \frac{d}{dt} \beta_k^\dagger(z') \beta_l^\dagger(z'')(t) &= \frac{2i}{l} \{ E_k(z') + E_l(z'') \} \beta_k^\dagger(z') \beta_l^\dagger(z'') \end{aligned} \quad (\text{A.54})$$

Writing the Bogoliubov modes with m_F components $\mathbf{b}_{z_1} = \left(\beta_1(z_1) \ \beta_0(z_1) \ \beta_{-1}(z_1) \right)$ as $\mathbf{b} = \left(\mathbf{b}_{z_1} \ \mathbf{b}_{z_2} \ \dots \ \mathbf{b}_{z_1}^\dagger \ \mathbf{b}_{z_2}^\dagger \ \dots \right)$ yields to the correlation matrix of the form

$$\Gamma = \mathbf{b} \mathbf{b}^\dagger = \begin{pmatrix} \mathbf{b}_{z_1} \mathbf{b}_{z_1}^\dagger & \mathbf{b}_{z_1} \mathbf{b}_{z_2}^\dagger & \dots & & & \\ \mathbf{b}_{z_2} \mathbf{b}_{z_1}^\dagger & \mathbf{b}_{z_2} \mathbf{b}_{z_2}^\dagger & & & & \\ & \ddots & & & & \\ \vdots & & & \mathbf{b}_{z_{n-1}}^\dagger \mathbf{b}_{z_{n-1}} & \mathbf{b}_{z_{n-1}}^\dagger \mathbf{b}_{z_n} & \\ & & & \mathbf{b}_{z_n}^\dagger \mathbf{b}_{z_{n-1}} & \mathbf{b}_{z_n}^\dagger \mathbf{b}_{z_n} & \end{pmatrix}. \quad (\text{A.55})$$

The following unitary matrix $\mathcal{E}(t)$ solves equation (A.54) by an exponential ansatz and evolves the correlation matrix in time, $\Gamma(t) = \mathcal{E}(t) \Gamma(0) \mathcal{E}^\dagger(t)$, with

$$\mathcal{E}(t) = \text{diag} \left[e^{-\frac{2i}{l} E_1(z_1)t}, e^{-\frac{2i}{l} E_0(z_1)t}, e^{-\frac{2i}{l} E_{-1}(z_1)t} \dots, e^{\frac{2i}{l} E_1(z_n)t}, e^{\frac{2i}{l} E_0(z_n)t}, e^{\frac{2i}{l} E_{-1}(z_n)t} \right]. \quad (\text{A.56})$$

A.6 Cumulant Expansion

In chapter 6 we apply a specific expansion of the field operator in terms of phase-density formalism which describes the quasi-condensate in the limit of weak interactions and low density fluctuations. Thereby, we assume the phase fluctuations to vary smoothly between neighboring points. However, when computing first order correlations of the type

$$\langle \hat{\Psi}_i^\dagger(z) \hat{\Psi}_j(z') \rangle = \langle \sqrt{\hat{n}_i(z)} e^{i[\hat{\theta}_j(z') - \hat{\theta}_i(z)]} \sqrt{\hat{n}_j(z')} \rangle, \quad (\text{A.57})$$

z and z' are not neighboring points of the lattice any more. Thus, the difference in the fluctuation of the phase can become arbitrary large since the fluctuations are uncorrelated at large distances. This can be seen also from Figure 6.8, where the correlations of the phase fluctuations decrease with distance. Hence, fluctuations can differ arbitrary large at points far apart from each other. In order to cure this divergence, we introduce a cumulant expansion of the exponential in powers of the phase difference up to second order in fluctuations, thereby using the short-writing $\vartheta \equiv \delta\hat{\theta}_i(z) - \delta\hat{\theta}_i(z')$:

$$\langle e^{i\vartheta} \rangle = e^{\langle -\vartheta^2 \rangle / 2}. \quad (\text{A.58})$$

For any operator with zero mean it can be proven by induction that the following identity holds using Wick's theorem

$$\begin{aligned} \langle e^{i\vartheta} \rangle &= \left\langle \sum_{n=0}^{\infty} \frac{i^n}{n!} \vartheta^n \right\rangle \stackrel{\langle \vartheta \rangle = 0}{=} \left\langle \sum_{k=0}^{\infty} \frac{i^{2k}}{(2k)!} \vartheta^{2k} \right\rangle = \sum_{k=0}^{\infty} \frac{(-1)^k}{(2k)!} \langle \vartheta^{2k} \rangle \\ &\stackrel{\textcircled{*}}{=} \sum_{k=0}^{\infty} \frac{(-1)^k}{(2k)!} \frac{2k!}{k! 2^k} \langle \vartheta^2 \rangle^k = \sum_{k=0}^{\infty} \frac{1}{k!} \left(\frac{-\langle \vartheta^2 \rangle}{2} \right)^k \\ &= e^{\langle -\vartheta^2 \rangle / 2}. \end{aligned} \quad (\text{A.59})$$

$\textcircled{*}$ to proof: $\langle \vartheta^{2k} \rangle = \frac{2k!}{k! 2^k} \langle \vartheta^2 \rangle^k$

1. base case: $k = 1 \Rightarrow \langle \vartheta^2 \rangle = \langle \vartheta^2 \rangle$

2. step case: $k = n + 1$:

$$\begin{aligned} \langle \vartheta^{2(n+1)} \rangle &= \langle \vartheta^{2n} \vartheta^2 \rangle \stackrel{Wick}{=} \langle \vartheta^{2n} \rangle \langle \vartheta^2 \rangle (2n + 1) = \frac{(2n)!}{n! 2^n} \langle \vartheta^2 \rangle^n \langle \vartheta^2 \rangle (2n + 1) \\ &= \frac{(2n)!}{n! 2^n} \langle \vartheta^2 \rangle^{n+1} \frac{(2(n+1) - 1) 2(n+1)}{2(n+1)} = \frac{2(n+1)!}{(n+1)! 2^{n+1}} \langle \vartheta^2 \rangle^{n+1}. \end{aligned}$$

With this, we can now compute the first order correlation function from equation (A.57) as follows

$$\begin{aligned}
\langle \hat{\Psi}_i^\dagger(z) \hat{\Psi}_j(z') \rangle &= \langle \sqrt{\delta \hat{n}_i(z)} e^{i(\hat{\theta}_j(z') - \hat{\theta}_i(z))} \sqrt{\delta \hat{n}_j(z')} \rangle \\
&= \sqrt{n_i n_j} e^{i(\theta_j - \theta_i)} e^{\langle -\vartheta^2 \rangle / 2} \left\{ 1 + \frac{i}{2n_i} \langle \delta \hat{n}_i(z) \vartheta \rangle + \frac{i}{2n_j} \langle \vartheta \delta \hat{n}_j(z') \rangle \right. \\
&\quad - \frac{1}{8n_i^2} (\langle \delta \hat{n}_i^2(z) \rangle - \langle \delta \hat{n}_i(z) \vartheta \rangle^2) \quad \quad \quad \text{(A.60)} \\
&\quad - \frac{1}{8n_j^2} (\langle \delta \hat{n}_j^2(z') \rangle - \langle \vartheta \delta \hat{n}_j(z') \rangle^2) \\
&\quad \left. + \frac{1}{4n_i n_j} (\langle \delta \hat{n}_i(z) \delta \hat{n}_j(z') \rangle - \langle \delta \hat{n}_i(z) \vartheta \rangle \langle \vartheta \delta \hat{n}_j(z') \rangle) \right\}.
\end{aligned}$$

For small fluctuations, the cumulant expansion agrees (up to second order) with the standard expansion of (A.57), which can be seen from expanding $e^{\langle -\vartheta^2 \rangle / 2}$ for small ϑ^2 and neglecting the quartic terms in (A.60). Since the computation of the QFI from dynamic susceptibilities is performed within a quadratic theory our results agree with the first order correlation functions extracted from the cumulant expansion. However, the same does not apply to the second order correlator in the computation of the variance. Future work should therefore carefully consider the potential effects of the cumulant expansion, for instance, in order to achieve an improved estimation of the variance. The above equations could be taken as a starting point for generally extracting higher-order correlation functions for smoothly varying phase fluctuations.

Bibliography

- [1] L. Pezzé, A. Smerzi, M. K. Oberthaler, R. Schmied, and P. Treutlein. Quantum metrology with nonclassical states of atomic ensembles. *arXiv:1609.01609v3*.
- [2] C. D. Hamley, C. S. Gerving, T. M. Hoang, E. M. Bookjans, and M. S. Chapman. Spin-nematic squeezed vacuum in a quantum gas. *Nature Physics*, 2012. *arXiv:1111.1694*, doi:10.1038/nphys2245.
- [3] P. Kunkel, M. Prüfer, H. Strobel, D. Linnemann, A. Frölian, T. Gasenzer, M. Gärtner, and M. K. Oberthaler. Spatially distributed multipartite entanglement enables EPR steering of atomic clouds. *Science*, 360(6387):413–416, 2018. doi:10.1126/science.aao2254.
- [4] M. Gessner, P. Feldmann, C. Klempt, L. Santos, and A. Smerzi. Heralded Generation of Macroscopic Superposition States in a Spinor Bose-Einstein Condensate. *arXiv:1712.03864v1*.
- [5] J. Peise, I. Kruse, K. Lange, B. Lücke, L. Pezzè, J. Arlt, W. Ertmer, K. Hammerer, L. Santos, A. Smerzi, and C. Klempt. Satisfying the Einstein–Podolsky–Rosen criterion with massive particles. *Nature Communications*, 6, 2015. doi:10.1038/ncomms9984.
- [6] J. G. Bohnet, B. C. Sawyer, J. W. Britton, M. L. Wall, A. M. Rey, M. Foss-Feig, and John J Bollinger. Quantum spin dynamics and entanglement generation with hundreds of trapped ions. *Science*, 352(6291):1297–1301, 2016. doi:10.1126/science.aad9958.
- [7] H. Pu, C. K. Law, S. Raghavan, J. H. Eberly, and N. P. Bigelow. Spin-mixing dynamics of a spinor Bose-Einstein condensate. *Physical Review A - Atomic, Molecular, and Optical Physics*, 60(2):1463–1470, 1999. doi:10.1103/PhysRevA.60.1463.
- [8] S. L. Braunstein and C. M. Caves. Statistical Distance and the Geometry of Quantum States. *Physical Review Letters*, 72(22), 1994. doi:10.1103/PhysRevLett.72.3439.
- [9] C. W Helstrom. Quantum detection and estimation theory. *Journal of Statistical Physics*, 1(2):231–252, 1969. doi:10.1007/BF01007479.
- [10] L. Pezzé and A. Smerzi. Entanglement, nonlinear dynamics, and the heisenberg limit. *Physical Review Letters*, 102(10), 2009. doi:10.1103/PhysRevLett.102.100401.
- [11] P. Hyllus, W. Laskowski, R. Krischek, C. Schwemmer, W. Wieczorek, H. Weinfurter, L. Pezz, and A. Smerzi. Fisher information and multiparticle entanglement. *Physical Review A - Atomic, Molecular, and Optical Physics*, 022321:1–10, 2012. doi:10.1103/PhysRevA.85.022321.
- [12] P. Hauke, M. Heyl, L. Tagliacozzo, and P. Zoller. Measuring multipartite entanglement through dynamic susceptibilities. *Nature Physics*, 12(8):778–782, 2016. *arXiv:1509.01739*, doi:10.1038/nphys3700.
- [13] C. Mora and Y. Castin. Extension of Bogoliubov theory to quasicondensates. *Physical Review A - Atomic, Molecular, and Optical Physics*, 67(5):24, 2003. *arXiv:0212523*, doi:10.1103/PhysRevA.67.053615.

- [14] L. Anthony. Bose-Einstein condensation in the alkali gases: Some fundamental concepts. *Reviews of Modern Physics*, 73(2):307–356, 2001. arXiv:0206046, doi:10.1103/RevModPhys.73.307.
- [15] Y. Kawaguchia and M. Ueda. Spinor Bose-Einstein condensates, 2012. doi:10.1016/j.physrep.2012.07.005.
- [16] G. E. Marti and D. Stamper-Kurn. Spinor Bose-Einstein gases. 2015. arXiv:1511.01575.
- [17] J. M. Radcliffe. Some properties of coherent spin states. *Journal of Physics A: General Physics*, 4(3):313–323, 1971. doi:10.1088/0305-4470/4/3/009.
- [18] E. Wigner. On the Quantum Correction For Thermodynamic Equilibrium. *Physical Review Letters*, 40(5):749–759, 1932. doi:10.1103/PhysRev.40.749.
- [19] N. N. Bogoljubov. On a new method in the theory of superconductivity. *Il Nuovo Cimento*, 7(6):794–805, 1958. URL: <http://link.springer.com/10.1007/BF02745585>, doi:10.1007/BF02745585.
- [20] K. Geier. Private Communication. 2019.
- [21] P. Feldmann, M. Gessner, M. Gabbrielli, C. Klempt, L. Santos, L. Pezzè, and A. Smerzi. Interferometric sensitivity and entanglement by scanning through quantum phase transitions in spinor Bose-Einstein condensates. *Physical Review A*, 97(3), 2018. arXiv:1712.03896, doi:10.1103/PhysRevA.97.032339.
- [22] D. M. Stamper-Kurn and M. Ueda. Spinor Bose gases: Symmetries, magnetism, and quantum dynamics. *Reviews of Modern Physics*, 85(3):1191–1244, 2013. arXiv:1205.1888, doi:10.1103/RevModPhys.85.1191.
- [23] T.-L. Ho. Spinor Bose Condensates in Optical Traps. *Physical Review Letters*, (2), 1998. doi:10.1103/PhysRevLett.81.742.
- [24] T. Zibold, E. Nicklas, C. Gross, and M. K. Oberthaler. Classical Bifurcation at the Transition from Rabi to Josephson Dynamics. *Physical Review Letters*, 105(20):204101, 2010. doi:10.1103/PhysRevLett.105.204101.
- [25] H. Strobel, W. Muessel, D. Linnemann, T. Zibold, D. B. Hume, L. Pezzè, A. Smerzi, and M. K. Oberthaler. Fisher information and entanglement of non-Gaussian spin states. *Science*, 345(6195):424–427, 2014. arXiv:1507.03782, doi:10.1126/science.1250147.
- [26] E. P. Gross. Structure of a quantized vortex in boson systems. *Il Nuovo Cimento Series 10*, XX(x), 1961. URL: <http://link.springer.com/article/10.1007/BF02731494>.
- [27] L. P. Pitaevskii. Vortex lines in imperfect Bose gases. *J. Exptl. Theoret. Phys. (U.S.S.R.)*, 13(40):646–651, 1961. URL: <https://link.springer.com/content/pdf/10.1007/BF02731494.pdf>.
- [28] C. K. Law, H. Pu, and N. P. Bigelow. Quantum Spins Mixing in Spinor Bose-Einstein Condensates. *Physical Review Letters*, 81, 1998. doi:10.1103/PhysRevLett.81.5257.
- [29] P. Kunkel, M. Prüfer, S. Lannig, R. Rosa-Medina, A. Bonnini, M. Gärtner, H. Strobel, and M. K. Oberthaler. Simultaneous Readout of Noncommuting Collective Spin Observables beyond the Standard Quantum Limit. 2019. arXiv:1904.01471.

-
- [30] C. D. Hamley, C. S. Gerving, T. M. Hoang, E. M. Bookjans, and M. S. Chapman. Spin-nematic squeezed vacuum in a quantum gas. *Nature Physics*, 8(4):305–308, 2012. arXiv:1111.1694, doi:10.1038/nphys2245.
- [31] S. Sachdev. *Quantum Phase Transitions*. Cambridge University Press, 2 edition, 2011. doi:10.1017/CB09780511973765.
- [32] R. P. Feynman, F. L. Vernon, and R. W. Hellwarth. Geometrical Representation of the Schrödinger Equation for Solving Maser Problems. *Journal of Applied Physics*, 28(1):49–52, 1957. doi:10.1063/1.1722572.
- [33] M. A. Nielsen and I. L. Chuang. *Quantum Computation and Quantum Information: 10th Anniversary Edition*. Cambridge University Press, 2010. doi:10.1017/CB09780511976667.
- [34] J. J. Sakurai and E. D. Commins. *Modern Quantum Mechanics*. AAPT, revised edition, 1995.
- [35] E. Davis, G. Bentsen, T. Li, M. Schleier-smith, V. P. Mall, and S. Ca. Advantages of Interaction-Based Readout for Quantum Sensing. *Proc. SPIE 10118, Advances in Photonics of Quantum Computing, Memory, and Communication X*, 2017. doi:10.1117/12.2257033.
- [36] R. Schmied and P. Treutlein. Tomographic reconstruction of the Wigner function on the Bloch sphere. *New Journal of Physics*, 13, 2011. doi:10.1088/1367-2630/13/6/065019.
- [37] Y. Lee Loh and M. Kim. Visualizing spin states using the spin coherent state representation. *American Journal of Physics*, 83(1):30–35, 2015. doi:10.1119/1.4898595.
- [38] J. D. Fraser. Spontaneous Symmetry Breaking in Finite Systems. *Philosophy of Science*, 83(4):585–605, 2016. doi:10.1086/687263.
- [39] J. van Wezel and J. van den Brink. Spontaneous Symmetry Breaking in Quantum Mechanics. *American Journal of Physics*, 75(2), 2006. arXiv:0609177, doi:10.1119/1.2730839.
- [40] I. Boettcher, J. M. Pawłowski, and S. Diehl. Ultracold atoms and the Functional Renormalization Group. *Nuclear Physics B - Proceedings Supplements*, 228:63–135, 2012. doi:10.1016/j.nuclphysbps.2012.06.004.
- [41] D. J. Amit and V. M. Mayor. Field theory, the renormalization group, and critical phenomena. *World Scientific*, 2005.
- [42] J. Cardy. Phase transitions in simple Systems. *Scaling and Renormalization in Statistical Physics*, pages 1–15, 2015. doi:10.1017/cbo9781316036440.002.
- [43] L. Onsager. A 2D Model with an Order-Disorder Transition. *Physical Review Letters*, 56(41):680–683, 1949. doi:10.1103/PhysRev.65.117.
- [44] T. Koma and H. Tasaki. Symmetry breaking and finite-size effects in quantum many-body systems. *Journal of Statistical Physics*, 76(3-4):745–803, 1994. doi:10.1007/BF02188685.

- [45] J. L. van Hemmen. A Note on the Diagonalization of Quadratic Boson and Fermion Hamiltonians. *Zeitschrift für Physik B - Condensed Matter*, 277(38):271–277, 1980. doi:10.1007/BF01315667.
- [46] M.-W. Xiao. Theory of transformation for the diagonalization of quadratic Hamiltonians. 2009. arXiv:arXiv:0908.0787v1.
- [47] G. C. Wick. The Evaluation of the Collision Matrix. *Phys. Rev.*, 80(2), 1950. doi:10.1103/PhysRev.80.268.
- [48] H. Cramér. *Mathematical Methods of Statistics*. Princeton University Press, 1946. doi:10.1086/256571.
- [49] J. Ma and X. Wang. Fisher information and spin squeezing in the Lipkin-Meshkov-Glick model. *Phys. Rev. A*, 80(1), 2009. URL: <https://link.aps.org/doi/10.1103/PhysRevA.80.012318>, doi:10.1103/PhysRevA.80.012318.
- [50] O. Gühne, G. Tóth, and H. J. Briegel. Multipartite entanglement in spin chains. *New Journal of Physics*, 7, 2005. doi:10.1088/1367-2630/7/1/229.
- [51] J. Jensen and A. R. Mackintosh. *Rare earth magnetism: structures and excitations*. 1991.
- [52] K. Ryogo. Statistical-Mechanical Theory of Irreversible Processes. I. General Theory and Simple Applications to Magnetic and Conduction Problems. *Journal of the Physical Society of Japan*, 12(6), 1957. doi:10.1143/JPSJ.12.570.
- [53] R. Costa de Almeida. to be submitted. 2019.
- [54] M. Prüfer, P. Kunkel, H. Strobel, S. Lannig, D. Linnemann, C.-M. Schmied, J. Berges, T. Gasenzer, and M. K. Oberthaler. Observation of universal dynamics in a spinor Bose gas far from equilibrium. *Nature*, 563(7730):217–220, 2018. doi:10.1038/s41586-018-0659-0.
- [55] P. Kunkel, M. Prüfer, H. Strobel, D. Linnemann, A. Frölian, T. Gasenzer, M. Gärtner, and M. K. Oberthaler. Spatially distributed multipartite entanglement enables EPR steering of atomic clouds. *Science*, 360(6387), 2018. arXiv:1708.02407, doi:10.1126/science.aao2254.
- [56] J. I. Cirac, L.-M. Duan, and P Zoller. Quantum entanglement in spinor Bose-Einstein condensates. *Physical Review A - Atomic, Molecular, and Optical Physics*. doi:10.1103/PhysRevA.65.033619.
- [57] H. J. Lipkin, N. Meshkov, and A. J. Glick. Validity of many-body approximation methods for a solvable model: (I). Exact solutions and perturbation theory. *Nuclear Physics*, 62(2):188–198, 1965. doi:[https://doi.org/10.1016/0029-5582\(65\)90862-X](https://doi.org/10.1016/0029-5582(65)90862-X).
- [58] J. J. Bollinger, W. M. Itano, D. J. Wineland, and D. J. Heinzen. Optimal frequency measurements with maximally correlated states. *Physical Review A - Atomic, Molecular, and Optical Physics*, 54(6):R4649—R4652, 1996. doi:10.1103/PhysRevA.54.R4649.
- [59] D. Leibfried, E. Knill, S. Seidelin, J. Britton, R. B. Blakestad, J. Chiaverini, D. B. Hume, W. M. Itano, J. D. Jost, C. Langer, R. Ozeri, R. Reichle, and D. J. Wineland. Creation of a six-atom ‘Schrödinger cat’ state. *Nature*, 438(7068):639–642, 2005. doi:10.1038/nature04251.

- [60] T. Monz, P. Schindler, J. T. Barreiro, M. Chwalla, D. Nigg, W. A. Coish, M. Harlander, W. Hänsel, M. Hennrich, and R. Blatt. 14-Qubit Entanglement: Creation and Coherence. *Physical Review Letters*, 106(13):130506, 2011. doi:10.1103/PhysRevLett.106.130506.
- [61] H. Lee, P. Kok, and J. P. Dowling. A quantum Rosetta stone for interferometry. *Journal of Modern Optics*, 49(14-15):2325–2338, 2002. doi:10.1080/0950034021000011536.
- [62] M. Vengalattore, S. R. Leslie, J. Guzman, and D. M. Stamper-Kurn. Spontaneously modulated spin textures in a dipolar spinor Bose-Einstein condensate. *Physical Review Letters*, 100(17):4–7, 2008. arXiv:0712.4182, doi:10.1103/PhysRevLett.100.170403.
- [63] C. S. Gerving, T. M. Hoang, B. J. Land, M. Anquez, C. D. Hamley, and M. S. Chapman. Non-equilibrium dynamics of an unstable quantum pendulum explored in a spin-1 Bose-Einstein condensate. *Nature Communications*, 2012. arXiv:arXiv:1205.2121v1, doi:10.1038/ncomms2179.
- [64] H. F. Song, N. Laflorencie, S. Rachel, and K. Le Hur. Entanglement entropy of the two-dimensional Heisenberg antiferromagnet. *Phys. Rev. B*, 83(22), 2011. doi:10.1103/PhysRevB.83.224410.
- [65] M. A. Cazalilla, R. Citro, T. Giamarchi, E. Orignac, and M. Rigol. One dimensional bosons: From condensed matter systems to ultracold gases. *Rev. Mod. Phys.*, 83(4), 2011. doi:10.1103/RevModPhys.83.1405.
- [66] A. Khodja, R. Steinigeweg, and J. Gemmer. Relevance of the eigenstate thermalization hypothesis for thermal relaxation. *Physical Review E*, 91(1):12120, 2015. doi:10.1103/PhysRevE.91.012120.
- [67] N. D. Mermin and H. Wagner. Absence of ferromagnetism or antiferromagnetism in one- or two-dimensional isotropic Heisenberg models. *Physical Review Letters*, 17(22):135, 1966. doi:10.1103/PhysRevLett.17.1307.
- [68] P. C. Hohenberg. Existence of long-range order in one and two dimensions. *Physical Review Letters*, 158(2):383–386, 1967. doi:10.1103/PhysRev.158.383.
- [69] A. Görlitz, J. M. Vogels, A. E. Leanhardt, C. Raman, T. L. Gustavson, J. R. Abo-Shaeer, A. P. Chikkatur, S. Gupta, S. Inouye, T. Rosenband, and W. Ketterle. Realization of Bose-Einstein Condensates in Lower Dimensions. *Physical Review Letters*, 87(13):130402, sep 2001. doi:10.1103/PhysRevLett.87.130402.
- [70] V. N. Popov. On the theory of the superfluidity of two- and one-dimensional bose systems. *Theoretical and Mathematical Physics*, 11(3):565–573, 1972. doi:10.1007/BF01028373.
- [71] D. S. Petrov, G. V. Shlyapnikov, and J. T.M. Walraven. Regimes of quantum degeneracy in trapped 1D gases. *Physical Review Letters*, 85(18):3745–3749, 2000. doi:10.1103/PhysRevLett.85.3745.
- [72] C.-M. Schmied. Emergence of Structure in a Quenched (Quasi) One-dimensional Spin-1 Bose-Einstein Condensate in Comparison with Experiments. *Master Thesis*, 2016.

- [73] T. Bergeman, M. G. Moore, and M. Olshanii. Atom-Atom Scattering under Cylindrical Harmonic Confinement: Numerical and Analytic Studies of the Confinement Induced Resonance. *Physical Review Letters*, 91(16):163201, 2003. doi:10.1103/PhysRevLett.91.163201.
- [74] A. L. Gaunt, T. F. Schmidutz, I. Gotlibovych, R. P. Smith, and Z. Hadzibabic. Bose-Einstein Condensation of Atoms in a Uniform Potential. *Phys. Rev. Lett.*, 110(20), 2013. doi:10.1103/PhysRevLett.110.200406.
- [75] S. Lellouch, T.-L. Dao, T. Koffel, and L. Sanchez-Palencia. Two-component Bose gases with one-body and two-body couplings. *Phys. Rev. A*, 88(6), 2013. doi:10.1103/PhysRevA.88.063646.
- [76] N. T. Phuc, Y. Kawaguchi, and M. Ueda. Effects of thermal and quantum fluctuations on the phase diagram of a spin-1 ^{87}Rb Bose-Einstein condensate. *Phys. Rev. A*, 84(4):43645, 2011. doi:10.1103/PhysRevA.84.043645.
- [77] N. K. Whitlock and I. Bouchoule. Relative phase fluctuations of two coupled one-dimensional condensates. *Phys. Rev. A*, 68(5), 2003. doi:10.1103/PhysRevA.68.053609.
- [78] S. Lannig. Private Communication. 2019.
- [79] U. Schollwöck. The density-matrix renormalization group in the age of matrix product states. *Annals of Physics*, 326(1), 2011. doi:<https://doi.org/10.1016/j.aop.2010.09.012>.
- [80] P. B. Blakie, A. S. Bradley, M. J. Davis, R. J. Ballagh, and C. W. Gardiner. Dynamics and statistical mechanics of ultra-cold Bose gases using c-field techniques. 2008. arXiv:arXiv:0809.1487.
- [81] C.-M. Schmied, T. Gasenzer, M. K. Oberthaler, and P.G. Kevrekidis. Stability analysis of ground states in a one-dimensional trapped spin-1 Bose gas. 2019. arXiv:1905.03069.
- [82] T. Weigand. Lecture notes on quantum field theory. *Heidelberg University*, 2011. URL: <https://www.thphys.uni-heidelberg.de/~weigand/Skript-QM2011/skript.pdf>.
- [83] S. Uchino, M. Kobayashi, and M. Ueda. Bogoliubov theory and Lee-Huang-Yang corrections in spin-1 and spin-2 Bose-Einstein condensates in the presence of the quadratic Zeeman effect. *Phys. Rev. A*, 81(6):63632, 2010. doi:10.1103/PhysRevA.81.063632.

Erklärung

Ich versichere, dass ich diese Arbeit selbstständig verfasst habe und keine anderen als die angegebenen Quellen und Hilfsmittel benutzt habe.

Heidelberg, den 24.7.2019

.....